

MULTI-MILLION-YEAR CYCLIC RAMP-UP OF VOLATILES IN A LOWER CRUSTAL MAGMA RESERVOIR TRAPPED BELOW THE TAMPAKAN COPPER-GOLD DEPOSIT BY MIO-PLIOCENE CRUSTAL COMPRESSION IN THE SOUTHERN PHILIPPINES

^{1,2}Bruce D. Rohrlach and ^{1,3}Robert R. Loucks

¹ *Research School of Earth Sciences, Australian National University, Canberra, Australia.*

² *Consultant, Legaspi City, Philippines.*

³ *Geoscience Research, Lakewood, Colorado, USA*

Abstract - Magmatic-related porphyry copper and high-sulphidation epithermal copper-gold ore deposits are spatially and temporally clustered in arc segments that underwent crustal shortening during magmatic differentiation. In the ductile lower crust or uppermost mantle, geodynamically induced horizontal compression inhibits propagation of subvertical dykes and can keep buoyant magmas trapped in sheet-like, subhorizontal chambers. Layered ultramafic-mafic cumulates crystallise within these chambers until the regional stress regime relaxes or until further magmatic differentiation generates the buoyancy needed to overpower the stress field and permit magma ascent. In the hot lower crust or uppermost mantle, magma chambers tend to last long enough to experience multiple episodes of replenishment by primitive magma, partial mixing of arriving mafic and resident evolved melts, and fractional crystallisation of those hybrids. Over a succession of replenishment and partial-crystallisation cycles, the melt's concentration of incompatible chemical components (H₂O, Cl, SO₃, etc.) follows a "sawtooth ramp-up" time series. Multi-cycle magma chambers thereby become exceptionally fertile for magmatic-hydrothermal Cu metallogeny. In this case study of the late Miocene to Recent magmatism in the Tampakan ore district of southern Mindanao, Philippines, we integrate the regional tectonic history with local geological, geochronological, petrochemical and crustal stress data, and with magma chamber thermal modelling, formulate a model for arc-scale porphyry Cu-Au metallogenesis in compressional arc segments. Porphyry copper and high-sulphidation epithermal mineralisation within the giant Tampakan Cu-Au deposit (2500 Mt @ 0.48% Cu and 0.2 g/t Au) is hosted by a cluster of four overlapping stratovolcanoes constructed over the past 7 M.y. by intermittent emissions from a lower-crustal magma chamber having the same lifespan. This time interval spans the pre-, syn- and late-collision stages of the Sangihe arc in southern Mindanao where crustal compression commenced at ~7 Ma and peaked at ~4 to 3 Ma. The Tampakan porphyry Cu ore (4.24 to 4.26 Ma) and high-sulphidation Cu-Au ore (3.24 to 3.28 Ma) formed during peak crustal compression. Geochronologic and geochemical studies of the Tampakan volcanic complex identify five mafic-to-felsic differentiation cycles, punctuated by major mafic-magma replenishments into the basal chamber between the late Miocene and present, as the arc underwent a transition from relatively non-compressive subduction to collision. ²³⁸U-²⁰⁶Pb geochronology on 471 zircon samples parameterise time series in chemical compositions of volcanic rocks and phenocrysts, and time-series in magmatic temperature, oxygen fugacity and wt % H₂O in the pre-eruptive melt over the past 7 M.y. The time series of U/Ti, U/Ge and Th/Ti ratios in hundreds of dated detrital zircon grains resolve multiple, million-year-scale magma recharge-mixing-and-crystallisation cycles within a long-lived, lower-crustal magma reservoir near the arc Moho at 18 to 22 km depth (~5 to 6 kbars, by Al-in-hornblende geobarometry). The "sawtooth" cyclic ramp-up of these element ratios in zircons and their parent melts coincides with a 7 M.y. long sawtooth cyclic ramp-up in concentrations of volatiles and crystal-incompatible trace elements in erupted melts of basaltic andesite to dacite composition. At ~6.3 Ma, silicic andesite (62% SiO₂) of the early mafic-to-felsic differentiation cycle had only ~3 wt% H₂O in the melt and U/Ti \cong 20 in zircon, whereas by ~1.3 Ma the late-cycle silicic andesite (62% SiO₂) had ~7.5 wt% H₂O in the melt and U/Ti \cong 80 in zircon, due to inheritance of H₂O and U and other incompatible components from prior cycles. Porphyry-Cu-ore-related volcanics and epizonal plutons display trace-element evidence that the melts segregated from high pressure (lower-crustal) cumulates consisting largely of olivine, Al-rich augite and hornblende, but little or no plagioclase. Higher Sr/Y ratios in later cycles of the Tampakan igneous complex represent differentiation of increasingly hydrous hybrid melts in the lower crust. Retardation and suppression of plagioclase crystallisation by high magmatic water activities and by high load pressure allowed residual

melt fractions to avoid depletion of Sr and Eu during fractionation crystallisation. Higher pressure and H₂O activities in melts foster prolific crystallisation of hornblende earlier in the crystallisation sequence of later cycles, thereby depleting the melt in Y and heavy REE, and driving up its Sr/Y and Eu/Yb ratios to produce the distinctive chemical signatures characteristic of porphyry-copper ore-forming magmas worldwide throughout Phanerozoic time

Introduction

The Tampakan copper-gold deposit in southern Mindanao, Philippines, is a giant high-sulphidation epithermal (Cu-Au) deposit that is developed on older, erosionally exhumed, deeper-level porphyry-Cu mineralisation. The deposit is located within the municipality of Tampakan, Province of South Cotabato in southern Mindanao, Philippines, at approximately 06°28'30"N latitude and 125°03'00"E longitude, 40 km NNW of General Santos City. It lies at 600 to 1200 metres elevation along the southern portion of the Central Mindanao Cordillera. Mineralisation is hosted by altered diorite intrusions and andesitic lava flows that form a late Miocene volcanic basement sequence and an erosionally dissected, late Miocene to Pleistocene stratovolcanic complex. The Tampakan district lies at the northern end of the Miocene-to-Holocene-age Sangihe volcanic arc which extends from northern Sulawesi to southern Mindanao. The district lies between strands of the Cotabato strike-slip fault zone (Fig. 1).

The Tampakan deposit was discovered by WMC Resources Ltd in 1992 and is currently owned by Indophil Resources Ltd and its Philippine partner Sagittarius Mines Ltd. It has a preliminary inferred resource of 2500 million tonnes (Mt) grading 0.48% copper, and includes a higher-grade core with an indicated and inferred resource of 1100 Mt grading

0.7% copper and 0.3 g/t gold (Subang *et al.*, 2004). The total estimated *in-situ* metal content is 12.5 Mt of copper (Cu) and 500 tonnes (16 Moz) of gold (Au). It is the second largest known Cu-Au resource within the western Pacific, after the giant, diatreme-hosted, Grasberg Cu-Au deposit in Irian Jaya. The Tampakan deposit is the first exploration discovery within a newly defined metallogenic province in the southern portion of the Central Mindanao Cordillera, and lies within a syn- to post-collisional tectonic setting related to terrane accretion and arc-arc collision. This collision is associated with widespread thrust faulting and folding within the arc, and subduction polarity reversal. Intense intra-arc compressional deformation penecontemporaneous with mineralisation is observed in all well investigated Cenozoic Cu-dominant Cu ± Au metallogenic provinces around the rim of the Pacific basin.

A poorly understood feature of oceanic-island-arc and continental-arc metallogeny is the highly variable endowment of Cu and Au mineralisation in different arcs and arc segments. A second poorly understood feature of arc metallogeny is its usual development as province-scale metallogenic pulses lasting a few million years that punctuate much longer periods of metallogenically infertile magmatism in the same regions. Many of the major mineralised porphyry and epithermal provinces that contain multiple deposits display a long history of subduction-related magmatism (15 to >60 M.y.). Magmatic

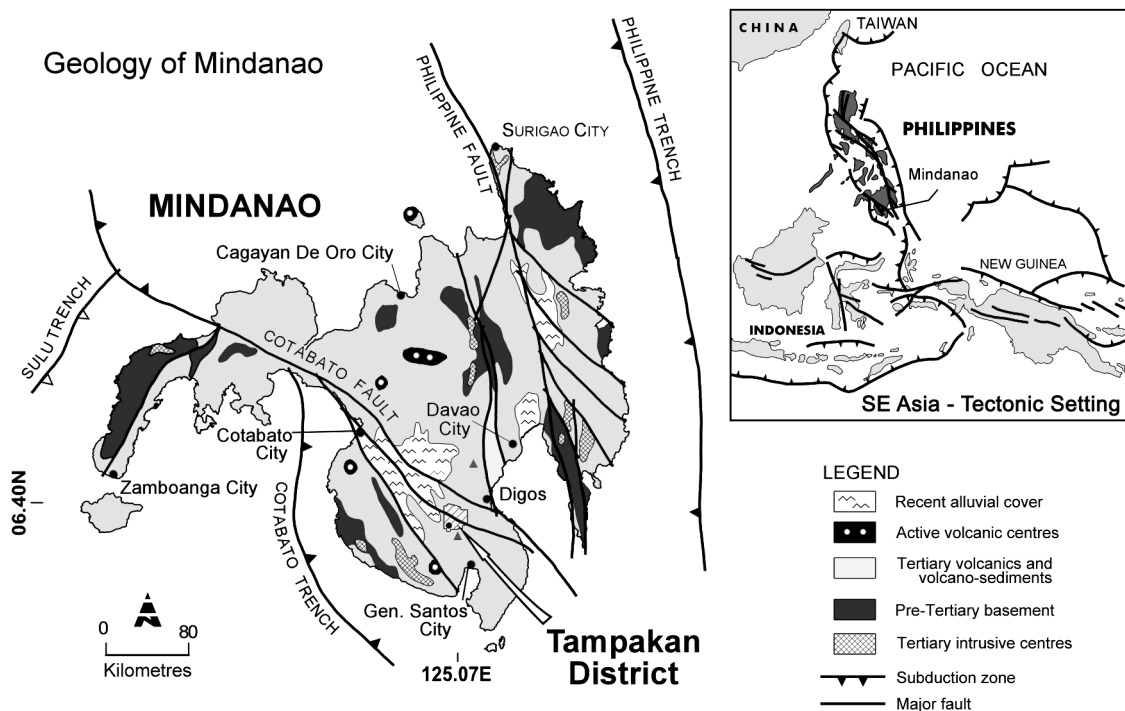


Figure 1: Geology of Mindanao, southern Philippines, and location of the Tampakan deposit within the transressional Cotabato Fault Zone.

differentiation, enrichment of incompatible elements and volatile exsolution are processes that occur in nearly all intra-arc intrusives. However, the emplacement of ore-forming magmas within mineral districts and provinces typically spans a brief time interval (~3 to 10 M.y.). Examples of these short-lived pulses of mineralisation include the various mineral belts of the Andean cordillera [4 to 12 Ma, 20 to 22 Ma, 33 to 41 Ma, 55 to 60 Ma in different segments – Titley and Beane (1981)]; the southwest continental US [39 to 40 Ma, 52 to 59 Ma, 62 to 67 Ma in different regions – Titley and Beane (1981)]; the Philippines [1 to 5 Ma]; New Guinea [1 to 6 Ma] and the New Ireland/Solomon Islands/Fiji region [0 to 4 Ma].

The regional tectonic factors that accompany and contribute to these brief, migratory pulses of metallogenically fertile magmatism are often poorly understood and poorly characterised in district-scale ore-genesis studies. An understanding of the fundamental tectonic controls on province-scale metallogenesis is required in any holistic model for magmatic-related Cu-Au mineralisation. The most appropriate regions to study this problem are those where mineralisation is sufficiently young that the pre-, syn- and post-mineralisation variations in tectonic setting can be tightly constrained. The late Neogene to Recent volcanic island arcs of southeast Asia and the southwest Pacific are suitable localities for this type of study. The Pliocene age of the Tampakan deposit enables interpretation of the petrology, petrochemistry and geochronology of the ore-bearing and barren magmatic suites in the context of the reasonably well constrained tectonic framework for Mindanao in the late Cenozoic. In this paper, we identify the relevant tectonic-plate-scale cause-and-effect relationships responsible for magmatic metallogenic fertility in the Tampakan district, and we determine the diagnostic petrochemical characteristics of ore-forming magmas in the Tampakan district; these characteristics are representative of the broader spectrum of magmas that produce large porphyry and high-sulphidation Cu ± Au ore deposits of Phanerozoic age globally.

Regional Tectonic Setting

The Philippine archipelago is the site of recent small-scale collisions between extinct early Cenozoic arc systems on the Philippine Sea Plate and continental fragments or island-arc fragments that were rifted from the southeast margin of the Eurasian Plate during Tertiary opening of marginal basins. The principal tectonic element of the archipelago is the elongate Philippine Mobile Belt (PMB; Rangin, 1991) that is bounded to the east by the Philippine subduction system and to the west by the Manila-Negros-Sulu and Cotabato subduction systems. The crustal “raft” that comprises the Philippine archipelago is bisected along its north-south axis by the ~2000-km-long sinistral Philippine Fault (inset to Fig. 1). Taiwan and several segments of the western seaboard of the Philippines that include Zambales, Mindoro, Palawan, western Panay and southern Mindanao, represent collision zones caused by convergent interaction between the Eurasian Plate and the Philippine Sea Plate along the multi-strand boundary zone that comprises the PMB (Pubellier *et al.*, 1991).

According to Hall (1996, 2002) and sources cited therein, a major reorganisation of tectonic plates in the Southwest Pacific and Sundaland region accompanied the late Oligocene (30 to 25 Ma) arrival of the “horn” promontory of northwestern continental Australia (now the Birds Head of Irian Jaya, Seram, Buru, and east arm of Sulawesi) at the north-dipping trench along which the Mesozoic oceanic crust of the Indo-Australian Plate had been subducting under the Sundaland-Philippine Sea Plate. The continental promontory’s arrival at the trench divided the Indo-Australian oceanic lithosphere north of Australia into two segments lying west and east of the promontory. The eastern segment was continuous from the Molucca Sea to the Solomon Sea, but that continuity was soon destroyed at ~25 Ma, isolating the Molucca Sea portion, when northern New Guinea arrived at the Philippine-Halmahera-South Caroline Trench situated on the southern edge of the Philippine Sea Plate.

The Molucca Sea oceanic lithosphere fragment lay between southern Mindanao and northern Sulawesi during the Miocene. Clockwise rotation of the Philippine Sea Plate at 25 Ma initiated the Sangihe subduction system along the western margin of the attached Molucca Sea Plate fragment, and by 20 Ma the Molucca Sea Plate was subducting westward at the Sangihe Trench. This subduction zone generated volcanism between 15 and 5 Ma in southern Mindanao. Hall (1996) suggests that at 20 Ma, the proto-Cotabato Fault Zone propagated along the northern edge of the Zamboanga Peninsula as a sinistral strike-slip fault that partly accommodated the clockwise rotation of the Philippine Sea Plate. The Cotabato Fault became a transfer zone along which the southern Mindanao (Zamboanga Peninsula, Daguma Range and the Sarangani Peninsula) portion of the ancestral Zamboanga-Negros-Panay-Luzon arc was translated southeastward to dock with the northern half of Mindanao at the Miocene-Pliocene transition (Rangin 1991; Pubellier *et al.*, 1991; Hall 1996).

The Molucca Sea Plate began to subduct eastward along the Halmahera Trench at around 15 Ma. The Molucca Sea Plate was doubly subducting eastward and westward at 15 Ma, and by 10 Ma the plate was bounded by sinistral strike-slip systems on the north (Cotabato Fault Zone) and on the south (Sorong Fault Zone) (Hall, 1996). At the Miocene-Pliocene transition (6 to 4 Ma), immediately preceding and during porphyry mineralisation at Tampakan (4.24 to 4.26 Ma), the southern portion of Mindanao (Sarangani Peninsula, Zamboanga Peninsula and Daguma Range) was moving southeastward along the Cotabato Transfer Fault Zone which separated basement of Eurasian affinity in the south from basement of oceanic affinity – Philippine Sea Plate – in the north (Fig. 2).

The 5 to 3 Ma period was a dynamic one in the southern Philippines as continental crust of southern Mindanao docked with arc-thickened oceanic crust of northern Mindanao. The 5 Ma date marks the commencement of a prolonged and continuing period of compression throughout southeast Mindanao and was synchronous with porphyry Cu and high-sulphidation epithermal Cu-Au mineralisation in the Tampakan district. Compressional structures related

to this oblique collision include NW-trending sinistral strike-slip faults that define pressure ridges and horst blocks along the Cotabato transfer fault, widespread thrust faults which are east-verging in the southern Mindanao terrane and west-verging in the northern Mindanao terrane (Fig. 3) (Quebral *et al.*, 1996; Domingo *et al.*, 1995), thrust-related ramp anticlines which display dual vergence (Fig. 3), and regional folding (Figs. 6 and 7). Compression during the 5 to 3 Ma period in southeastern Mindanao was compounded by final closure of the northern Molucca Sea as the Sangihe and Halmahera arcs came into frontal collision.

As the central Philippines collided with the continental Palawan block in the late Miocene, jamming the Manila Trench there, the Philippine Trench was initiated along the opposite, eastern margin of the central Philippines at around 8 Ma and propagated southward to the latitude of Mindanao by about 5 Ma (Ozawa *et al.*, 2004). The compressional stress associated with establishment of the new subduction-thrust system was transmitted westward through the interior of Mindanao, contributing to the accumulation of compressional stress within the collision terrane of central and southern Mindanao. Furthermore, a segment of the

Halmahera arc (southern Pacific Cordillera) accreted onto east Mindanao by collision between 5 and 4 Ma (Lallemand *et al.*, 1998).

During this Pliocene compressional period, the Philippine Fault was initiated as a sinistral strike-slip fault within the Philippine Mobile Belt to partly accommodate the oblique component of convergence between the Philippine Sea Plate and the Philippine Mobile Belt (Aurelio *et al.*, 1991; Barrier *et al.* 1991). However, compressional stress was generated faster than it was accommodated by the proto-Philippine Trench and Philippine Fault Zone, so distributed compressional deformation became increasingly focused into a developing subduction thrust zone that became the Cotabato Trench along the southwestern margin of Mindanao (Figs. 3, 4 and 5).

A new geodynamic setting for the southern Philippines was ushered in at ~3 Ma. The Zamboanga Peninsula, Daguma Range and Sarangani Peninsula were tectonically incorporated into the Philippine Mobile Belt. Establishment of the Philippine Trench constitutes an eastward jump of the western margin of the Philippine Sea Plate, thereby tectonically isolating the Philippine Mobile Belt as a crustal "raft" that was trapped between the east-dipping Manila-

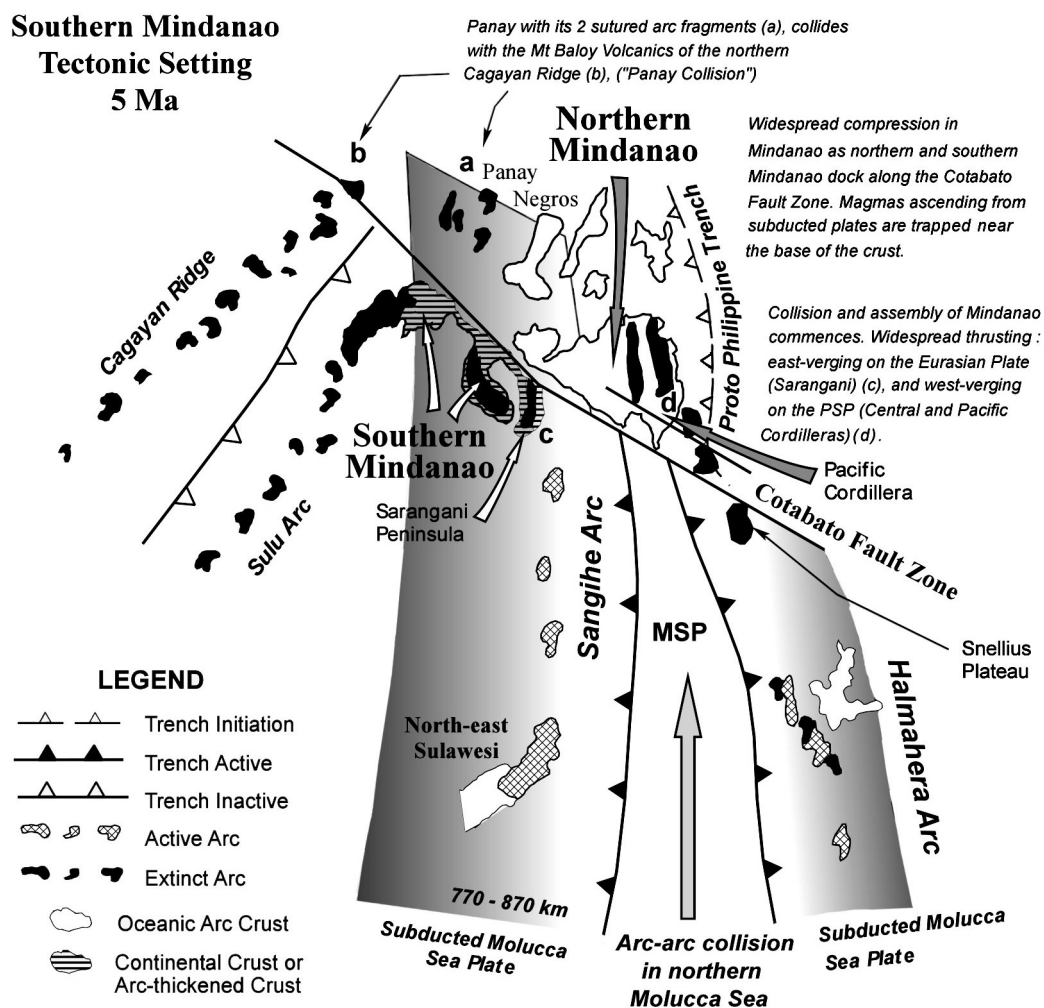


Figure 2: Schematic tectonic reconstruction of southern Mindanao during the Mio-Pliocene collision event at 5 Ma. The docking of northern and southern Mindanao along the Cotabato Fault Zone occurred synchronously with arc-arc collision between the northern end of the Sangihe and Halmahera arcs.

Negros-Cotabato subduction system and the west-dipping Philippine Trench subduction zone. During the late Pliocene and Pleistocene through to the present, the docking of the two terranes along the Cotabato Fault was completed and the Molucca Sea Plate's two outward facing subduction zones (Sangihe and Halmahera) were replaced by the Philippine Trench and Cotabato Trench subduction zones that now dip under the Philippine archipelago. This period of subduction polarity reversal was marked by extensive and rapid uplift of significant portions of Mindanao. Collision is currently ongoing south of the Pujada Peninsula, off the southeast coast of Mindanao (Fig. 4), where segments of the Halmahera arc that have been dislocated by strike-slip faulting are partly under-thrust beneath the Sangihe Trench (Lallemand *et al.*, 1998; Pubellier *et al.*, 1999).

The history of convergence between the Philippine Sea Plate and the Sunda Block of the Eurasian margin, and the partitioning of this convergence into subduction systems, is illustrated in Fig. 5. By integrating the area above the curve that defines the deficit in total convergence, after accounting for convergence at active subduction zones (Fig. 5, shaded black area), we derive a first-order estimate of the portion of the plate convergence that is partitioned into intra-plate compressive deformation. Southern Mindanao has been under significant crustal compression since 7 Ma, with compression peaking between 4 and 2 Ma

(Fig. 5). There is widespread thrusting of Pliocene age throughout southeastern Mindanao and in the Tampakan district. This shortening is implicated in rapid uplift between 3.92 and 4.32 Ma which unroofed the Tampakan porphyry system by ~2 km within a time frame of ~350 K.y. (See 'Geochronology' below). The progressive slowing in subduction rate of the Molucca Sea Plate at the Halmahera and Sangihe trenches, due to the Cotabato suture collision that commenced at ~5 Ma, coincides with the convergence between the Philippine Sea Plate and the Sunda Block becoming increasingly accommodated by intra-plate thrusting and folding in southern Mindanao. It is also synchronous with initiation of thrusting at the nascent Philippine Trench. At present there is a small component of convergence (A-Su on Fig. 5; 8.4 mm y^{-1}) which is not accommodated by subduction. This suggests that crustal shortening is still ongoing in southern Mindanao, albeit waning in intensity. Quaternary to Recent uplift of limestone terraces along the western shoreline of Sarangani Bay (pers. observ.) indicate ongoing uplift. The component of convergence available for partitioning into crustal compression is diminishing as current subduction systems become established and as the sinistral Philippine Fault Zone propagates farther south and absorbs some convergence in this region.

The Molucca Sea Plate has submerged into the upper mantle below the over-riding and colliding Eurasian and Philippine

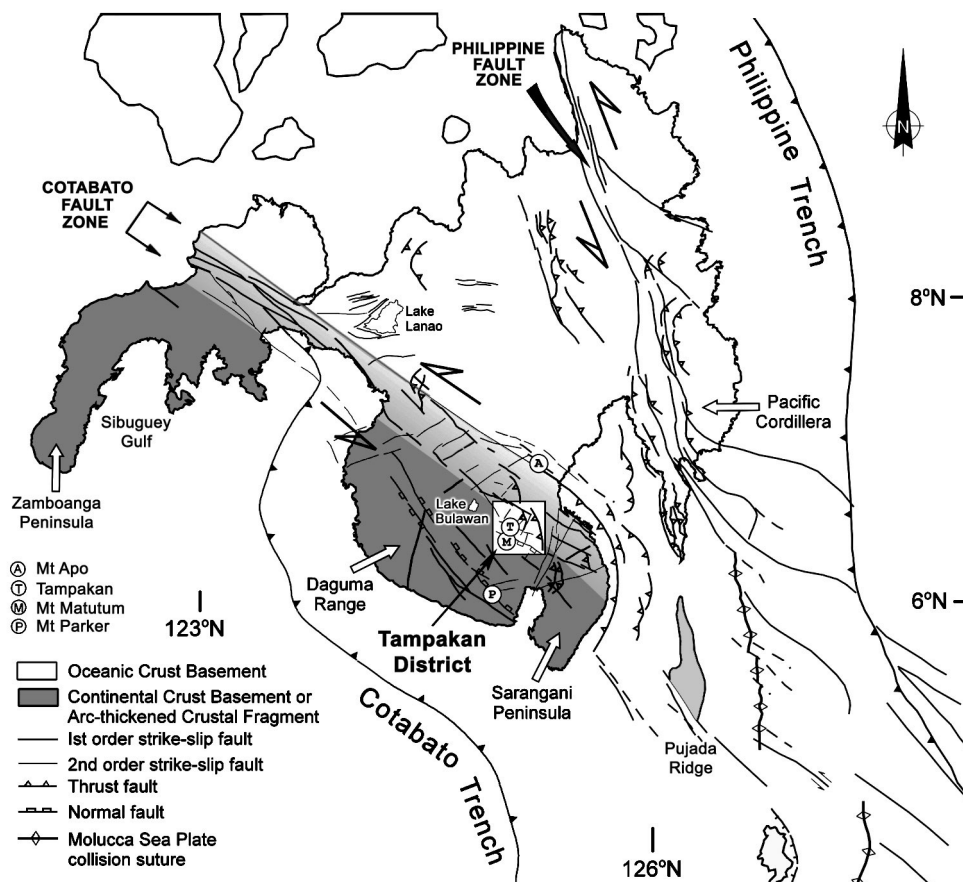


Figure 3: *Principal strike-slip and thrust faults in Mindanao. The Tampakan district lies within a ~100-km-wide corridor of sinistral wrench faulting along the Cotabato Fault Zone. Widespread thrust faulting that occurs in proximity to the Tampakan district developed during the Mio-Pliocene collision event in southeast Mindanao. These thrust faults verge to the east in the Tampakan district and Sarangani Peninsula, and verge to the west on the southern portion of the Pacific Cordillera.*

lithospheric plates in southern Mindanao; however, arc-arc collision is ongoing in the southern Molucca Sea. The Sangihe and Halmahera volcanic arcs face each other and are underlain by opposite-dipping Benioff zones. The west-dipping portion of the Molucca slab beneath the Sangihe Arc and the Celebes Sea can be traced to at least 650 km depth by earthquake foci (Seno and Kurita, 1978; Cardwell *et al.*, 1980), whereas the east-dipping portion of the doubly subducted Λ -shaped Molucca slab can only be traced

seismically to around 250 km depth beneath the Halmahera Arc (Hatherton and Dickinson, 1969; Silver and Moore, 1978; Hamilton, 1979; Hall, 1996). The Tampakan district lies along the trace of the suture between northern and southern Mindanao defined by the Cotabato Fault Zone, and falls within a zone of compressional structures defined by thrusting and folding that developed during subduction reversal associated with the transition from the Sangihe-Halmahera to the Cotabato-Philippine subduction pairs.

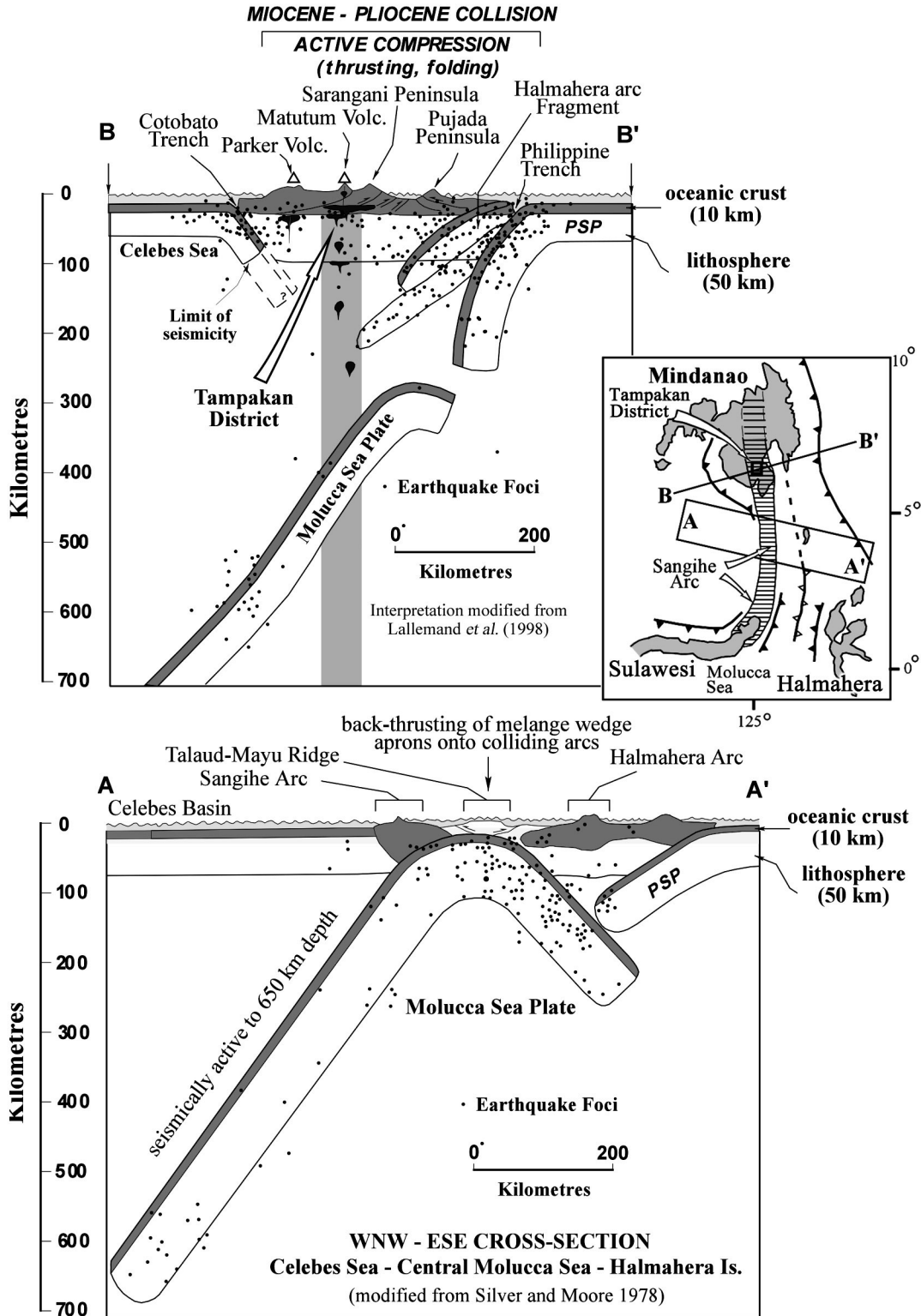


Figure 4: Geometry of subducted ocean floor beneath the collision zone that contains the Tampakan district in southern Mindanao (top), and in the Molucca Sea between Mindanao and Sulawesi where arc-arc collision is presently occurring. Stacking of arc fragments occurs below southeast Mindanao. The Molucca Sea Plate is subsiding into the mantle below the collision zone.

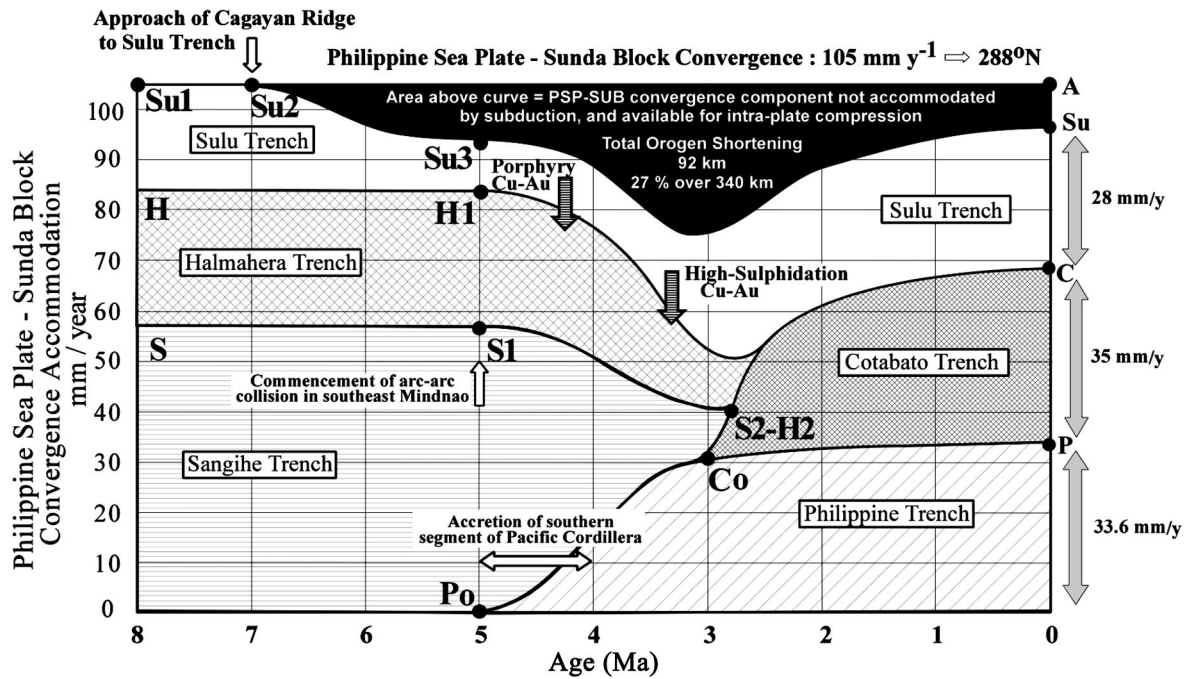


Figure 5: Temporal history of convergence-parallel accommodation of the Philippine Sea Plate motion, relative to the Sunda Block, that is accommodated at subduction zones in southern Mindanao. Residual convergence that is not accommodated by subduction is represented as distributed intra-plate compression (black shading). The geological controls for the tie-points (labelled dots) are discussed by Rohrlach (2002).

District Geology

The geology of southern central Mindanao is dominated by three segments of the Sangihe volcanic arc; i). the Daguma Range (magmatically active from ~17 to 18 Ma; Pubellier *et al.*, 1993, Sajona 1994); ii). the Sarangani Peninsula (~10 to 12 Ma; Pubellier *et al.*, 1993, Sajona *et al.*, 1994); and iii). the southern Central Mindanao Cordillera which was volcanically active from ~8.5 Ma to the present in the Tampakan district. The Tampakan district is flanked to the west by the Cotabato Basin and to the east by the Sarangani Basin (Fig. 6). The Cotabato Basin separates the Daguma and southern Central Mindanao Cordillera arc segments. It has a long history, initially as a fore-arc basin developed between early Miocene arc volcanism in the Daguma Range and the Sangihe Trench, and more recently, as a developing back-arc basin behind the Daguma Range (Pubellier *et al.*, 1991) as a result of new subduction along the Cotabato Trench. The basin comprises an extensive alluvial plain with several NW-trending ridges (e.g., the Roxas Range) that define *en echelon* folds developed over buried splays of the Cotabato Fault Zone (Fig. 7). Middle Miocene to Pleistocene basin sediments within the Roxas Range comprise bathyal marine mudstone and conglomerate, progressively shallower marine limestone, sandstone, and recent non-marine alluvium. The shallowing palaeo-sedimentary environment reflects prolonged uplift of the region. Coarsely bedded Pleistocene conglomerate beds along the eastern margin of the basin onlap the cordillera west of the Tampakan deposit, and are intruded by Pleistocene-age volcanic plugs in the Tampakan district. The beds are tilted towards the west at 30 to 40° by basin-margin thrust faults. The Sarangani Basin separates the Central Mindanao Cordillera from the Sarangani Peninsula arc segment and is an intra-arc basin that developed within an active synclinal flexure

on the western limb of the Sarangani ramp anticline (Fig. 6). This north-south trending topographic depression is filled by Pliocene-age volcanoclastic sediments and limestones. The volcanoclastic sediments were eroded from the adjacent, actively uplifting arc segments to the east and west. The presence of water-lain tuff interbedded with conglomerate and limestone along the western margin of the basin indicate active volcanism in the hinterland during folding and basin development. Much of the volcanoclastic component was probably sourced from the early to middle Pliocene Tampakan volcano which was the nearest volcanic centre during the Pliocene.

Southern Mindanao has been affected by two styles of deformation. The earliest and most persistent deformation took the form of lithospheric-scale wrench faulting along a Miocene plate boundary that coincides with the ~100-km-wide zone of sinistral faulting that comprises the suturing Cotabato Fault system (Pubellier *et al.*, 1991). The second style of deformation comprises folding and thrusting that developed during collision of the Sangihe and Halmahera arcs in southeastern Mindanao, and during subsequent subduction polarity reversal that formed the Philippine and Cotabato trenches. The thrust faults and ramp-anticlines that dominate east-west geological cross-sections of the southern Pacific Cordillera and Sarangani Peninsula (Quebral *et al.*, 1996; Domingo *et al.*, 1995) are also present within the southern Central Mindanao Cordillera segment of the Sangihe Arc and the Tampakan district (Fig. 3). The Tampakan district is fault-bounded against the western margin of the Sarangani Basin by an east-verging thrust fault which dips westward under the district – the Central Cordilleran Thrust Fault (Fig. 6). The district lies on a ramp anticline that developed in the hanging wall of this thrust fault and which folds the early Miocene volcanic basement (Fig. 7).

The Tampakan district is centred on a deeply eroded polygenetic volcanic complex which was active episodically from the Late Miocene to late Quaternary period. The volcanics and intrusives are dominated by mafic to silicic andesite flows and intrusives of Late Miocene to Middle Pliocene age, with lesser basaltic andesite flows of Late Miocene age and dacitic flow domes and plugs of Pleistocene age. The Tampakan porphyry mineralisation is hosted by Late Miocene and early Pliocene volcanics whereas the Tampakan high-sulphidation deposit is hosted also by younger, middle Pliocene volcanic and intrusive rocks. Digital terrain model (DTM) images of the Tampakan district that have been enhanced using algorithms that simulate solar illumination, clearly identify a deeply dissected, central-vent stratocone that forms the core of the district (Fig. 8). This eroded volcanic centre is overlapped to the south by the juvenile and dormant Mt Matutum stratocone. The digitally enhanced topographic images reveal the preserved basal third of an andesitic stratocone that is erosionally truncated at an elevation of ~1200 to 1300 metres above sea level. The Tampakan deposit lies below the western lip of the truncated surface (Fig. 8). The Tampakan volcanic centre comprises a series of sequentially rebuilt and eroded volcanic centres that have accumulated the Tampakan Andesite Sequence over a 4.5 M.y. interval extending from ~7 to ~2.5 Ma. The eroded topographic stratocone remnant identified in the DTM dataset is a middle Pliocene age stratocone that dominated the volcanic landscape at the time of Tampakan high-sulphidation Cu-Au mineralisation.

The Tampakan Andesite Sequence has a grossly circular distribution, and on a regional-scale unconformably overlies a northwest-trending basement antiform (Fig. 7). The 10 to 15° radial dip angle of andesite lava flows on the flanks of the volcanic structure, and the diameter of the base of the inferred volcanic cone (~18 km) suggest that the original middle Pliocene volcanic summit may have had an elevation of ~3000 metres above sea level, similar in scale

to the 2950 metre-high Quaternary Mt Apo volcanic centre that lies ~60 km to the north in the Davao district. Strands of the Cotabato wrench fault zone that transect the district are the Alip River Fault and the Buayan Fault (Fig. 7). Prominent northeast-trending photo-lineaments lie parallel to mineralised zones within the deposit and cross-cut a district-wide zone of advanced argillic to intermediate argillic and silicic alteration (Fig. 7).

Deposit Geology

The spatially coupled high-sulphidation-epithermal Cu-Au and porphyry Cu deposits at Tampakan are located on the western rim of an eroded middle Pliocene volcanic centre (Fig. 8), and on the western margin of a series of annular to elliptical topographic anomalies in the core of the eroded volcanic edifice (Fig. 7). High-sulphidation mineralisation and acid alteration form a manto-like zone of mineralisation extending along an erosion surface that exhumed a low-grade porphyry Cu system. Epithermal mineralisation post-dates porphyry mineralisation by ~1 M.y. (See 'Geochronology' below).

High-Sulphidation Mineralisation

High-sulphidation mineralisation at Tampakan accounts for most of the resource that has been defined to date. Mineralisation covers a lateral area of ~1.6 by 2.0 km (Fig. 9) and forms a generally stratabound and gently-dipping zone between 200 and 500 metres thick on the western flank of the volcanic centre. The zone of high-sulphidation mineralisation and advanced-argillic/silicic alteration crops out at ~1200 metres above sea-level (ASL) in the northern part of the deposit and extends to ~600 metres ASL at the southern end. The stratabound zone of partial to massive silicification displays multi-phase brecciation, acid leaching and vuggy porosity, and is developed within a district-scale advanced-argillic lithocap that exceeds 90 km² in area (Fig. 7). The principal host rocks are the Tampakan Andesite Sequence of Late Miocene to

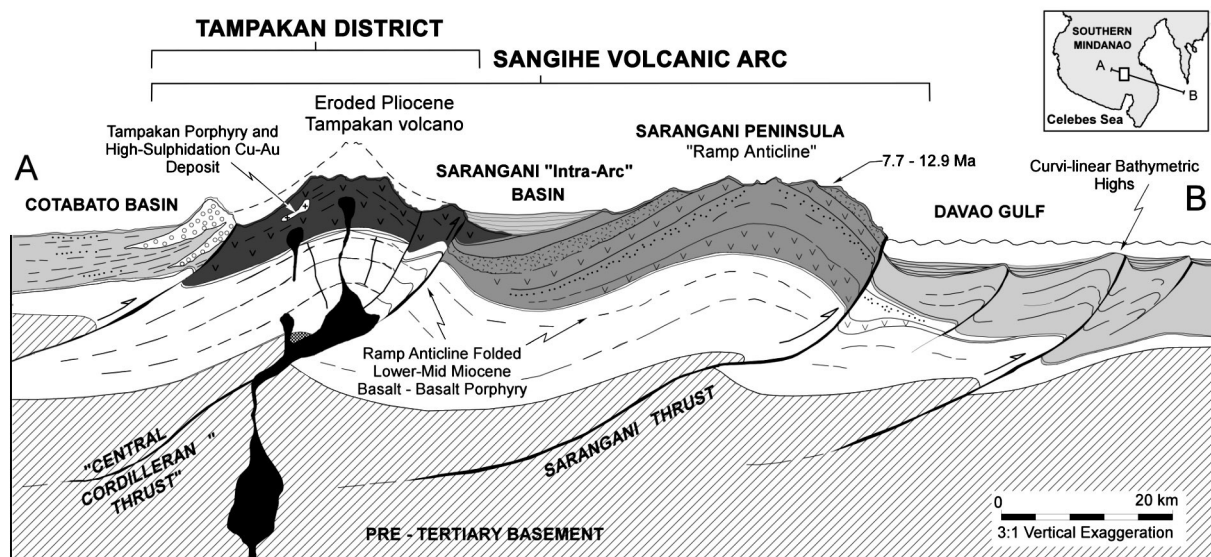


Figure 6: Geological cross-section through south-central Mindanao, showing location of the Tampakan district on a ramp-anticline developed over a Pliocene collision-stage thrust fault. Major folds and thrusts affect latest-Miocene rocks. Thrust faults are east-verging throughout the southern Central Mindanao Cordillera, Sarangani Peninsula and in seafloor sediments of the Davao Gulf (Quebral *et al.* 1996). The convex-to-east geometry of Sarangani Peninsula reflects the largest of the collision-stage thrust faults observed in southeast Mindanao.

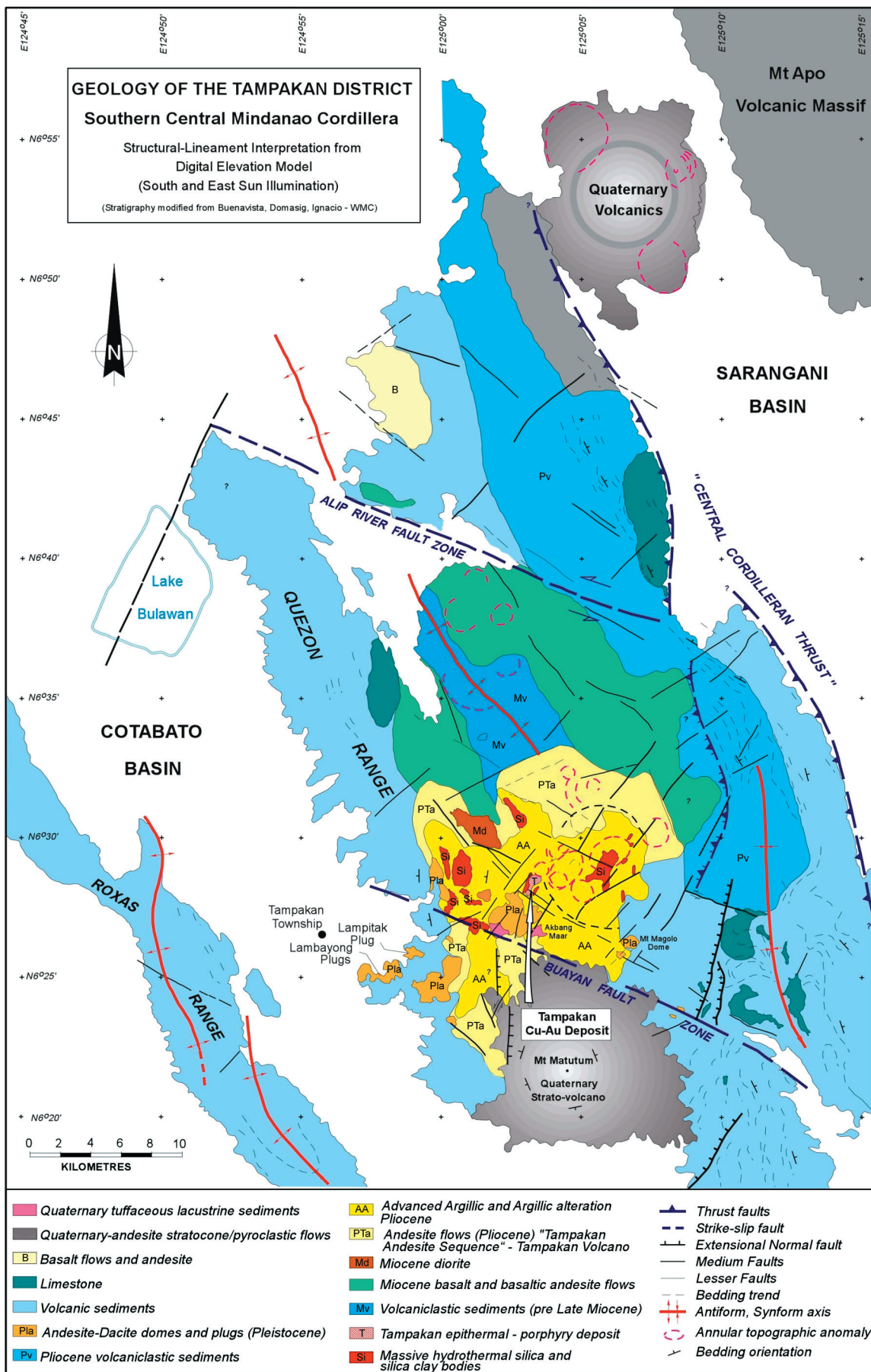


Figure 7: Geology of the Tampakan district, southern Mindanao.

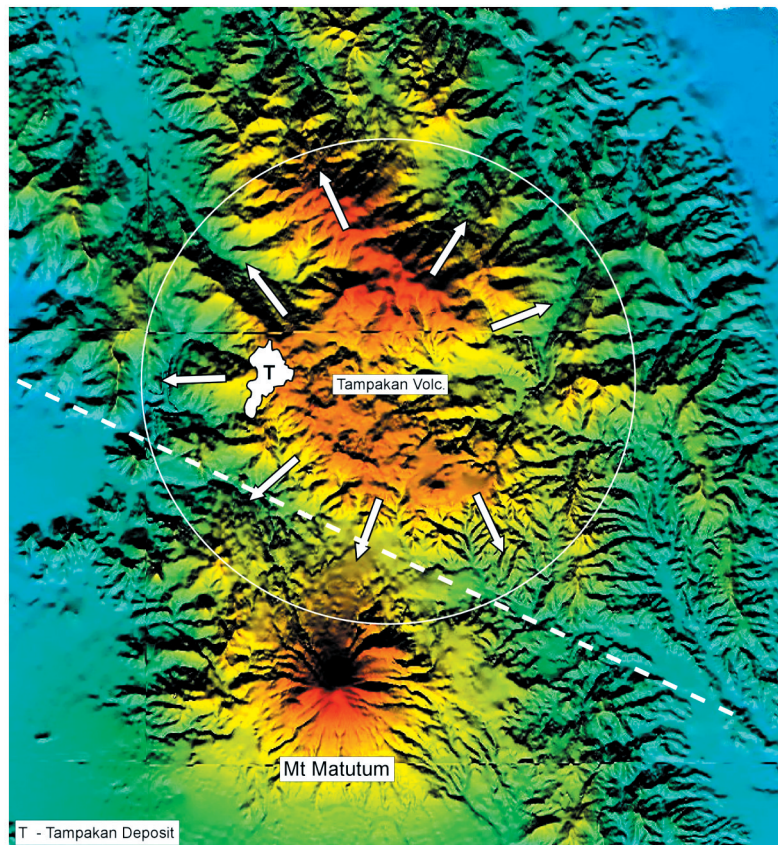


Figure 8: Digital terrain model of the Tampakan district enhanced by a digital illumination from the south. The Tampakan deposit (T) is located on the western rim of a deeply eroded mid-Pliocene-age andesitic stratovolcano.

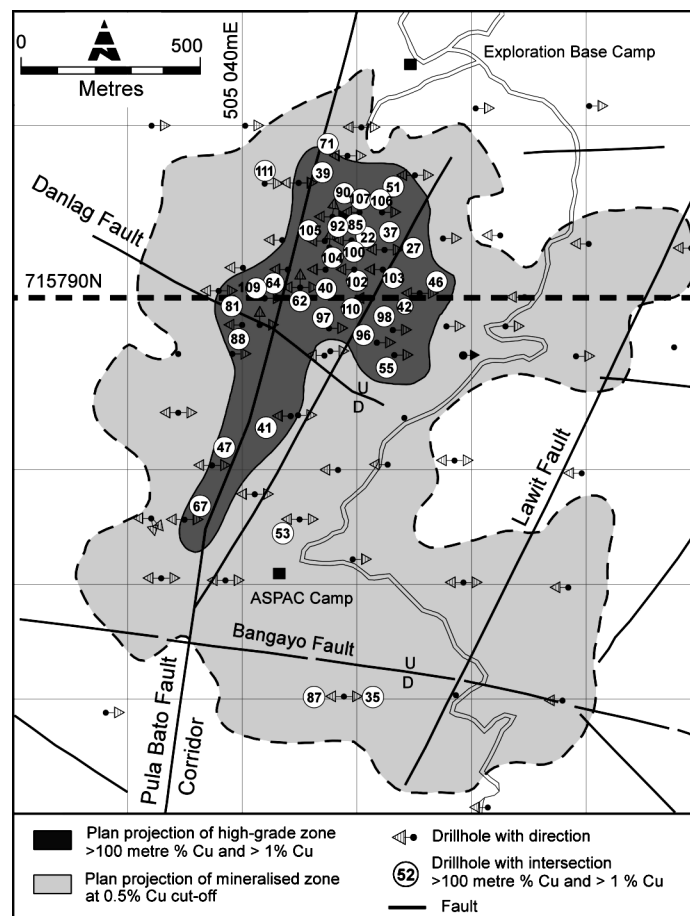


Figure 9. Plan of the projected outline of mineralisation above a cut-off of 100 metres at 1.0 % Cu. The location of cross-section 715790 mN (Figs. 10a, b and 11) is shown. Diagram is modified from Middleton *et al.*, (2004).

mid-Pliocene age. They comprise porphyritic hornblende-pyroxene andesite and silicic andesite flows that dip at 10 to 20° towards the WSW, sub-parallel to the mineralised lithocap in the deposit. Hornblende-diorite porphyry stocks intrude the Tampakan Andesite Sequence in the deposit environs. They vary from holocrystalline and equigranular to crowded-porphyry-textured intrusives with 70 to 80% phenocrysts. The intrusives form apophysis-like dykes and stocks, and tend to be altered but weakly mineralised.

High-sulphidation mineralisation displays both structural and stratigraphic controls. The Pula Bato Fault Zone comprises a NNE-trending series of faults that transect the Pliocene volcanic edifice and lie along the long-dimension of the Tampakan orebody. High-sulphidation mineralisation pinches downward along the NNE-trending Pula Bato Fault Zone, and mushrooms upward into a broad, manto-like, stratabound zone of advanced-argillic alteration that encapsulates the central zones of high-sulphidation ore. Detailed mapping of alteration assemblages using mineral infra-red spectra collected using a portable spectrometer (PIMA II; Rohrlach 2002) locally defines upward-flaring zones of advanced-argillic alteration that 'flower' into semi-concordance with stratigraphy at shallow levels. This geometry suggests the existence of structurally-rooted feeder faults with steep marginal alteration zones that flare at shallow levels where the faults intersect high-level zones of stratigraphic permeability. A detailed review of alteration textures within the deposit is presented in Rohrlach *et al.*, (1999).

The uppermost zone of hydrothermal alteration at Tampakan comprises argillic-altered porphyritic andesites (Fig. 10b) that overlie patchy zones of massive hydrothermal silica in the upper portions of the manto (Fig. 10a). The textures of the silica bodies include massive hydrothermal silica, multi-cycle silicified hydrothermal breccias, phenocrystic vuggy silica and clotted vuggy silica (Rohrlach *et al.*, 1999). Mineralisation within the silica bodies is typically fracture-controlled and comprises vug-filling sulphides, plus sulphides in hydrofractures, stringer veins and breccia veins. Common sulphide assemblages include i). bornite + digenite + enargite ± pyrite/tetrahedrite/molybdenite, ii). bornite + chalcocopyrite + pyrite, and iii). late-stage pyrite + covellite. The silica bodies lie along the upper portion of the manto and are underlain by extensive domains of 'silica-clay' (50 to 90% free silica; Fig. 10a) and 'clay-silica' (10 to 50% free silica; Fig. 10a) that correspond to pyrophyllite + dickite and pyrophyllite + dickite + diaspore alteration assemblages (Fig. 10b). The close proximity of diaspore-bearing alteration zones immediately below zones of massive silica (Fig. 10b) reflect their high degree of acid leaching at shallower levels in the hydrologic system.

The massive silica bodies and the diaspore-bearing alteration zones 'collectively' define a nearly flat-lying blanket on section 715790 mN (Fig. 10b), although this zone of most intense acid-leaching has an overall gentle dip to the southwest across the orebody. Alunite is present in the advanced-argillic alteration zone, although it is rare due to the relatively low potassium content of the andesitic

precursor lithologies. Mineralisation becomes increasingly disseminated at deeper levels in the clay-silica alteration zones. The textures that are present in the pyrophyllite-, dickite- and diaspore-bearing zones of silica-clay alteration include massive silica-clay, porphyritic silica-clay and clotted silica-clay. These are described in detail by Rohrlach *et al.*, (1999) and are depicted in photographic plates in Rohrlach (2002) and Middleton *et al.*, (2004). The zone of higher-grade high-sulphidation mineralisation on section 715790 mN (>1.0% Cu) forms a blanket that is approximately 50 to 150 metres thick (Fig. 11) and coincides with the broad zone of silica-clay alteration. It overlies lower-grade mineralisation at depth that is associated with porphyry Cu ore that formed during a prior mineralising event. Sericitic alteration becomes increasingly prominent at deeper levels in the deposit. Shallow areas of pyrophyllite-dickite-sericite alteration are transitional to deeper zones of sericitic alteration that in turn are transitional downward to sericite-chlorite alteration.

The alteration textures within the advanced-argillic lithocap reflect upward-intensifying degrees of acid-leaching and silicification. The vertical increase in acidity of hydrothermal fluids progressively transformed pre-existing potassic and propylitic alteration assemblages to sericite-chlorite- and phyllic-altered andesite with good textural preservation. At shallower levels, increased intensity and duration of acidic alteration resulted in complete cation leaching to produce massive homogeneous silicified rock above several fluid conduits (Rohrlach *et al.*, 1999). The vertical zonation in alteration textures and mineralogy through the lithocap is produced by progressively increasing hydrolysis of magmatic SO₂ to H₂S and H₂SO₄ and subsequent, lower-temperature dissociation of H₂SO₄ to yield H⁺ ions in solution. These reactions progress to greater degrees at lower temperatures (Rye *et al.*, 1992). Mixing with oxidising meteoric ground water at shallower levels oxidised some H₂S to H₂SO₄, further acidifying the fluids. Together, these sources of sulphuric acid account for the increasing degree of acid-leaching and residual silica enrichment at high levels.

High-sulphidation mineralisation is characterised by pyrite, bornite, enargite and digenite, with lesser chalcocite, chalcocopyrite, covellite and molybdenite. Although the high-sulphidation-stage veins display variable mineralogy, there are several common sulphide associations that define broad stages of evolution from high-temperature hypogene assemblages to increasingly oxidised, low-temperature hypogene assemblages.

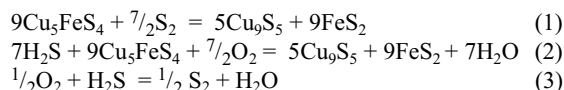
Stage 1: Pyrite+Bornite+Enargite ± Chalcocopyrite ± Molybdenite

The earliest recognised stage of mineralisation comprises pyrite+bornite+enargite ± chalcocopyrite ± molybdenite. An accessory sulphide assemblage occurs as microscopic blebs within bornite, and is characterised by a volatile element suite of Sn, V, Te and Sb. Colusite is a Cu-Sn-V-As-Fe sulphide that occurs with mawsonite (Cu-Fe-Sn sulphide) and goldfieldite (Te-bearing tetrahedrite) as fine anhedral inclusions within bornite.

Stage 2: Digenite+Chalcocite - High Temperature Oxidation.

Digenite is abundant within the high-sulphidation deposit and occurs as an alteration product of precursor Stage 1 bornite. Digenite forms replacement masses that marginally replace and envelop Stage 1 sulphides. Light grey paramorphic or lamellar chalcocite is ubiquitous as an exsolution product from digenite. Both bornite and locally pyrite are unstable during the conversion of bornite to digenite; however the other sulphide phases of Stage 1 (chalcopyrite, enargite, colusite, mawsonite and goldfieldite) are texturally stable during the transformation. The alteration of

bornite to digenite may involve the sulphidation reaction (1) and/or the oxidation reaction (2).



Increasing oxidation of an early high-sulphidation assemblage (Stage 1) by the downward encroachment of the mixing interface between cool oxidised surface waters and dense ascending magmatic vapours, as the hydrothermal system wanes, may result in increasing $f\text{O}_2$ and production of S_2 (3) in the H_2S stability field, both of which drive reactions (2) and (1) towards conversion of bornite to digenite.

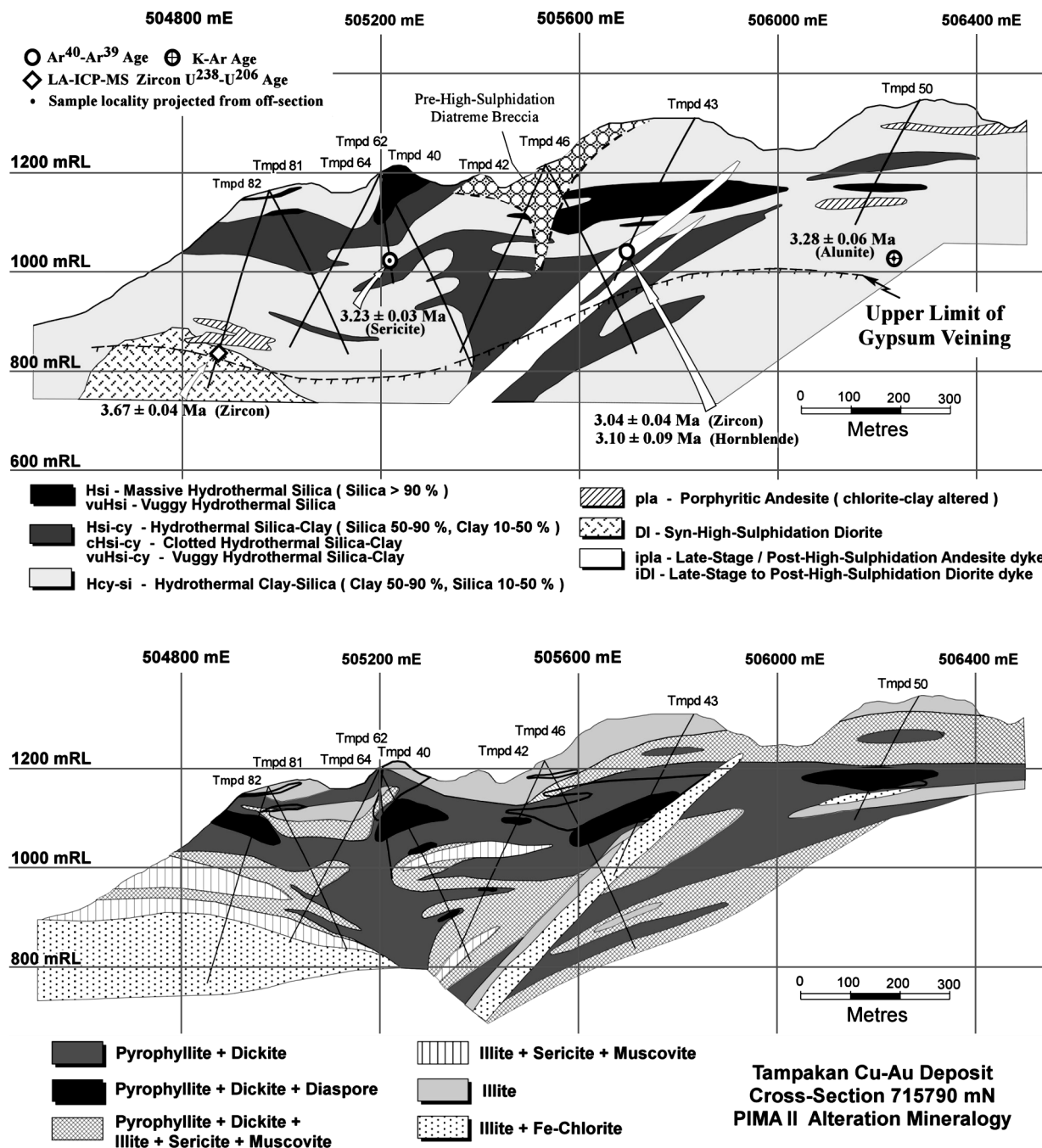


Figure 10: (a, top) Representative geological cross-section 715790 mN through the Tampakan deposit, and (b, bottom) alteration zonation on section 715790 mN defined from 1160 mineral infra-red spectra acquired by a PIMA II portable spectrometer. Additional alteration cross-sections generated from acquisition of PIMA II infra-red data are sourced in Rohrlach (2002). Alteration assemblages on both diagrams above show an upward mushrooming morphology that is centered on the Pula Bato Fault corridor shown in Fig. 9.

Stage 3: Pyrite+Covellite Veins

Late-stage pyrite+covellite veins are widespread within the upper portions of the lithocap, and overprint earlier sulphide assemblages. Paragenetically late alunite 'crackle veins' are commonly covellite-bearing. The alunite-covellite-pyrite assemblage reflects an increase in the oxidation state of the fluids as they cooled by mixing with shallow ground water, and reflects the transition to increasingly sulphate-dominated fluids as H₂S within the hydrothermal fluid was progressively oxidised.

Stage 4: Covellite+Idaite - Low Temperature Supergene Oxidation

Both covellite and idaite are widespread in the uppermost and oxidised portions of the lithocap, and in areas where further oxidation of pyrite and chalcopryrite produce low temperature Fe-oxide assemblages. Idaite commonly forms as an alteration product of chalcopryrite while digenite and chalcocite alter to covellite.

Stage 5: Supergene Gypsum ± Covellite Veins

Late-stage fibrous gypsum veins consistently overprint all high-sulphidation-related clay veins. They are pervasive in the sericite-chlorite alteration zone and in the underlying relict potassic alteration zones, but are absent in the upper portions of the advanced-argillic zone. Their distribution at depth is restricted to below a sharp sub-horizontal transition zone, typically less than a metre wide, above which the advanced-argillic sequence is highly friable and lacks gypsum, and below which the rock is compact and heavily impregnated by gypsum (Fig. 10a). We interpret this boundary to have formed as a downward-migrating sulphate-saturation

front, whereby cool descending meteoric waters dissolved sulphate from the advanced-argillic alteration blanket at shallow levels and re-precipitated sulphate as low-temperature gypsum veins at depth. A subset of gypsum veins contain minute flecks of covellite, suggesting that they precipitated from low-temperature oxidised fluids.

The transition in sulphide assemblages from Stage 1 through to Stage 5 records a continuum from high-temperature hypogene mineralisation, to high- and medium-temperature hypogene oxidation and finally to lower temperature oxidation and supergene weathering. The primary high-sulphidation assemblage of bornite + enargite + pyrite + chalcopryrite underwent continuous compositional adjustment as the hydrothermal system waned.

Isotopic and fluid inclusion evidence for fluid mixing between a vapour-rich two-phase magmatic fluid and meteoric waters at the base of the hydrostatically-pressured rock column within the volcanic edifice, and subsequent radial outflow of the hybrid fluids along a palaeo-aquifer on the western flank of the Tampakan volcanic complex, is discussed in the palaeohydrological study of Rohrlach (2002). The P-T-enthalpy-salinity-density coordinates for the high-sulphidation-stage magmatic fluids were calculated by Rohrlach (2002) for the site of two-phase magmatic fluid exsolution (~900°C, ~800 bars, >99% vapour with ~4.4 wt.% NaCl equiv.); immediately below the lithostatic-hydrostatic interface (two-phase fluid, ~500°C, P_{Lith} ≅ 550 b, 96.9% vapour that holds 85% of the systems Cl); immediately above the lithostatic-hydrostatic interface (two-phase fluid, ~375°C, P_{Hyd} ≅ 200 b, 61.7% vapour that holds 4% of the systems Cl after decompression); and at points along the mixing path in the

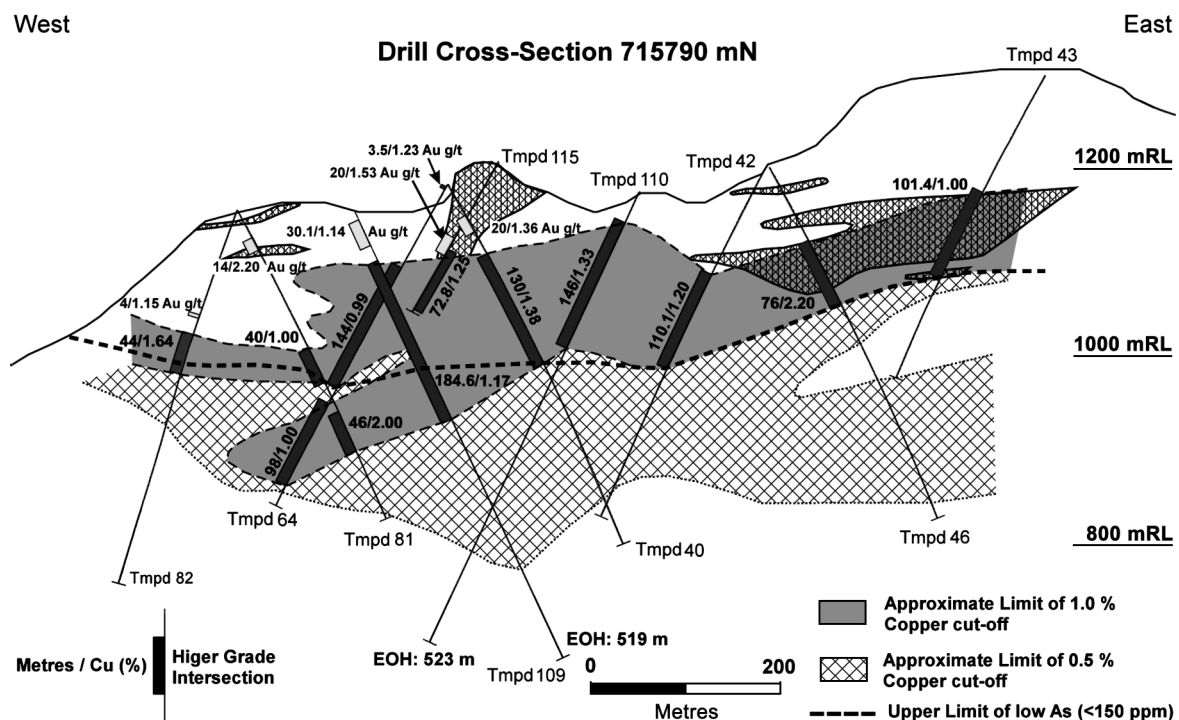


Figure 11: Significant assay intersections on section 715790 mN (modified from Middleton *et al.*, 2004). The zones of massive silica alteration are depicted by the tight cross-hachure pattern at shallow levels across the manto. Additional assay cross-sections through the deposit are presented in Middleton *et al.*, (2004).

hydrostatic domain (375-100°C, P_{Sat}) (Rohrlach *et al.*, 2003). The high-sulphidation-stage magmatic vapour rapidly condensed during isenthalpic decompression at the lithostatic-hydrostatic interface and cooled instantaneously from ~500 to 375°C. The condensed vapour was modestly saline (~5 wt.% NaCl) and mixed with meteoric water at a constrained depth of ~2 km. Most of the exsolved magmatic chloride (~81 to 85%, and metal) was transported through the ductile rock column to the site of ore deposition by a dense vapour phase.

Porphyry-Cu Mineralisation

Porphyry Cu-Au mineralisation is widespread in the lower part of most drill-holes that penetrate below the high-sulphidation mineralisation into the zone of sericite-chlorite alteration. The principal sulphide and oxide minerals in equilibrium with porphyry-stage anhydrite-biotite-alteration are chalcopyrite, bornite, pyrite, magnetite (up to 8%), subordinate specular hematite and molybdenite. Porphyry-Cu mineralisation is dominated by pink-grey coloured, multi-directional, crudely laminated veins with medial crack-seal textures that contain traces of bornite and/or chalcopyrite and/or pyrite. Anhydrite-bearing veins are less prevalent. Chalcopyrite is the dominant sulphide and occurs as disseminated grains, as anhedral inclusions within and along the margins of hydrothermal magnetite grains, and as elongate laths that extend along cleavage planes of hydrothermal biotite grains. Bornite is subordinate to chalcopyrite, and both these sulphides are always in textural equilibrium, often forming composite sulphide grains. Molybdenite and hematite are minor phases in the potassic alteration zone. Porphyry-stage sulphides also occur as fracture-controlled disseminations within the wallrock to quartz-dominated and lesser anhydrite-bearing veins.

The porphyry sulphide assemblage lacks the association of enargite/digenite/chalcocite/covellite that is typical of the overprinting high-sulphidation epithermal mineralisation. The chalcopyrite+bornite+pyrite mineral association occurs within the sericite+chlorite alteration zone and areas of relict potassic alteration in the deepest drill tested portions of the deposit. At higher levels within the phyllic and lower advanced-argillic facies, the porphyry quartz veins are grey-coloured and bleached as they become over-printed by acidic conditions of the significantly younger advanced-argillic lithocap. Porphyry quartz veins are *only* observed in the lower portion of the lithocap below an unconformity between magmatic cycles 3 and 4a that unroofed the porphyry system prior to high-sulphidation mineralisation (see 'Geochronology' below). Specular hematite is more abundant within the outer sericite+chlorite alteration facies than in the inner potassic biotite-anhydrite-magnetite zone. The presence of hypogene hematite – locally replaced by chalcopyrite – may reflect more oxidised conditions at shallower levels where Cp+Py+Hem (\pm Mt \pm Bn) occurs in preference to Cp+Py+Mt (\pm Bn) in the porphyry-stage ore.

Geochronology

Forty-four radiometric ages from 28 representative lavas, intrusive plugs and dykes from the Tampakan volcanic complex, and limestones from the surrounding district, were dated by either ^{40}Ar - ^{39}Ar step-heating, K-Ar total fusion, zircon ^{238}U - ^{206}Pb by excimer laser-ablation ICP-MS, or by correlation of limestone $^{87}\text{Sr}/^{86}\text{Sr}$ with the secular variation of $^{87}\text{Sr}/^{86}\text{Sr}$ in Neogene seawater as given by Hodell *et al.*, (1990). Only a brief summary of dating results can be presented here; see Rohrlach (2002) for a detailed account of methods and results. ^{238}U - ^{206}Pb ages were also obtained

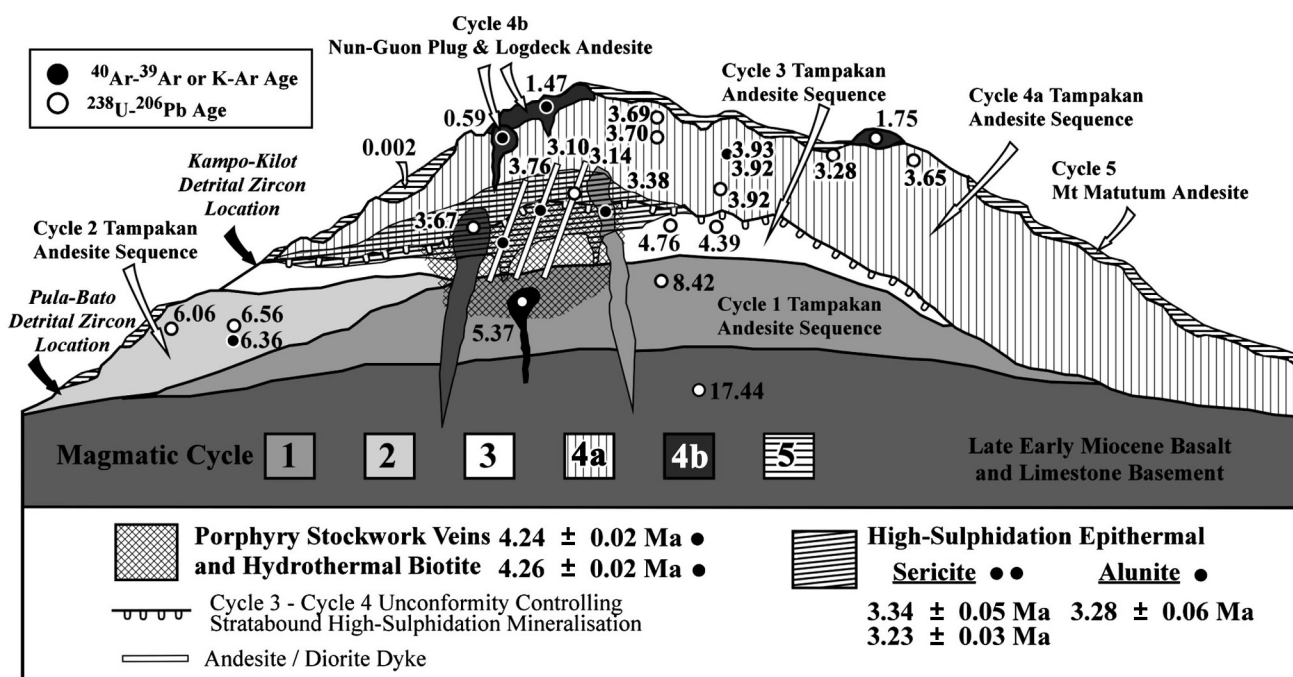


Figure 12: Schematic east-west profile looking north through the Tampakan igneous complex and showing the age relationship of magmatic and hydrothermal events. Ages obtained for magmatic sequences are shown on the diagram, whereas ages obtained for the alteration minerals are shown in the legend. Porphyry mineralisation was exposed at the surface during the early Pliocene by an erosional unconformity that separates Cycle 3 from Cycle 4a magmatism. High-sulphidation mineralisation was localised along this unconformity during the latter part of Cycle 4a magmatism and stratocone rebuilding.

by laser ablation ICP-MS for two suites of detrital zircons that were eroded from the western flank of the Tampakan volcanic complex. The age dating constrains stages of uplift, erosion, sedimentation, folding and faulting, and tightly constrains the duration and the timing of petrochemical evolution of the Tampakan magmatic system and the timing of porphyry Cu and high-sulphidation Cu-Au mineralisation. Two sets of detrital zircons from streams that drain the western flank of the volcanic centre at Pula Bato and Camp Kilot (Fig. 12) yielded 144 representative detrital zircon ages by ELA-ICP-MS. The frequency of detrital zircon ages reveals a long history of zircon crystallisation, and hence magmatic activity that extended from 7.29 Ma to the Holocene. Four episodes of profuse magmatic/volcanic activity (Fig. 13) are defined by peaks in age frequency that extend from ~7 to 6 Ma (late Miocene cluster), 5.3 to 4.1 Ma (Early Pliocene cluster), 3.6 to 2.5 Ma (Middle Pliocene cluster) and 0.3 Ma to the present (Late Quaternary cluster) (Fig. 13). The whole-rock igneous and volcanic rock ages from the Tampakan district coincide with the three early peaks in detrital zircon ages, and corroborate three principal episodes of volcanism that erupted during the Late Miocene, Early Pliocene, and Middle Pliocene.

Volcanic History

Geochronologic studies reveal that the Tampakan district has experienced frequent and extensive magmatic activity over the past 8.5 M.y. An episodic and long-lived succession of andesitic stratovolcano-building events extended from the late Miocene to present, and are separated by erosional unconformities. These episodes of volcanism and magmatism are here termed magmatic Cycles 1 to 5. Cycles 2, 3, 4a and 5 were major stratocone-building events.

The oldest dated rocks in the Tampakan district are limestones that are intercalated with porphyritic augite-phyric basaltic andesites that underlie the Tampakan volcanic complex. The $^{87}\text{Sr}/^{86}\text{Sr}$ of a reefal limestone unit sampled from the southeast side of Mt Matutum indicates an upper early Miocene age of 17 Ma (Fig. 12). The intercalated basement basalts are folded about a broad NNW-trending anticline, so the limestone age places a lower age limit on folding within the district. The oldest dated andesite that erupted onto this basement has an age of 8.34 ± 0.32 Ma obtained by ^{238}U - ^{206}Pb on zircons from an andesite unit near the base of drill-hole Tmpd 8, deep in the Tampakan porphyry deposit. This event is not represented in the detrital zircon dates, which suggests that the sequence is not exposed on the western flank of the volcanic centre. A 7 to 6 Ma basaltic-andesite to andesite sequence is well represented in detrital zircon populations (Figs. 12 and 13). This age cluster is also represented by two ^{238}U - ^{206}Pb zircon ages of 6.06 ± 0.04 Ma and 6.56 ± 0.05 Ma, and a ^{40}Ar - ^{39}Ar age of 6.36 ± 0.05 Ma, which were taken from outcrops of lavas at low elevations along the northwest and southwest flank of the volcanic centre. They lie deep in the Tampakan volcanic pile and belong to Cycle 2 magmatism (Fig. 12). They form part of an underlying and deeply eroded volcanic centre that developed in the late Miocene. Andesites of this age have not been identified in dated samples from drill-holes in the

Tampakan orebody, despite the occurrence of older and younger cycles in the deposit. Cycle 2 volcanics may have been completely eroded down to the Cycle 1 substrate below the Tampakan deposit, where they occurred at higher elevations of the volcanic complex.

The Cycle 1 sequence in the lowermost part of drill-hole Tmpd 8 is intruded by a diorite stock dated by ^{238}U - ^{206}Pb (zircon) at 5.3 ± 0.3 Ma (Figs. 12 and 13). The stock is overprinted by porphyry-ore-stage quartz veins associated with disseminated biotite-chlorite-anhydrite alteration. This age correlates with the onset of a second, albeit subdued, rise in age frequency of detrital zircons (Fig. 13), which extends from ~5.3 to 4.1 Ma. Two ^{238}U - ^{206}Pb (zircon) ages of 4.39 ± 0.08 Ma and 4.76 ± 0.06 Ma were obtained from andesites collected from the deeper portions of drill-holes Tmpd 34 and 87. These pre-mineralisation lavas host porphyry-Cu-stage quartz veins, and belong to an early Pliocene, Cycle 3 magmatic event that erupted during a third phase of volcanic edifice construction extending from ~5.3 to 4.1 Ma (Fig. 13), following substantial erosion of the underlying Cycle 2 volcanic edifice (Fig. 12).

Cycle 4 units of the Tampakan Andesite Sequence are extensively dated. They define a middle Pliocene stage of stratocone construction (Cycle 4a) and a late Pliocene to Pleistocene stage of evolved andesitic to dacitic intrusives and volcanic plugs (Cycle 4b). Cycle 4a andesite lavas occur in the upper portion of the drill-holes in the deposit and host high-sulphidation mineralisation and associated advanced-argillic alteration but *lack porphyry-stage quartz veins*. The andesite lavas in drill-holes Tmpd 13 and 33, surface exposures of andesite on the Tampakan drill grid, and numerous high-elevation outcrops in the district are dated as middle Pliocene age and belong to the Cycle 4a andesitic stratocone that is recognisable in the DTM image (Fig. 8). These flows are intruded by dykes and stocks of pre-, syn- and post-high-sulphidation age. The age distribution of rocks dated from the Cycle 4a sequence is broadly coeval with the third peak in frequency of detrital zircons (Fig. 13). Cycle 4b magmatism is represented in the detrital zircon dataset by a minor cluster of 3 detrital zircon ages between 1.8 and 1.3 Ma (Fig. 13). The paucity in ages is consistent with their isolated and scattered outcrop distribution, comprising small, evolved andesitic to dacitic intrusive plugs and extrusive flow-dome complexes located around the southern and southwestern quadrant of the volcanic centre. The Logdeck Andesite, which overlies the southern part of the Tampakan orebody, yielded an age of 1.47 ± 0.05 Ma by ^{40}Ar - ^{39}Ar . A hornblende-bearing andesite in the southeast quadrant of the Cycle 4a Tampakan volcanic edifice contained zircons dated at 1.75 ± 0.16 Ma. A K-Ar age of 1.47 Ma was obtained for the Lote Plug, and a K-Ar age of 0.86 Ma was determined for the Lambayong volcanic plug (Sajona, 1994). The Nun-Guon plug was dated as 0.59 ± 0.03 Ma by ^{40}Ar - ^{39}Ar and as 0.59 ± 0.02 Ma by K-Ar. Cycle 4b dacites of Pleistocene age mark a transition to dacitic magmatism. They are widely distributed and do not form a major stratovolcanic edifice in the manner of magmatic Cycle 4a. The youngest magmatic event recorded by the detrital zircon ^{238}U - ^{206}Pb data is the pyroclastic cover sequence that erupted onto the

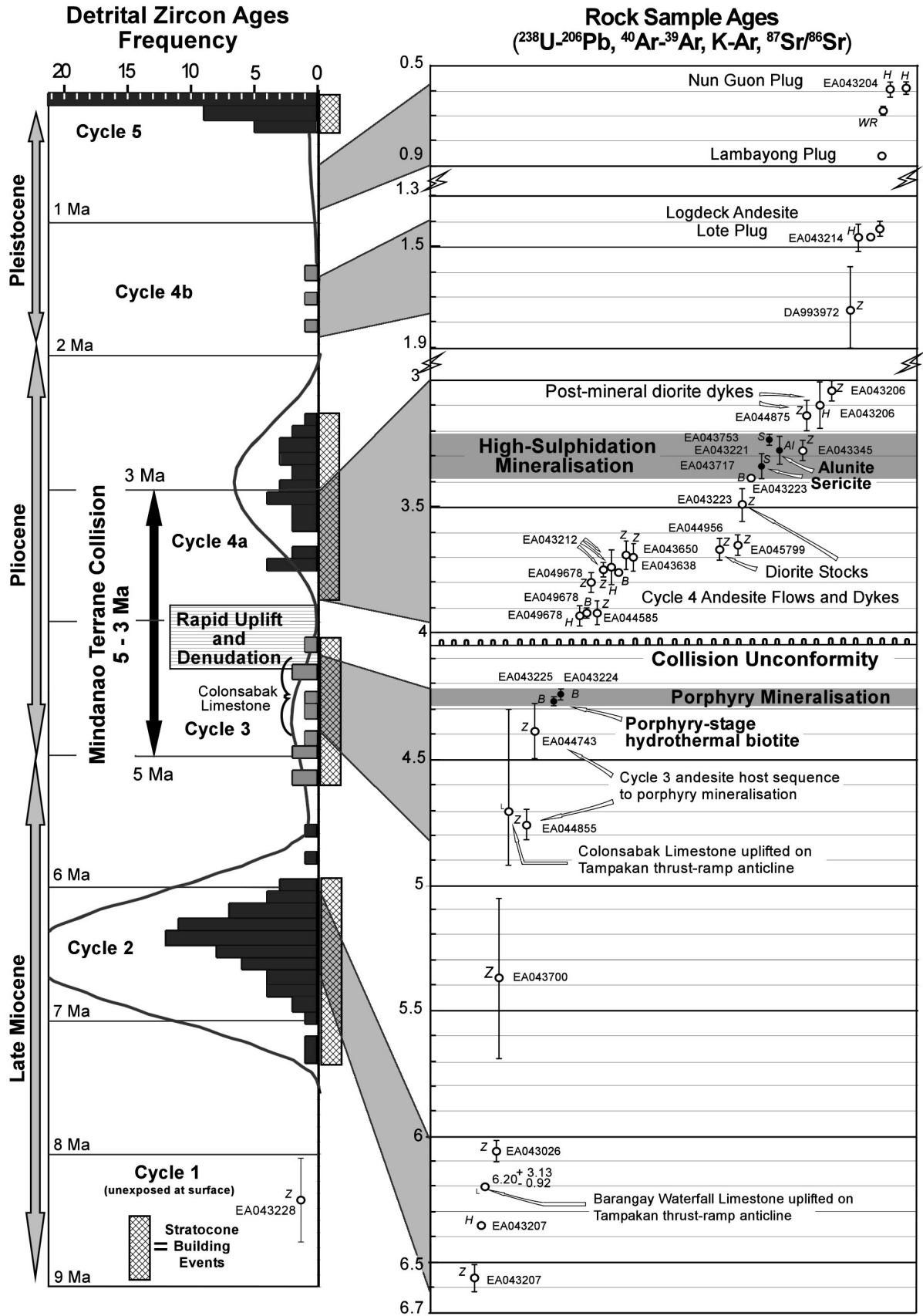


Figure 13: Time sequence of volcanic and intrusive magmatic rocks in the Tampakan district, illustrating the principal stratocone-building events and erosional unconformities. Ages of detrital zircon grains collected from the west flank of the volcanic complex are shown on the left panel and define four peaks of magmatic activity. Corresponding rock ages are shown on the right-hand side. Abbreviations: Z = zircon ²³⁸U-²⁰⁶Pb age; H, B, S = hornblende, biotite and sericite ⁴⁰Ar-³⁹Ar age; L = limestone ⁸⁷Sr/⁸⁶Sr age; Al = alunite K-Ar age, and WR = whole-rock K-Ar age.

incised Tampakan volcanic edifice from the overlapping Mt Matutum stratocone, the youngest volcano in the complex, which was constructed during the last 300 Ka.

Ages of Mineralisation

Porphyry mineralisation is dated by ^{40}Ar - ^{39}Ar ages on two samples of hydrothermal biotite from a relict potassic alteration facies near the base of drill-hole Tmpd 8. Two concordant ages of 4.24 ± 0.02 Ma and 4.26 ± 0.02 Ma indicate that porphyry mineralisation occurred near the end of magmatic Cycle 3. These ages post-date Cycles 1 and 3 dates for rocks that host the lower portions of the porphyry Cu deposit. The hydrothermal biotite dates are minimum ages, as they record the time at which biotite cooled below its closure temperature for argon loss. Nevertheless, the true age of porphyry mineralisation must lie between the 4.25 Ma average date of the biotite samples and the 4.39 Ma date for the youngest Cycle 3 andesite sample that hosts porphyry veins.

The high-sulphidation mineralisation event is constrained by three concordant K-Ar and ^{40}Ar - ^{39}Ar ages obtained from hydrothermal alunite and sericite. The alunite was extracted from covellite+pyrite-bearing veins and has an age of 3.28 ± 0.06 Ma. This is concordant with two ^{40}Ar - ^{39}Ar ages of 3.34 ± 0.05 and 3.23 ± 0.03 Ma obtained from hydrothermal sericite within the advanced-argillic lithocap. Thus the age of high-sulphidation mineralisation is constrained to lie between 3.39 and 3.20 Ma at the level of one standard-deviation uncertainty of the ages. These ages are consistent with the 3.93 ± 0.04 Ma to 3.69 ± 0.06 Ma age range of Cycle 4a andesite flow units in the upper portions of the Tampakan deposit that are altered by the high-sulphidation event, and with the 3.14 ± 0.06 Ma and 3.04 ± 0.04 Ma age of two weakly altered, post-mineralisation andesite and diorite dykes that post-date acid-sulphate alteration (Fig. 13).

The difference between the mean age of the two porphyry-stage biotite samples (4.25 ± 0.01 Ma) and the mean age of the three high-sulphidation-stage sericite and alunite ages (3.26 ± 0.02 Ma) is a million years. This interval is significantly greater than the possible lifespan of a major porphyry system (Cathles *et al.*, 1997). The Lepanto high-sulphidation epithermal and Far Southeast porphyry deposit "pair" are associated with a hydrothermal system of ~300 000 years duration (Arribas *et al.*, 1995), and the Ladolam deposit evolved from a porphyry to epithermal environment over a similar duration of ~300 000 years (Moyle *et al.*, 1990). The Tampakan porphyry and high-sulphidation epithermal deposits formed from separate magmatic-hydrothermal systems, and although they are not products of the same high-level volcano-scale hydrothermal system, they are related in the context of a consanguineous succession of igneous intrusions from the same deep lower-crustal magmatic reservoir (see the 'Petrochemistry, Magma Mixing and Volatile Ramping' and 'Magmatic Physico-Chemical Properties' sections below).

Constraints on Uplift and Unroofing

Cycle 4a eruptive units dated at between 3.93 and 3.69 Ma lack porphyry-stage quartz veins but host high-sulphidation

mineralisation and alteration, and lie directly on Cycle 3 and Cycle 1 andesites which host porphyry-stage quartz veins associated with hydrothermal biotite of 4.26 to 4.24 Ma in age. These geochronological data and the contrasting depth regimes of the two mineralisation types reveal the presence of a major unconformity representing kilometre-scale erosional loss between preserved units of eruptive Cycles 3 and 4a. The unconformity has not been identified texturally in drill-core due to the extensive acid-sulphate alteration, silicification and hydrothermal brecciation, suggesting the unconformity may have served as an aquifer for palaeo-ground-water flow, which ascending magmatic volatiles condensed to form the stratabound high-sulphidation system. This unconformity is responsible for unroofing the porphyry system to depths near the outer edges of its potassically-altered core in the time frame between hydrothermal biotite alteration at 4.24 to 4.26 Ma (or ~50 K.y. prior, to allow for cooling of hydrothermal biotite through its closure temperature) and the commencement of eruption of Cycle 4a andesites at 3.93 Ma. Some 2 km or more of overburden must have been eroded from above the Tampakan porphyry system within a time-frame of ~370 K.y. An anomalously high erosion rate of 5.4 mm/year over a 370 K.y. time frame is required to remove ~2 km of overburden from above the lithostatically-pressured porphyry veins. The long-term average erosion rate for the Tampakan volcanic centre between 3 Ma and the present, based on reconstruction of volcanic topography, is 0.75 mm/year – identical to the estimate by Ruxton and McDougall (1967) for long-term erosion of a similar stratovolcano in nearly identical climatic conditions in New Guinea. The geochronologically constrained rate of erosion for the Tampakan Cycle 3 sequence between 4.30 Ma and 3.93 Ma (assuming ~2 km of unroofing), prior to eruption of the Cycle 4a sequence on the unroofed porphyry system, implies catastrophic landslides and/or volcanic sector collapse during the pulse of rapid uplift associated with thrust-and-fold deformation of early Pliocene age. Crustal compression, collision-stage thrust faulting and attendant uplift were in maximum effect in the time interval during porphyry and younger high sulphidation mineralisation at Tampakan. The erosional unconformity between Cycles 3 and 4a magmatism became an important control on the distribution of younger high-sulphidation mineralisation within the deposit.

Petrochemistry

In the Tampakan district, volcanic and hypabyssal intrusive rocks comprise porphyritic basaltic andesites, andesites, silicic andesites and dacites that record magmatic evolution processes during an arc-arc-collision event that generated the world-class Cu-Au ore system. The time series of chemical variations from basaltic andesite to dacite define multiple cycles of magmatic differentiation in lower-crustal and sub-volcanic magma chambers that fed a succession of overlapping volcanic centres that developed during the late Miocene to Recent epochs. They are highly oxidised calc-alkaline magmas having petrochemical features typical of subduction-generated arc magmas, such as relative enrichment in the large-ion-lithophile elements Cs, Rb, Ba,

U, K, Pb and Sr due to transport of these fluid-mobile elements from the slab into the source region of the melts. They also exhibit typical arc-type relative depletions in the high-field-strength elements Nb, Ta and Ti. Pliocene-Pleistocene members of the suite display petrochemical signatures atypical of felsic arc magmas, such as high abundances of Sr and Eu and exceptional depletions of Y and heavy REE's that are explicable by protracted fractionation of magmas in the lower crust under high pressure and high magmatic water activity. The principal petrographic distinction of the Tampakan igneous suite is the high abundance of hydrous minerals such as hornblende and biotite in basaltic andesites as well as in more evolved andesites, silicic andesites and dacites. The hydrous mineral phases become modally more abundant over time. The post-middle-Miocene magmatic rocks evolved from ordinary augite-bearing basaltic andesites that lack hydrous phenocryst phases in the latest Miocene, to augite-hornblende andesites in the early Pliocene, to a predominance of pyroxene-free, hornblende- and biotite-bearing silicic andesites in the middle Pliocene and Pleistocene. During the tectonic collision that affected the Tampakan district, there was a progressive increase in the modal abundance of hydrous mineral phases in erupted magmas, a decrease in the modal abundance of anhydrous mineral phases, and an appearance of the hydrous mineral phases, hornblende and biotite, at successively earlier (less silicic) stages of the crystallisation sequence.

Along-Arc Variations in Mineralogy

Analyses of magmatic rocks from the succession of igneous complexes along the Sangihe arc allow investigation of the petrologic and petrochemical variations, from south to north, in the context of their pre-, syn- and post-collision tectonic settings. The increase in modal abundance of hydrous mineral species that are observed in the Tampakan segment of the Sangihe arc during the ~0-6 Ma period of arc compression is also reflected in along-arc variations of

the proportion of rocks with hydrous phenocryst phases. Pre-collision magmatism associated with active subduction currently occurs off the northern portion of Sulawesi in the southern Molucca Sea between 0 and 4°N. A presently active collision zone occurs in the northern Molucca Sea between 4 and 6°N where magmatism is sparse compared to the pre-collisional areas farther south. Late Neogene magmatism associated with early- to syn-collision and slab stalling occurs in southeastern and central Mindanao (6 to 9°N) in the Tampakan and Mt Apo districts, whereas Plio-Pleistocene post-collisional magmatism occurs in northern Mindanao and further northward to Camiguin Island (~9.2°N). Igneous petrochemical data were compiled from this extensive section of the Sangihe arc along which the southward-propagating collision zone has migrated during the Late Neogene and Quaternary. Data compiled from Corpuz, (1992), Castillo *et al.*, (1999), Elburg and Foden, (1998), Morrice *et al.*, (1983), Polve *et al.*, (1997), Prouteau *et al.*, (2000), Sajona *et al.*, (1994, 1997, 2000) and Tatsumi *et al.*, (1991) span ~8.3 degrees of latitude (0.9 to 9.2°N; ~960 km) along the arc. There is a latitude-dependant variation in the degree of differentiation of young (<5 Ma) igneous rock types. The Tampakan district contains the highest proportion of evolved magmatic rocks, with ≥ 60% SiO₂, compared to arc segments farther north and south. Rocks from the neighbouring Mt Apo district north of Tampakan also have a high proportion of evolved andesites and dacites, reflecting advanced magmatic differentiation. These districts are the only two that contain syn-collisional to recent post-collisional magmatism. The northern Molucca Sea (4 to 6°N) is currently undergoing collision, but the paucity of subaerial magmatism in this latitude interval precludes statistically reliable petrological comparison with the Tampakan and Mt Apo districts.

Fig. 14 illustrates regional systematic trends in the proportion of rocks containing olivine, orthopyroxene, clinopyroxene, hornblende and biotite as phenocrysts, from

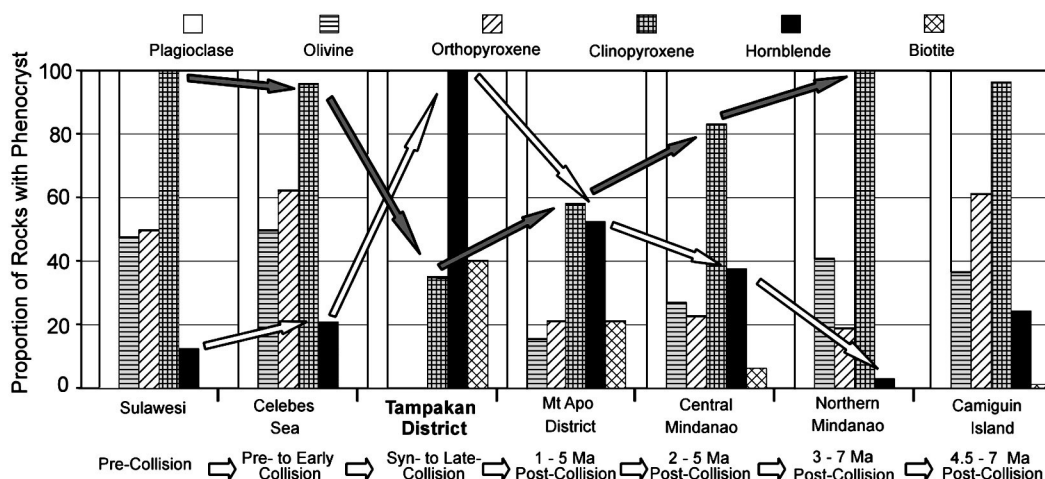


Figure 14: *Along-Sangihe-arc trends in the proportion of magmatic rocks that contain anhydrous phenocrysts (plagioclase, olivine, orthopyroxene, clinopyroxene) and hydrous phenocrysts (hornblende, biotite).* Systematic trends are observed northward along the Sangihe arc that reflect a rise in magmatic water activity as the arc becomes increasingly compressional in the Sulawesi to Tampakan interval, with a corresponding increase in the proportion of hydrous mineral phases that are stabilised by the high water activities. Northward from Tampakan, there is a gradual decrease in the proportion of hydrous mineral phases, and increase in anhydrous phases, as the horizontal compressive stress is relieved increasingly by subduction along the Cotobato Trench to the west and by the Philippine Trench to the east. The Late Neogene and Quaternary (<5 Ma) syn-collisional rocks from the Tampakan district lie at the peak of the spatial trends in rising magmatic water activity and proportional abundance of hydrous mineral phases.

south-to-north between the six southernmost districts within the Sangihe arc. These volcanic rocks erupted in varying stress fields associated with their pre-, syn- or post-collision setting during the Late Neogene and Quaternary. The Tampakan district is unique relative to the adjacent non-mineralised districts in that magmatic rocks of <5 Ma lack olivine and orthopyroxene. These smooth trends indicate that hornblende progressively becomes more dominant as the arc is traversed from actively subducting regions in a pre-collision setting (northeastern Sulawesi), to marginal areas undergoing early collision (Celebes Sea), and then to syn-collision and late-collision segments of the arc (Tampakan district). Hornblende progressively, and eventually totally, usurps clinopyroxene and orthopyroxene as the principal mafic phenocryst phase in rocks with >54 wt % SiO₂. Likewise, a traverse northward along the arc from areas of active collision (Tampakan district) to areas of increasingly post-collision magmatism (Mt Apo district, central Mindanao and northern Mindanao) is associated with trends in which hornblende-bearing rocks decrease in their proportional abundance, and an antithetic trend in which the proportion of rocks with clinopyroxene as a phenocryst phase increases.

The net effect of crustal stress on magmatic differentiation along the Sangihe arc is that volcanism becomes increasingly silicic and hydrous (hornblende ± biotite-bearing) as horizontal compressive stress within the lithosphere increases from that of normal subduction to collision. The reverse trend occurs as the stress within the lithosphere is progressively relieved after collision by initiation of new subduction zones, the Cotobato and Philippine Trenches west and east of the central Mindanao orogen. That is, erupted magmas become less evolved, less hydrous and progressively more clinopyroxene-bearing (at the expense of hornblende) as collisional stress is relieved along new subduction zones.

Rare Earth Element Chemistry

The lanthanide elements and yttrium are useful as indicators of the identities and approximate proportions of cumulus minerals involved in differentiation processes that produced samples of evolved melts from normal arc-basaltic parents. Seven selected N-MORB-normalised REE profiles for the Tampakan igneous suite are presented in Fig. 15. The middle Miocene Sulop basaltic andesite sequence (sample EA045800) displays a REE pattern of relatively flat middle (MREE) to heavy (HREE) rare earth elements that reflects a combination of pyroxene and plagioclase fractionation, similar to the MORB pattern and consistent with the lack of hornblende in petrographic samples. It exhibits a strong negative Eu anomaly due to a predominance of plagioclase fractionation. The sample is a plagioclase-olivine-pyroxene basalt and represents volcanism in the Tampakan sector of the Sangihe arc during normal subduction, prior to the late Miocene onset of compression.

The Cycle 2 magmatic sequence represented by sample EA043207 (6.56 Ma; Figs. 12 and 15) shows a slight concavity in the shape of the HREE patterns that reflects the effect of prior augite and hornblende fractionation which removes the MREE's and HREE's from the melt. The REE profile shows increasing LREE concentrations relative to the middle Miocene sequence, whereas the HREE values decrease modestly. The steepening of the LREE to MREE segment and the diminishment of the Eu anomaly suggests that plagioclase fractionation is decreasing, and hornblende plus augite fractionation collectively produce a steeper LREE to MREE segment of the normalised REE trend. However, the REE profile for this sample shows the least 'hornblende fractionation effect' relative to younger cycles of magmatism. This is corroborated by the relatively low calculated magmatic water contents relative to younger samples (Table 1).

Table 1: Samples selected for determination of magmatic physico-chemical parameters, and resulting values.

Sample	Age	Cycle	Rock-type	Physico-Chemical Variables								
				Temp	fO ₂	H ₂ O	P _{Sat}	P	MD	D _{ex}	HD	S _m
	Ma			(°C)	ΔNNO	(%)	Bar	Kbar	g/cc	Km	g/cc	ppm
EA043228	8.34	1	Cpx-Hbl? BA (flow)									311
EA043207	6.36	2	Cpx-Hbl la (flow)	T _O = 872	+2.5	4.7	1352			5	0.278	
DA993948	~ 6.0	2	Cpx>>Hbl la (flow)	T _{Si} = 860		4.1	1094			4.1	0.230	
EA049678	3.80	4a	Hbl-Cpx-Bt la	T _O = 805	+2.4	5.6	1750			6.5	0.385	
EA043212	3.75	4a	Hbl-Cpx SA (dyke)	T _{HP} = 800		6.0	1987			7.4	0.427	188
EA044956	3.67	4a	Hbl Granodiorite	T _{HP} = 806		5.8	1901			7.0	0.410	
EA045799	3.65	4a	Hbl-Cpx la (flow)	T _O = 909	+1.7	4.4	1248			4.6	0.244	
EA043206	3.04	4a	Hbl-Cpx la (dyke)	T _O = 865	+1.5	5.1	1725			6.4	0.349	312
DA993972	1.75	4b	Hbl-Cpx la (flow)	T _{HP} = 875		5.4	1961			7.3	0.381	
EA043214	1.47	4b	Hbl-Bt SA Dome	T _{HP} = 765	+2.0	8.2	3335	5.1	2.34	12.4	0.605	
EA045009	0.86	4b	Hbl Dacite Plug	T _{Si} = 785		7.2	2747	5.0	2.33	10.2	0.535	
EA043204	0.59	4b	Hbl-Bt Dacite Plug	T _O = 807	+2.4	6.7	2404	6.0	2.36	8.9	0.481	57
EA045002	~0.1	5	Hbl-Bt la	T _O = 866	+2.2	4.9	1450			5.4	0.299	
EA046389	~0.1	5	Hbl-Bt la	T _O = 829	+2.5	5.5	1752			6.5	0.372	

Cycle = magmatic cycle; BA = Basaltic andesite; la = Intermediate andesite; SA = Silicic andesite; T_O = temperature by QUILF; T_{HP} = temperature by hornblende-plagioclase geothermometry; T_{Si} = temperature inferred from temperature vs SiO₂ correlation of 11 data points; fO₂ = oxygen fugacity, given as log units fO₂ above the nickel metal-nickel oxide reference buffer; P = total pressure (lithostatic load); P_{Sat} = H₂O partial pressure = minimum bound on confining pressure; H₂O = dissolved water in melt; MD = melt density at calculated pressure (P); D_{ex} = minimum depth of hydrothermal fluid exsolution at lithostatic pressure; HD = hydrothermal fluid density during initiation of exsolution (excluding solutes); S_m = sulphate concentration in melt.

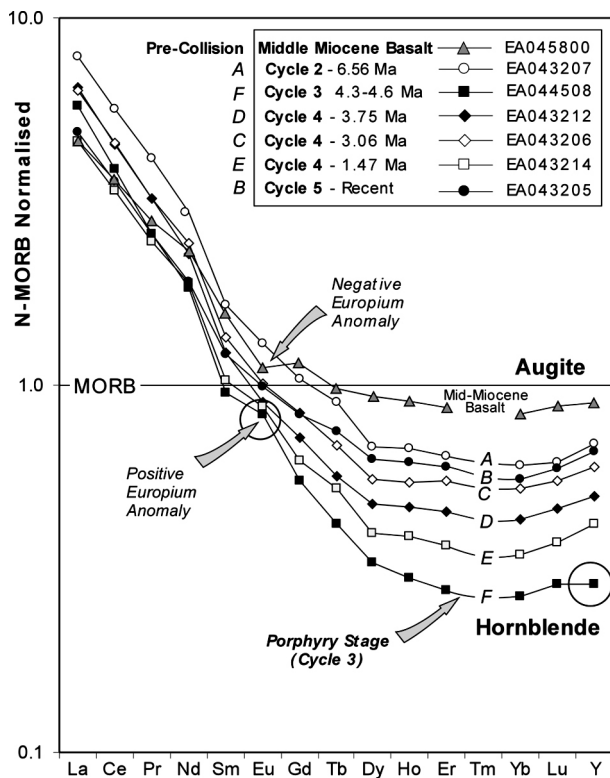


Figure 15: *N-MORB-normalised profiles of rare earth elements from selected rocks from the Tampakan district.*

The entire suite of Late Miocene to Recent magmatic rocks displays moderate to high degrees of hornblende fractionation, evident as a strong depletion of heavy REE, with a minimum around Er and in some cases by a weak positive Eu anomaly (Nagasawa and Schnetzler, 1971). Plagioclase and augite fractionation is dominant in the early part of successive magmatic cycles with minor hornblende fractionation, however hornblende becomes increasingly dominant through the course of each cycle and becomes the principal, or sole, mafic fractionating phase at the dacitic end of the later magmatic cycles. The porphyry Cu-Au mineralisation at Tampakan is associated with the rocks that show the greatest degree of hornblende fractionation at the end of Cycle 3.

lacks augite. Several units within the later part of Cycle 4 exhibit a positive Eu-anomaly (e.g. EA043214; Fig. 15), suggesting Eu^{2+} accumulation in residual silicate melt due to substantial delay in onset of plagioclase saturation. REE trends for Cycle 5 magmas from the Quaternary Mt Matutum stratovolcano show a regression to less depleted MREE and LREE values, consistent with decreasing hornblende fractionation and increasing augite fractionation. This regression is also associated with a renewed phase of magma chamber recharge and mixing in the lower crust to form more mafic hybrids (Fig. 19).

The REE data for the Tampakan series reveal successively evolving magmatic cycles (Cycles 1 to 5). During the commencement of each cycle, augite fractionation is either dominant (Cycles 1 and 2) or significant (Cycles 4 and 5). During progressive differentiation of Cycles 2, 3 and 4, both augite and plagioclase become progressively less important while hornblende becomes progressively more important as a fractionating phase. The evolution in the REE patterns described above is consistent with the element ratios in detrital zircons (Fig. 19) that show a corresponding, time-dependant, cyclic evolution in chemistry.

Sr and Y Systematics

Anomalous trends in several major and trace elements that partition into plagioclase (Sr, Al_2O_3) and hornblende (Y, HREE, FeO) are observed in the Tampakan suite relative to other representative arc segments in the western Pacific. Although Sr is enriched in most arc sequences relative to back arc and MORB basalts, due to fluid transfer of Sr from the subducting slab to the mantle wedge source region of melts, the behaviour of Sr during magmatic differentiation is typically that of a compatible element that decreases in abundance during magmatic differentiation. Plagioclase is the major sink for Sr because of the high $D^{\text{Plagioclase/Melt}}$ for Sr ($D^{\text{Labradorite/Melt}} \approx 3$; $D^{\text{Andesine/Melt}} \approx 6$; Blundy & Wood, 1991) and high modal abundance of plagioclase (>50%) in the crystallising mineral assemblage of evolved basalts, basaltic andesites and augite andesites at upper-crustal pressures. The data for representative arcs in Fig. 16a all show Sr behaving as a compatible element, with the exception of the Tampakan district where Sr increases markedly during magmatic differentiation. The rise in Sr with SiO_2 is a feature of evolving melt compositions, inasmuch as the Tampakan volcanics are not plagioclase cumulates to a significant degree, and contamination of the melt by Sr-bearing limestone

In Cycle 3 – which culminates in the formation of porphyry Cu ore from a dacitic melt – the *entire* NMORB-normalised REE pattern moves to substantially lower values (Fig. 15) relative to Cycle 2, with a severe depletion in the MREE to HREE's. This downward shift is produced by decreasing plagioclase fractionation and a progressive switch from augite to hornblende fractionation. A decrease in plagioclase fractionation is also indicated by a shift from no Eu anomaly (A – EA043207) in Cycle 2 to a positive Eu anomaly in Cycle 3.

The REE profiles for rocks from the first part of Cycle 4 (D and C; Fig. 15) occur at the transition of Cycle 3 to 4 (3.75 Ma; Fig. 19) and at the early stage of Cycle 4 (3.06 Ma; Fig. 19). They show an increase in MREE and HREE normalized values back to levels intermediate between Cycles 2 and 3. They lack the positive Eu anomaly typical of evolved Cycle 3 silicic andesites. These samples at the start of Cycle 4 coincide with the mid-Pliocene recharge of a parental, lower-crustal magma reservoir (Fig. 19), during which resident dacitic magmas of Cycle 3 mixed with primitive magmas from the mantle. During this recharge and mixing event, the predominance of hornblende fractionation at the end of Cycle 3 (Profile F in Fig. 15) decreased relative to augite fractionation during the transition from profiles F to D to C, resulting in shallowing and flattening of the MREE to HREE segment. During the latter part of Cycle 4, the N-MORB-normalised Er-Lu values decrease systematically in Cycle 4 rocks during magmatic differentiation. The progressive deepening trough in the MREE to HREE trends reflects progressive increase in hornblende fractionation throughout Cycle 4 magmatism. The increase in hornblende fractionation continues through the latter part of Cycle 4 until hornblende totally replaces augite as the principal mafic fractionating phase. Sample EA043214 is a hornblende-dacite which

sequences can be excluded because $^{87}\text{Sr}/^{86}\text{Sr}$ ratios in representative rocks of the district have typical mantle signatures (Rohrlach 2002). The high Sr values are attributed to retardation of plagioclase saturation due to high contents of dissolved H_2O in the melts, and to diminished modal abundance of plagioclase, because hornblende crystallisation consumes the melt's plagioclase-forming components, allowing Sr to accumulate within the melt to advanced stages of magmatic differentiation.

In most arc sequences, Y is residually enriched in the melt during magmatic differentiation because $Y D^{\text{Plagioclase/Melt}}$ and $Y D^{\text{Olivine/Melt}}$ are typically < 0.2 for basalts, andesites and dacites (Drake and Weill, 1975; Dunn and Sen, 1994; Ewart

and Griffin, 1994; Bindeman *et al.*, 1998; Beattie, 1994; Nielson *et al.*, 1992 and Kennedy *et al.* 1993), and $Y D^{\text{Pyroxene/Melt}}$ is < 1.0 for basalts and andesites having < 60 wt % SiO_2 and $\ll 1.0$ for cotectic pyroxene + plagioclase assemblages (Jenner *et al.*, 1994; Hack *et al.* 1994; Hart and Dunn, 1993; Larsen, 1979). Thus Y typically behaves as an incompatible element (accumulating in increasingly silicic residual melt fractions) as observed in the comparative Sangihe-Celebes, Halmahera and north Honshu arcs (Fig. 16b). In contrast, Y at Tampakan behaves as a compatible element, decreasing in abundance during differentiation. Hornblende is the major sink for Y because of high $D^{\text{Plagioclase/Melt}}$ for Y, $Y D^{\text{Olivine/Melt}} = 1.5$ for basaltic to andesitic melts, increasing to $Y D^{\text{Hornblende/Melt}} \geq 2.5$ for dacitic

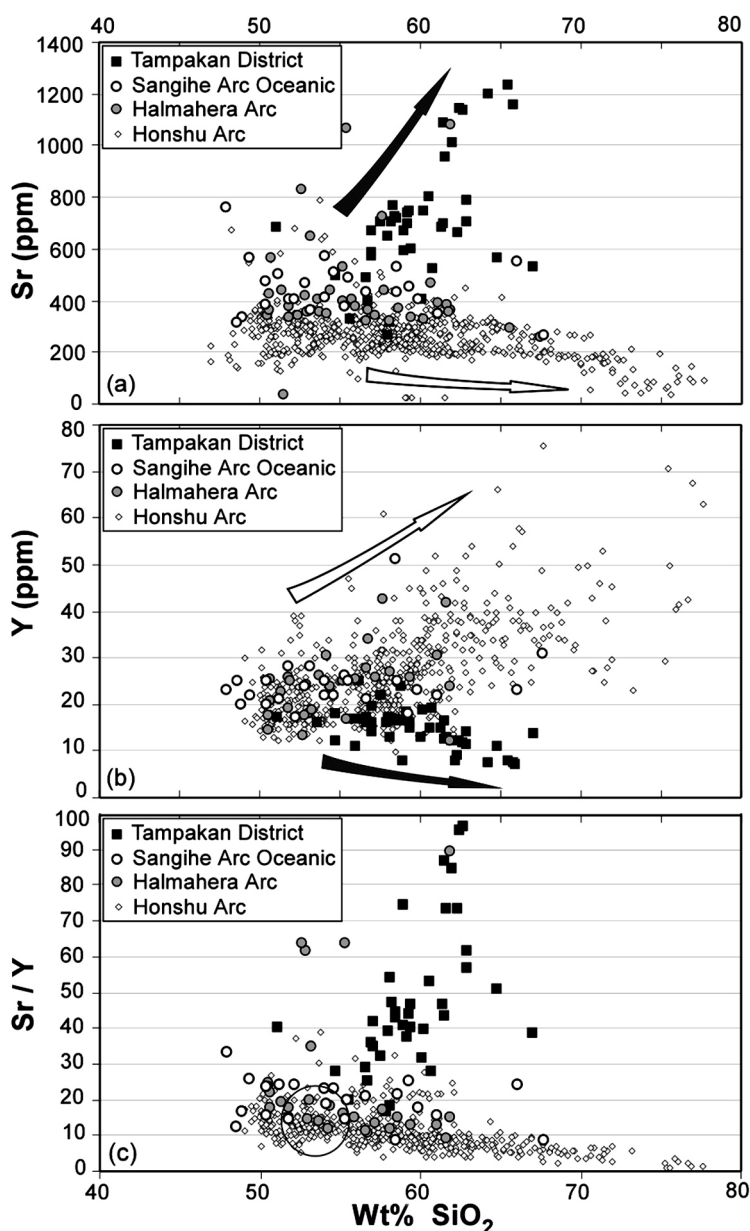
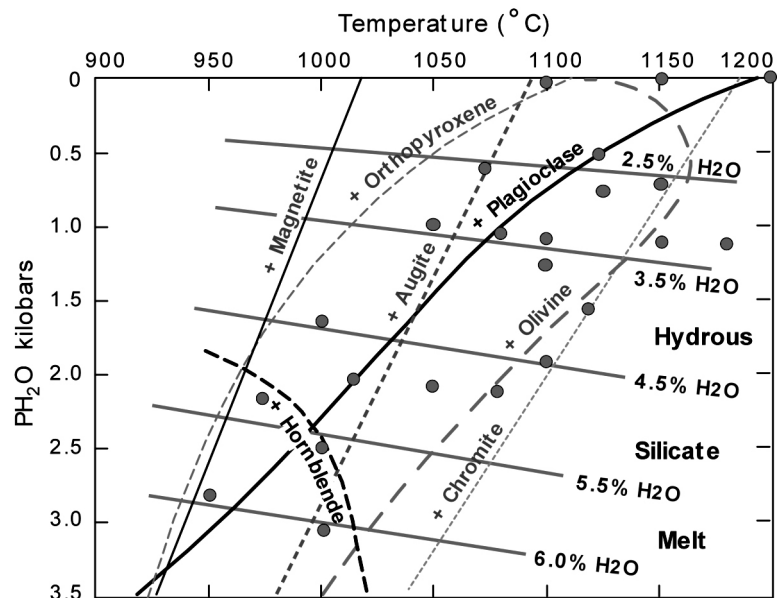


Figure 16: *Sr, Y and Sr/Y versus SiO_2 for the Tampakan district, for the Celebes Sea segment of the Sangihe arc, for the Halmahera arc, and for the north Honshu arc.* The data plotted include late Miocene and younger rocks from the Tampakan district ($n = 49$), the Sangihe arc segment in the eastern Celebes Sea ($n = 24$), the Halmahera Arc ($n = 43$) and the North Honshu arc ($n = 480$). The Sangihe-Celebes and Halmahera arcs are built on oceanic crust while the Tampakan district and the north Honshu arc are built on continental crust. The data for the comparative districts were compiled from Morris *et al.*, (1983); Ikeda, (1991); Kimura *et al.*, (2001); Yoshida and Aoki, (1984); Hayashi, (1985); Aoko and Fujimaki, (1982); Kanisawa *et al.*, (1994); Miyajima, (1990); Tamura, (1994); Ujike and Stix, (2000); Togashi *et al.*, (1992); Aoki *et al.*, (1989); Sakuyama and Nesbitt, (1986); Shuto and Yashima, (1990); Fujinawa, (1992); Suzuki, (2000); Tamura and Shuto, (1989) and Kobayashi and Nakamura, (2001).

Figure 17: Varying the wt % H₂O dissolved in the silicate melt strongly affects the order of mineral crystallisation from the melt (and consequently affects the relative rates of depletion or accumulation of various trace elements in the melt), as illustrated by this map of phase assemblages in a series of crystallisation experiments by Moore and Carmichael (1998) on a basaltic andesite composition from the Trans Mexican magmatic arc.

Each grey dot represents an experiment in which the crystallising mineral assemblage was identified, and the melt's content of dissolved water (grey contours labelled with wt % H₂O) was determined from the composition of the quenched glass according to the method of Moore *et al.*, (1998). At P_{H₂O} = 0 (dry), the crystallisation order of silicates from the cooling melt is plagioclase first, followed by olivine, orthopyroxene, and then augite. At P_{H₂O} > 3.5 kbar and >6.5 wt % H₂O dissolved in the melt, plagioclase is the last of those silicates to crystallise, and hornblende is first. (Saturation curves for magnetite and orthopyroxene in the hydrous melts are based on lower-temperature andesite experiments by Blatter & Carmichael, 1998). Because dissolution of H₂O in the melt depolymerises aluminosilicate polymer units in the melt (Burnham, 1979), minerals such as pyroxenes and especially feldspars that consume higher-order aluminosilicate polymer units of the melt are most severely depressed in saturation temperature as more H₂O dissolves in the melt. Increase in the supply of silica monomers allows the saturation temperature of orthosilicates, such as olivine to rise initially, but further additions of dissolved H₂O dilutes the concentrations of all other chemical components of the melt, which depresses the saturation temperatures of all anhydrous minerals. The thermal stability of hydrous minerals, such as hornblende (and biotite and epidote) is increased by H₂O addition at constant temperature, up to rather high concentrations (beyond the range of this diagram), beyond which the dilution effect takes over and saturation temperatures of hydrous minerals fall with further additions of dissolved H₂O in the melt. Increasing the lithostatic pressure at constant content of dissolved H₂O has much the same effect on crystallisation order of plagioclase and hornblende as the P_{H₂O} effect shown here, because increasing lithostatic pressure also depolymerises aluminosilicate melts, retarding plagioclase saturation to lower temperatures, relative to orthosilicates such as olivine, zircon and garnet, and relative to minerals that use silica dimers and other low-order polymer species in the melt. At any given value of dissolved H₂O > 5 wt%, hornblende reaches its maximum thermal stability and rank in the crystallisation sequence at lower-crustal/uppermost-mantle pressures in the 10-20 kbar range (Ulmer, 1988).



melts (Sisson, 1994; Ewart and Griffin, 1994). In the Tampakan district, hornblende fractionation from basaltic andesitic, andesitic and dacitic melts caused depletion of Y in the melts during magmatic differentiation.

Extrapolation of the trends for Sr and Y (Fig. 16) to more primitive, SiO₂-poor compositions for the strongly hydrous Tampakan series reveals a convergence with parental basalts of the relatively anhydrous magmatic differentiation series in the Sangihe and Halmahera arc segments farther south. The convergence of differentiation trends at the mafic end implies that all could have been derived from the same type of parent magma under different pressure-depth conditions of magmatic differentiation.

Phase-stability relationships defined from crystallisation experiments by Baker and Eggler, (1983) for a high alumina basalt from Atka Island, Aleutian arc, under water-saturated conditions at 2 kbars, reveal that at low magmatic water contents (2 to 3 wt.% H₂O), plagioclase crystallises at high-temperature, well before hornblende enters the crystallisation sequence at lower temperatures. However, there is a reversal in this crystallisation sequence at high magmatic water contents of around 6 wt.% H₂O. Additional phase relationships defined by Moore and Carmichael, (1998) from crystallisation experiments conducted on a primitive andesite at water-saturated conditions and varying pressure reveal that there is also a pressure dependence on the relative crystallisation sequence of plagioclase and hornblende (Fig. 17). Additional representations are shown in Rohlach (2002) for experimental data compiled for

olivine tholeiite melts, or evolved equivalents that lie close to the liquid line of ascent of an olivine tholeiite. In the case of the olivine tholeiite, at a pressure of 5 to 6 kbars that equals the calculated crystallisation pressure of the Tampakan suite (see the Magmatic Physico-Chemical Properties sections below), hornblende starts to crystallise at 1050°C whereas plagioclase starts to crystallise at ~920°C. The combination of extremely hydrous magmas (Table 1) at Tampakan, combined with their crystallisation in an extremely slow-cooling lower crustal reservoir at ~20 km depth below the Tampakan district, and their maintenance at high temperature for prolonged periods of time by episodic recharge (Fig. 19), are responsible for the reversal of the normal plagioclase-hornblende crystallisation sequence which in turn produced the reversed evolutionary trends in Sr and Y that record the lower crustal evolution of hydrous magmas at Tampakan.

Fig. 18 shows the Sr/Y ratios plotted against Y. Hydrous and/or high-pressure magmas, in which plagioclase crystallisation is retarded and hornblende saturation is brought forward in the crystallisation sequence, evolve to high Sr/Y ratios and low Y values as the melt's SiO₂ content increases, because the suppression of plagioclase crystallisation allows Sr to build up in the melt during early stages of differentiation while hornblende fractionation depletes the melt in Y. High Sr/Y ratios (>20) are one of several chemical characteristics of "adakites", a rock-type defined by Defant and Drummond (1990) to be the product of melting of eclogitic portions of the subducted slab.

Melting of subducting Molucca Sea Plate under Tampakan is exceedingly implausible, inasmuch as it is of Mesozoic age (Hall, 1996) and has been subducting throughout much of the Cenozoic and now extends to >600 km depth in the mantle (Silver & Moore, 1978; Lallemand *et al.*, 1998), whereas thermal modeling of subducting slabs by Peacock, (1990a,b) and Peacock *et al.*, (1994) indicate that the conditions that permit melting of the slab are restricted to; i). subduction of young (<10 M.y.) and hence warm oceanic crust; ii). initial stages of subduction wherein the leading edge of the subducting plate intrudes thermally undisturbed and hence hot mantle; and/or iii). high rates of shear heating.

Magma Mixing

The series of detrital zircon ages from the Tampakan district (see Geochronology section above) record semi-continuous volcanism from the late Miocene to Recent. This detailed chronological record allows the temporal framework of magmatism to be coupled with aspects of the evolving chemistry of the Tampakan magmatic system as recorded by the trace element composition of dated detrital zircon grains. Trends in the elemental compositions of the zircons provide insights into the chemical evolution of their parent melts and corroborate and illuminate the magmatic “cycles” discussed in the Geochronology section. Fig. 19 shows U/Ti ratios of suites of detrital zircons that were collected from two streams in the radial drainage system on the Tampakan edifice. The element ratio U/Ti was determined by excimer laser ablation ICP-MS on zircon grains whose ^{238}U - ^{206}Pb ages were determined by the same instrument.

The oscillations in the time series of the U/Ti ratio in the zircons mirror oscillatory trends in the differentiation indices (such as wt. % SiO_2) of magmas that built the Tampakan volcanic complex. The U/Ti ratio was selected for examination because the Ti content of residual melts decreases over the course of differentiation from basaltic

andesitic to rhyolitic stages, whereas U behaves as an incompatible element that accumulates in residual melts over the same differentiation interval. We anticipated that zircon crystallising from melts in the 58-68 wt % SiO_2 range would inherit a biased representation of the parent melt's evolving U/Ti ratio, and thereby could serve as a differentiation index of the zircon's parent melt. The high density of data points in Fig. 19 provides a high-resolution depiction of the evolving magmatic system in the Tampakan district prior to and during generation of the giant porphyry and high-sulphidation ore systems and the unusual petrochemical signatures discussed above. A succession of “ramps” is resolved whereby the magmatic system builds to more evolved compositions (higher U/Ti) in a series of cycles that are separated by abrupt downward steps wherein the magmatic system was re-set to more primitive compositions. Each of these ramps, which collectively extend from the latest Miocene to the present, correlates with the succession of magmatic cycles defined in the Geochronology section and illustrated in the bottom panel of Fig. 19 by the oscillatory trend in wt % SiO_2 in a smaller number of least-altered drill core samples from which zircons were also separated and dated by the same ELA-ICPMS method. The first ramp in U/Ti, from ~7.3 Ma to ~6 Ma, is equivalent to the first major period of stratocone construction in the Tampakan district (Geochronology section; Figs. 12 and 13) and is labelled Cycle 2. Cycle 1 is not resolved here, as it is represented by only one age date from an andesite sample from deep levels of the Tampakan porphyry deposit. Between ~6 and ~5.4 Ma the U/Ti ratios decrease, reflecting replenishment of the magma chamber by mafic magma having a low U/Ti ratio and blending of the silicic resident and replenishing mafic melt fractions, after which the U/Ti ratio begins to climb steeply again between ~5.4 and ~4.2 Ma. The development of this second ramp coincides with increasing compression within the district (Fig. 5) during docking of northern and southern

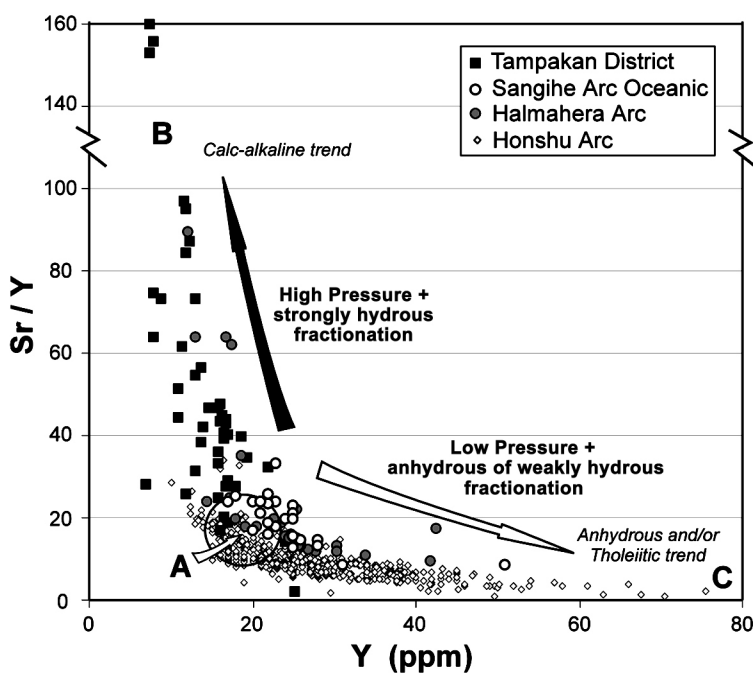
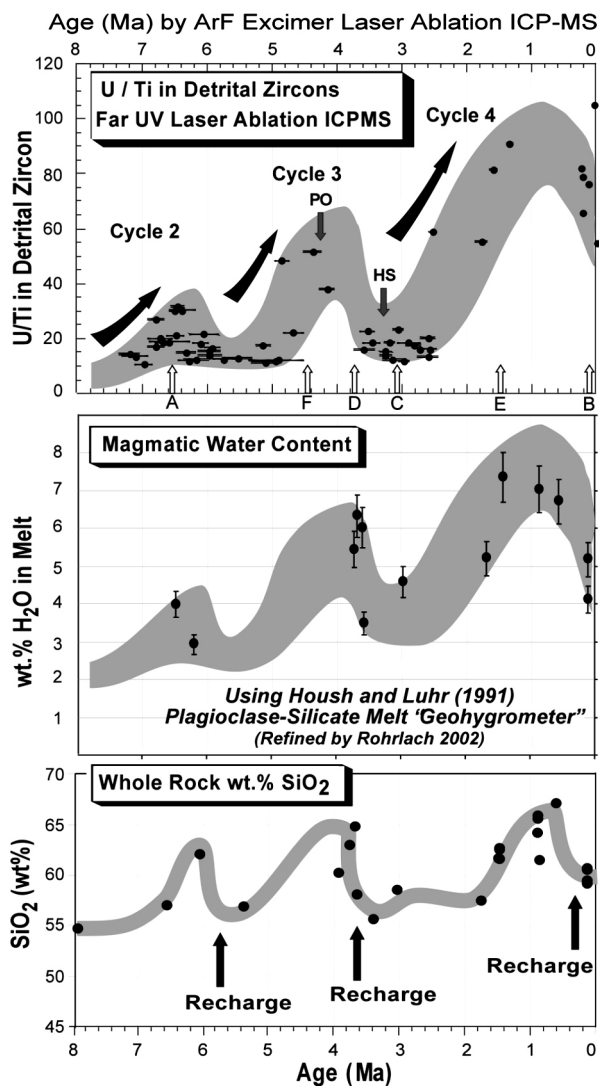


Figure 18: Plot of Sr/Y versus Y for the Tampakan district and several comparative arcs. The Tampakan suite displays an atypical trend wherein Sr/Y increases with increasing magmatic differentiation, opposite to the trend of decreasing Sr/Y with increasing magmatic differentiation that is observed in the Celebes Sea segment of the Sangihe arc, the Halmahera arc and the north Honshu arc. None of the last three arc segments is known to have significant magmatic-hydrothermal copper mineralisation in the time intervals represented by the datasets. High magmatic water contents (up to 8.2 wt.% H_2O ; Section 7) and high crystallisation pressures (6 kbars; Section 7) delay plagioclase saturation in the melt to substantially lower temperatures and advanced stages of differentiation, and advance hornblende saturation in the melt to earlier, more primitive stages of differentiation and at higher temperatures, relative to magmatic series which develop under water-poor conditions and/or low pressures. At Tampakan, the reversal of the usual order of appearance of plagioclase and hornblende in the crystallisation sequence produces the atypical trends in Sr/Y versus Y. Hydrous and high-pressure sequences evolve from A to B during magmatic differentiation whereas water-poor and low-pressure sequences evolve from A to C.



Mindanao along the Cotabato Fault Zone (Fig. 2). The formation of *porphyry copper mineralisation* at 4.26 to 4.24 Ma (Figs. 12 and 13) occurs at the dacitic end of the Cycle 3 ramp. The phase of stratocone construction associated with this magmatic ramp was eroded during unroofing of the porphyry system between 4.25 and 3.93 Ma (Geochronology section) due to high or catastrophic erosion rates as the collision event peaked during the middle Pliocene.

The magmatic system then underwent a replenishment and mixing event resulting in regression to more primitive compositions between ~3.8 and ~3.4 Ma, during the peak of the collision (Fig. 5) and following the evolved magmatism which produced porphyry copper mineralisation at the peak of the preceding ramp. The high-sulphidation epithermal Cu-Au mineralisation at Tampakan (3.39 to 3.20 Ma) is associable with a magma batch emitted from the lower-crustal chamber during the replenishment/mixing event. The third U/Ti ramp that is resolved by the zircon data extends from ~3.7 to ~0.6 Ma (Fig. 19) wherein U/Ti and other incompatible-on-compatible element ratios build to *greater values than in the preceding ramps, albeit within about the same SiO₂ range as preceding cycles*. This last ramp coincides with magmatic Cycle 4. The early part of Cycle 4 (~3.7 to ~2.5 Ma) was the principal stratocone building event during the middle Pliocene (Fig. 13), of

Figure 19: Upper panel - Detrital zircons were collected from streams on the western side of the Tampakan volcanic edifice and were dated by $^{238}\text{U}/^{206}\text{Pb}$ using a far-ultraviolet argon-fluoride excimer laser microprobe to ablate 25 to 200 μm spots in single crystals for isotopic and trace-element analysis of the ablated material by ICP-MS. As zircon crystallises, it inherits a biased version of the melt's U/Ti ratio, which is a magmatic differentiation index that rises as the melt's SiO₂ content rises. (Both U⁴⁺ and Ti⁴⁺ substitute in Zr⁴⁺ lattice sites). In the 8 to 0.06 Ma time series of ages of eruptive and intrusive units in the continuously evolving Tampakan igneous complex, the oscillations in the zircon's and the melt's U/Ti ratio represent cycles of magmatic differentiation by fractional crystallisation, punctuated by magma-chamber replenishments (labelled "recharge" in the lower panel) by mantle-derived mafic magma that mixed with residual andesitic or dacitic magma already in the lower-crustal chamber. PO and HS show the timing of porphyry and high sulphidation mineralisation.

The central and lower panels represent time series of variations in the dissolved H₂O content or SiO₂ content of magma batches that were erupted or intruded into the volcanic edifice. The age determinations in the central and lower panels are from U-Pb analyses of zircons separated from least-altered whole-rock samples collected from surface outcrops and drill core. Those samples were subjects of whole-rock XRF and ICP-MS analysis. The wt. % H₂O dissolved in the melt at various stages is calculated from our electron-microprobe measurements of the Ca/Na partition coefficient between plagioclase phenocryst rims and surrounding groundmass (quenched melt), and from the experimentally calibrated effect of dissolved H₂O (and temperature and pressure) on Ca/Na in plagioclase/melt.

The bottom panel shows the SiO₂ content of least-altered whole-rock samples from which datable zircons were extracted. The maximum SiO₂ content attained at the ends (tops) of differentiation cycles varies little among Cycles 2, 3, and 4, but the maximum U/Ti ratio ramps up by about 3-fold over the same time period, and the maximum H₂O content in successive cycles approximately doubles over the same time interval.

which the remnant landform is observed in topographic data (Fig. 8). Igneous rocks of the younger part of Cycle 4 comprise widely scattered and evolved hornblende-andesites and -dacites in the southern portion of the district. A minor regression in the U/Ti ratio and whole-rock SiO₂ occurred at the end of Cycle 4 (~0.6 Ma), prior to eruption of the Quaternary Mt Matutum Andesite (Cycle 5) which built a new stratocone that overlaps the southern flank of the older volcanic complex. The important aspect of the trends defined in Fig. 19 is that in each cycle the maximum height of the crest, at the top of each "ramp", is successively higher, and hence more evolved, than in each preceding ramp. This effect arises because i). U and H₂O are more highly incompatible components of the melt than is SiO₂ and hence climb relative to it, and because ii). hybrid melts at the start of new cycles inherited the accumulated U and H₂O (and Cl and SO₃, and other incompatible components) from evolved residual melts of the preceding cycle, and then added to the inherited accumulation by fractional crystallisation of U- and H₂O-poor cumulates in the current differentiation cycle. The half-wavelength, or evolving portions, of the three resolved differentiation ramps are between ~1 and 3 M.y. duration. This length of time is substantially longer than the life span of magma chambers in the upper crust (typically <400 K.y.) that are broadly equivalent to the construction period of individual stratovolcanoes. If each ramp, or mega-fractional crystallisation cycle were isolated magmatic systems related to independent and evolving chambers, with each being

replenished from the mantle with minimal melt storage in the lower-crust, then chemical inheritance between cycles would not be observed. The relatively long time intervals spanned by the major differentiation cycles implies that they occurred in a slow-cooling lower-crustal/upper-mantle magma chamber, as is also indicated by pressures of 5 to 6 kbar from Al-in-hornblende geobarometry on phenocrysts in silicic dacites (see Magmatic Physico-Chemical Properties section); these pressures correspond to lower-crustal depths under southern Mindanao.

The process of intermittent magma recharge and mixing in a continuously crystallising magma reservoir over a time interval of >7 M.y. is also reflected by evolutionary trends of compatible components such as wt % TiO_2 in whole-rock samples. Because TiO_2 is a relatively immobile component during hydrothermal alteration, we have selected it to illustrate the evolutionary process in complex multi-cycle melt fractionation events. Fig. 20 shows a representative plot of mixing relationships between evolved melt at the end of several magmatic cycles and a hypothetical mafic parental melt. The replenishing mafic end of the mixing series is not necessarily a primary, mantle derived melt, but simply a plausible, somewhat evolved end member for the mixing array. TiO_2 displays compatible behavior throughout the crystallisation interval of the sampled Tampakan series because of early crystallisation of titanomagnetite and ilmenite from the basaltic andesite stage onward. In this example, wherein the component of interest always displays compatible behavior, magmatic differentiation produces concave-upward depletion curves (Fig. 20). Linear mixing between TiO_2 -poor, silicic residual melt fractions and recharging mafic melts always produces hybrid melts that are more enriched in the compatible component at a given SiO_2 content. (Mg#, Ni and Cr contents ramp up in essentially the same way during generation of "adakites" by multi-cycle magmatic differentiation, without the commonly inferred implication that silicic melts of subducting eclogite were contaminated by peridotitic mantle wedge during ascent). The TiO_2 content of hybrid melts parental to successive cycles 1 to 5 climbs due to back mixing of successive silicic residual melts with a common parental melt. The inheritance implicit in this climb in TiO_2 content among successive

cycles corroborates previously described evidence that the petrochemical evolution toward copper metallogenic fertility was a multi-cycle recharge-and-differentiation process in a magma chamber that was exceptionally long-lived (late Miocene to Recent) because relatively evolved *buoyant* melts remained trapped near the Moho by the sustained compressive stress regime (see Mechanics of Lower Crustal Entrapment by Tectonic Stress section). Multi-cycle inheritance of incompatible components, most notably H_2O , eventually led to development of unusual andesitic and dacitic melts having no negative Eu anomalies, and exceptionally high Sr/Y and $\text{Fe}^{3+}/\text{Fe}^{2+}$ ratios (oxidation state).

Several textural features of the phenocrysts in the Tampakan suite also provide evidence of repeated magma injection and chemical disequilibrium between resident phenocrysts and the hybridising melts throughout the late Miocene to Recent epochs. Plagioclase phenocrysts commonly display sieve-like textures within the cores of large phenocrysts, along intermediate growth bands or along the exterior portion of phenocrysts. The sieve texture consists of interconnected lacy filaments of melt inclusions that comprise 10-30 % of the sieve-textured zones, and were trapped along resorbed surfaces of phenocrysts. In other examples of chemical disequilibrium within the hybrid magmas, "late-stage" biotite is replaced and mantled by hornblende. This reflects a temporary regression in the crystallisation sequence and is further evidence of crystal-liquid disequilibrium within the crystallising magma. Whereas plagioclase and hornblende phenocrysts display textural evidence of resorption during magma mixing and during shallow-level emplacement, uncorroded augite phenocrysts have remained in textural equilibrium with the melt, which indicates that the disequilibrium perturbations are toward more primitive melt compositions and mineral assemblages. Fe-Ti-oxide and hornblende-plagioclase temperature estimates for sample EA043214 (Magmatic Physico-chemical Properties section) reveal that it had been heated from $\sim 765^\circ\text{C}$ (hornblende-plagioclase temperature) to $\sim 906^\circ\text{C}$ (two-oxide temperature), corroborating the textural evidence for magma mixing during input of hotter, more primitive melt into the chamber.

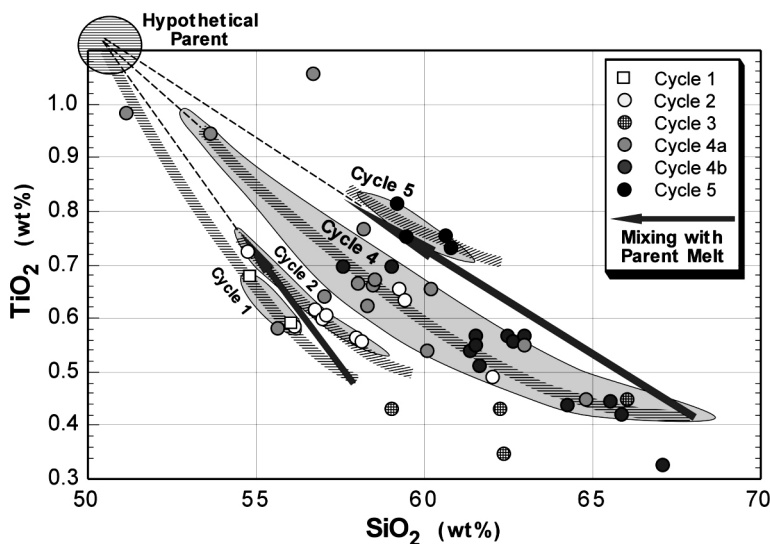


Figure 20: A plot of TiO_2 versus SiO_2 for the Tampakan igneous suite. The concentration of TiO_2 , and by corollary other melt-incompatible elements, decreases monotonically (pale grey curved trend lines of fractional crystallisation) within any single differentiation cycle, but increases in successive cycles 1 to 5 at intermediate to high silica contents, due to linear back mixing (heavy grey arrows) of evolved melts with a primitive parental melt. The effect is a product of the upward concave depletion curve that is characteristic of melt-incompatible elements.

Magmatic Physico-Chemical Properties

Magmatic physico-chemical parameters are calculated for 13 rocks from successive stages of the differentiation history of the Tampakan volcanic complex in order to constrain the magmatic temperature, oxygen fugacity, pressure of hornblende crystallisation, water content, H₂O partial pressure, depth at which water would begin to exsolve from the magma at lithostatic pressure, density of the exsolved supercritical brines, magmatic sulphur content, sulphur speciation and melt density. Physico-chemical parameters such as oxygen fugacity, magmatic water activity and sulphur speciation are important factors in controlling the metallogenic ore-forming capability of calc-alkaline melts.

Magmatic temperatures and oxidation states were calculated using the QUILF algorithms of Andersen *et al.*, (1993) (Fig. 21). The Fe-Ti-exchange geothermometer and oxygen barometer is not adequately calibrated at the low-temperature and high oxidation state of magmas that are commonly parental to porphyry-type copper-gold ore deposits, so we recalibrated the output of QUILF using data from five later, precise experimental studies to derive an empirical linear correction term for application to temperature estimates derived for rocks at oxygen fugacities greater than NNO+2 (Rohrlach and Loucks, 2000a). A correction term for magmatic fO_2 was also derived by comparison of QUILF output with the experimentally measured fO_2 and temperature that reproduce the mineral assemblage and compositions of Fe-Ti-oxides and other phenocrysts in the 1991 Pinatubo dacite. Temperatures of the Tampakan suite were also calculated by hornblende-plagioclase geothermometry (Holland and Blundy, 1994).

The calculated magmatic temperatures for the Tampakan suite vary from 765°C (hornblende-plagioclase

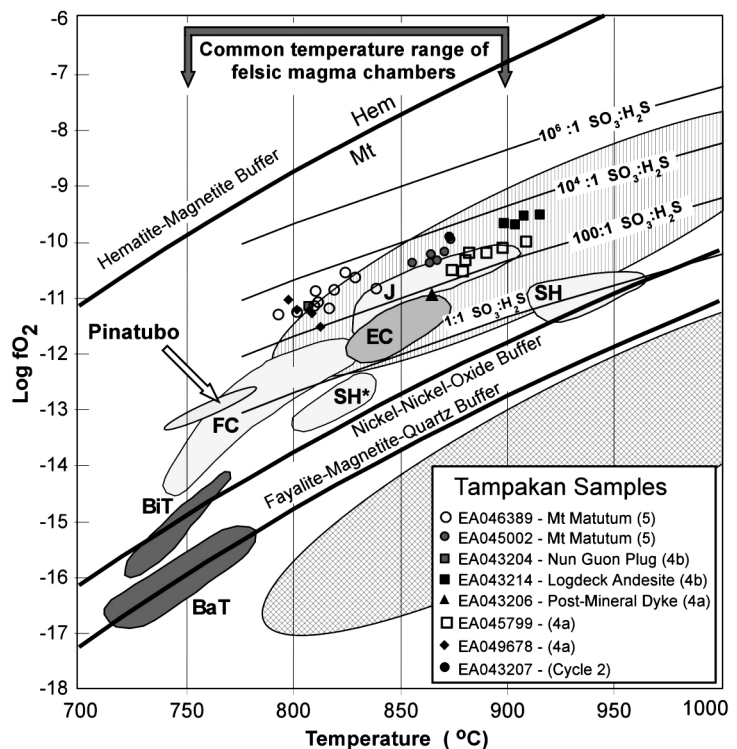
thermometer) to 909°C (two-oxide thermometer). The wide temperature range of the magmas is a function of the extensive composition range plotted. The disparity between the Fe-Ti-exchange geothermometer and the hornblende-plagioclase geothermometer for temperature estimates of sample EA043214 (909°C vs 765°C), in conjunction with disequilibrium corrosion and replacement textures in plagioclase, biotite and hornblende, indicate that magma mixing between cool resident magmas (765°C) and hot recharging magmas (> 909°C) occurred in a lower-crustal magma chamber.

The fO_2 range of the Tampakan suite varies from NNO+1.5 to NNO+2.5 and lies near the upper limit of the fO_2 range for typical Cu-Au ore-forming, oxidised I-type magmas. The magmas lie in the field where sulphur-as-sulphate (SO₃) predominates over sulphur-as-sulphide (H₂S) dissolved in the melt, with SO₃:H₂S ratios between ~200:1 and 6000:1. High sulphur concentrations in fresh magmatic apatite from the Tampakan district reveal that many of the melts were anhydrite-saturated (Rohrlach 2002), and that anhydrite saturation was a persistent feature of the dacitic stage of evolution. The series crystallised igneous anhydrite at ~67 wt.% SiO₂ in the melt over a significant portion of the late Miocene to Recent magmatic history, consistent with the SO₃:H₂S ratios determined above.

The aluminium-in-hornblende barometer of Anderson and Smith, (1995) was used to calculate crystallisation pressures of magmatic phenocrysts in three Cycle 4b dacite-porphyry units having rhyolitic groundmass (interstitial melt) compositions. This version of the barometer takes into account not only the fO_2 dependence, but also the temperature dependence of the partitioning of aluminium into the tetrahedral site of hornblende, which other calibrations of the barometer fail to consider. The three samples from the Tampakan suite for which the barometer

Figure 21: Titanomagnetite-hemoilmenite temperatures

and oxygen fugacities of Tampakan magmas, plotted with comparison data fields abbreviated as follows: BaT - Bandelier Tuff; BiT - Bishop Tuff; EC - El Chichón; FC - Fish Canyon Tuff; J - Julcani; SH - Mt St Helens; and SH* - Mt St Helens pumice (after Imai *et al.*, 1993). The field for the Mt Pinatubo dacite is plotted using the fO_2 and temperature constraints from Scaillet and Evans (1999). The fields of FC, SH, EC and J are displaced by 0.57 log units to lower values than represented in Imai *et al.*, (1993) to correct for the error in calibration of the Fe-Ti-oxide model at high fO_2 and $T < 900^\circ\text{C}$. The Pinatubo and the El Chichón fields plot at plausible SO₃:H₂S ratios for these series (~10:1) in which pyrrhotite coexisted with anhydrite. The plotted mineral buffers and SO₃:H₂S concentration ratios in the melt are calculated at 2 kbars. SO₃:H₂S contours are derived thermodynamically from Carroll & Rutherford's (1988) experimental finding that a sulphide/sulphate ratio 1:1 occurs in dacitic melt at $fO_2 \sim 1.35$ log units above FMQ at 950°C and 2 Kbar PH₂O. Poulson & Ohmoto (1990) showed that in felsic melts having wt% H₂O > wt% FeO, sulphide in the melt is bonded mainly to H, not Fe. The field of reduced S-type magmas (cross-hatched region) and oxidised I-type magmas (vertical hatched region) are plotted from Burnham and Ohmoto (1980). The Tampakan suite has similar, or slightly higher, fO_2 (relative to NNO) to the anhydrite-bearing Mt Pinatubo dacite, and are as oxidised as the high- fO_2 end-members of the high-sulphidation ore-forming magmas at Julcani, Peru.



was applied are the most highly differentiated units that have the lowest-variance phase assemblage (six phenocryst minerals + quartz-saturated melt + aqueous fluid), and which satisfy Gibbs Phase Rule requirements for successful application of the barometer (Rohrlach 2002). The pressure estimates are: Nun-Guon Plug (6.0 ± 0.6 kbars); Logdeck Andesite (5.1 ± 0.6 kbars); and Lambayong Plug (5.0 ± 0.6 kbars). These pressure estimates correspond to hornblende crystallisation depths of 17.6 to 21.1 km for mafic crust ($\rho = 2.90$ g/cc), or 18.6 to 22.3 km for granitic crust ($\rho = 2.75$ g/cc). The depth estimates obtained from both hornblende rims and cores from the Nun Guon Plug and Logdeck Andesite are indistinguishable within the calibration uncertainty of the barometer. These two units underwent most of their fractionation history in the lower-crust, and were emplaced at the surface directly from a deep, lower-crustal reservoir. The crustal thickness of southern Mindanao is ~ 31 km (Scripps Institute of Oceanography Global Crust Model - CRUST 2.0). These lower-crustal pressure estimates are consistent with the high-pressure mineral assemblages associated with the long-lived magmatic system at Tampakan (as outlined in the Petrochemistry section above).

Water contents dissolved in the melt were calculated for the Tampakan magmatic series using the method of Housh and Luhr, (1991), which experimentally calibrated the effects of dissolved H₂O and temperature and pressure on Na/Ca partitioning between plagioclase and melt. The program TWATER1™ was used to calculate the dissolved water content of the melt, given input data representing proportions of other chemical components in the melt, the chemical composition of the feldspar, and the pressure and temperature of crystallisation. Rohrlach and Loucks, (2000b) added data for 48 experiments to the experimental database of Housh and Luhr, (1991), and derived a refined empirical algorithm that better accounts for the effect of dissolved H₂O in depressing the activities of the melt's silica and albite components. Our calibration of the output of TWATER1™ using recently published experimental data yield a much improved standard precision of $\pm 8.85\%$ in retrieving water contents for experiments with H₂O > 4 wt. % that were less precisely retrieved ($\pm 14.4\%$) by the Housh and Luhr calibration. The dissolved water contents calculated for the Tampakan suite range from 4.1 wt. % H₂O up to 8.2 wt.% H₂O. The series has variable to generally high water contents, and a subset of the suite is extremely hydrous. The magmatic water contents display a time-dependent evolution that mimics cyclic trends in the chemistry of whole-rocks and of detrital zircons (see the Petrochemistry section).

The pressures and depths at which silicate-saturated aqueous fluid exsolved from ascending water-saturated melts below the Tampakan orebody were calculated using Moore *et al.*, (1998). The depth (km) of initial magmatic-hydrothermal fluid exsolution from 13 selected melts during their ascent (ignoring pressure effects of dissolved gases and salts) was calculated from the calculated fluid saturation pressures (P_{sat}) by assuming a density of 2.70 g/cc and $dP/dz = 265$ bars/km for the upper crust. The estimated depths for onset of fluid saturation within the Tampakan

melts vary from 4.1 to 12.4 km. Experimental data from Baker and Rutherford, (1992) indicate that SO₂ concentrations in H₂O-rich fluids co-existing with anhydrite have $P_{\text{SO}_2} \sim 110$ bars at $P_{\text{sat}} = 2200$ bars of pressure fluid. These are thus minimum depth estimates (for a pure H₂O system), because dissolved CO₂ and SO₂ within the melt will force fluid exsolution at deeper levels.

The density of the silicate melt was calculated for 3 samples using magmatic temperatures, crystallisation pressures and magmatic water contents. The melt densities (Table 1) were calculated using the tabulated temperatures and pressures together with mole fractions of oxide components (Al₂O₃, K₂O etc) and their partial molar volumes as reported by Lange and Carmichael, (1990), Kress and Carmichael, (1991) and the partial molar volume of dissolved water published by Ochs and Lange, (1999). For the Logdeck Andesite, Lambayong Plug and Nun-Guon Plug, which are considered to have the most reliable pressure estimates from Al-in-hornblende barometry, the hydrous melt densities average 2.34 g/cc (Table 1). These melts are highly buoyant relative to mafic lower crust that has densities on the order of 2.90 g/cc.

Table 1 lists estimates of the total sulphur concentration dissolved in the silicate melt for 4 samples. These values are based on the analysed sulphate concentration in apatite phenocrysts in those samples, and on the apatite/melt partition coefficient of sulphate calibrated as a function of temperature by Rohrlach (2002), using data compiled from Peng *et al.*, (1997), Baker & Rutherford, (1996), and Streck and Dilles, (1998). Fig. 21 shows that the Tampakan melts had sulphate/sulphide ratios averaging around 1000:1, so the indicated values for sulphate in the melt are equivalent to total dissolved sulphur. Samples having ≤ 188 ppm sulphur plot along the anhydrite saturation curve at their respective temperatures, which implies that evolved magmas of Cycle 4 were generally anhydrite-saturated.

In summary, the calculated physico-chemical properties of the long-lived Tampakan magmatic suite reveal that the magmas are highly oxidised, display substantial temperature fluctuations, and evolved at lower-crustal depths of ~ 18 to 22 km. They underwent progressive enrichment in magmatic water, and attained >8 wt. % H₂O, in a manner that mimics the high-resolution pattern of detrital zircon chemistry (see the Petrochemistry section). The magmas were highly buoyant relative to lower crustal country rocks, so some mechanism is required to keep these magmas entrapped for sufficient periods of time in the lower crust so as to generate the multi-million year trends of magmatic evolution that are presented in the Petrochemistry section.

Mechanics of Lower Crustal Entrapment by Tectonic Stress

Primitive magmas generated by melting of spinel or garnet lherzolite within the mantle are very buoyant relative to ambient peridotitic mantle (density ~ 2.8 g/cc for a hydrous picritic or tholeiitic melt at 20 kb, compared to ~ 3.2 g/cc for peridotite near its solidus at 20 kb). After segregation from the source region, the basaltic melts migrate up to the

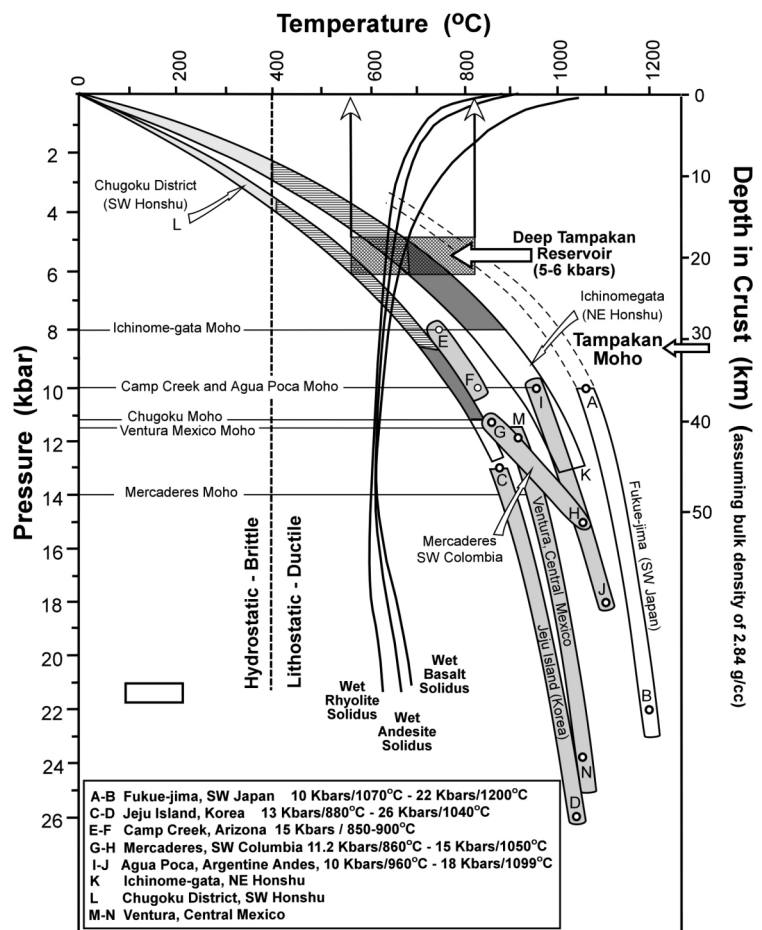
base of the crust or into the lower crust, where the density of mafic granulites and amphibolites is ~ 2.9 to 3.0 g/cc, so mafic magmas lose much of their buoyancy at the Moho. The stress regime in the vicinity of the mantle-crust boundary and at rheologic boundaries within the crust strongly influences whether picritic or basaltic melts continue to ascend by dyke propagation, or whether they stall as vertically prolate lenses, or propagate along subhorizontal hydraulic fractures and underplate the crust (or intra-plate the mid-crust) as laterally extensive magma chambers in which ultramafic and mafic layered cumulates develop. In stress regimes where the horizontal tectonic stresses are extensional or hydrostatic, dykes propagate as hydraulic fractures that open at the top and pinch shut at the tail until the magma lozenge reaches neutral buoyancy in a density-stratified crust, whereupon the magma body stalls and crystallises until segregated residual melt fractions have acquired enough compositional buoyancy to resume ascent. In contrast, when the lithospheric stress regime has the minimum stress axis (σ_3) oriented vertically (e.g. during tectonic collision events), and the horizontal

compressive stresses (σ_1 and σ_2) are of sufficient magnitude to inhibit subvertical propagation of dykes, buoyant magmas that are much more fluid than the country rock (making diapiric ascent unfeasible) can be trapped by the stress regime in subhorizontally propagating magma sheets.

The fluid pressure, P_f , at the upper tip of a dyke that is available to propagate the hydraulic fracture is $P_f = (\rho_{rx} - \rho_{melt}) Gz$, wherein ρ_{rx} is the density of the country rock, ρ_{melt} is the density of the magma, G is gravitational acceleration, and z is the height of the magma column. Table 1 showed that dacitic melts from eruptive Cycle 4b, having 6.7 to 8.2 wt% H₂O, contained a phenocryst assemblage that recorded a pressure of 5.5 ± 0.5 kb, which corresponds to $\sim 20.4 \pm 1.9$ km depth. These were overlain by a rock column with an average composition of andesite having an average density of ~ 2.75 g/cc and a lithostatic pressure gradient of ~ 0.2695 kb/km. At the indicated pressure, the dacitic melts have a density of 2.34 ± 0.02 g/cc (Table 1), so $dP_f/dz \approx 40$ bars/km of melt column. In the rheologically plastic lower crust, the horizontal deviatoric

Figure 22: Regional geothermal gradients in a representative suite of active magmatic arcs are defined by geothermobarometry on suites of lower-crustal and upper-mantle xenoliths in monogenetic volcanoes that sampled rock columns along new magma conduits through the lithosphere.

In several regions, xenoliths are derived only from the uppermost lithospheric mantle, while in other regions the xenolith suite spans the local crust-mantle boundary. The crustal and upper-mantle geotherms for the Ichinome-gata (K) and Chugoku (L) districts, of NE and SW Honshu respectively, are reproduced from Kushiro (1987). The remaining data are from: Fukue-jima [(A-B) Umino and Yoshizawa, 1996]; Jeju Island [(C-D) Choi *et al.*, 2001]; Mercaderes, SW Colombia [(G-H) Weber *et al.*, 2002; Conceição *et al.*, 2005; Rodriguez-Vargas *et al.*, 2005]; Camp Creek, Arizona [(E-F) Esperanca and Holloway, 1984; Esperanca *et al.*, 1988] and Ventura, Central Mexico [(O-P) Luhr and Aranda-Gómez, 1997]. The depth scale in km is calculated assuming an average arc-crust density of 2.84 g/cc (Kay and Kay, 1985). The mismatch between this scale and the Moho depth estimate for the Mercaderes district (14 kbars - 42 km, Weber *et al.*, 2001) is due to their assignment of a crustal density of 3.0 g/cc for a basaltic crust. The wet solidus for basalt/gabbro, andesite/tonalite and granite/rhyolite are from Stern *et al.*, (1975). Depth to Moho estimates are available from six of the localities based on petrology of the xenolith suites and/or independent seismic data. For the two localities where Moho depth estimates were not available (Fukue-jima and Jeju Island), the Moho depth is assumed to be equivalent to the nearby Chugoku District (11.1 kbars). All eight districts show temperatures at the Moho of around 760 to 860°C or higher, and all districts have Moho temperatures which are hotter than the wet solidus for basalt, andesite and rhyolite. The estimated depth at which the deep magmatic reservoir resides in the lower crust below the Tampakan district (5 to 6 kbars, 18 to 22 km; Al in hornblende geobarometry) is shown by the light grey band. The band encapsulates the range of ambient temperatures for lower-crustal rocks surrounding the deep chamber, prior to chamber emplacement, as inferred from the illustrated geotherms in other arcs. The dashed vertical line at 400°C represents the brittle-ductile transition. The geothermal gradient in the Tampakan district is likely to be similar to that of other island arc settings such as Ichinome-gata, Chugoku and Fukuwe-jima in Japan and Jeju Island in Korea, where crustal thicknesses are broadly comparable to the crustal thickness in the Tampakan district (~ 31 km). These data yield lower-crustal temperature estimates, at 18 to 22 km below Tampakan, in the range of 560 to 810°C . These temperatures straddle the temperature range of the wet-basalt to wet-rhyolite solidi (~ 620 to 680°C). The conclusion to be drawn from these data is that large, hydrous, calc-alkaline magma chambers entrapped at depths of 18 to 22 km would conductively cool extremely slowly, and, if country rock temperatures are above $\sim 650^\circ\text{C}$, then low volume, residual fractionated melts could be preserved indefinitely, until relaxation of the tectonic compressive stress permits their buoyant ascent. These data, together with detailed thermal modelling by Rohlach (2002), show that a large and deep lower crustal chamber may survive between successive recharge events throughout the period of compressive deformation.



stress, σ_h , that is responsible for crustal shortening and for inhibiting propagation of subvertical dykes is well approximated by the relation $\sigma_h \approx V \cdot \eta / W$, wherein V is the fractional shortening rate, η is the average viscosity of the deforming medium, and W is the distance over which the deformation occurs (England and McKenzie, 1982; Liu *et al.*, 2000).

In the Thermal Modelling of Magma Chamber Longevity section on chamber lifespan and cooling rate, we present a compilation of geotherms in six arcs, derived from geothermobarometry on xenoliths of upper-mantle and lower-crustal country rock sampled by new magma conduits that fed *monogenetic* volcanoes. Along these six geotherms, undisturbed by passage of prior batches of magma, the temperatures at 5.5 ± 0.5 kb (corresponding to the top of the Tampakan magma chamber) lie in the range of 560 – 810°C and average $\sim 685^\circ\text{C}$. At these temperatures, country rock having an average composition of diorite has a viscosity on the order of 10^{23} to 10^{21} Pa-sec (Talbot, 1999). Viscosities in this range also typify gabbroic compositions at 700 – 800°C in the vicinity of the Moho.

The data in Fig. 5 and the relation $\sigma_h \approx V \cdot \eta / W$ permit a rough estimate of the magnitude of the regional average σ_h as subduction convergence in south-central Mindanao ground to a halt while new subduction-thrust systems were being established along the Philippine Trench and the Sulu Trench to accommodate the continuing convergence between the Philippine Sea Plate and Eurasia. The diffuse deformation zone spans the interval from the Philippine Trench to the Sulu Trench, a distance of ~ 631 km in the direction of plate convergence.

According to the vertical width of the black band at the top of Fig. 5, the amount of plate convergence not accommodated by subduction at the Sulu, Cotobato, and Philippine trenches was 13.5 mm/yr at the time of Tampakan porphyry copper mineralisation, and 30 mm/yr during high-sulphidation mineralisation. Taking these rates as estimates of V , 631 km for W , and 10^{22} Pa-sec for η , we obtain $\sigma_h \approx 68$ bars during porphyry-copper mineralisation and $\sigma_h \approx 151$ bars during high-sulphidation mineralisation.

The result calculated in the earlier paragraph, $(\rho_{rx} - \rho_{melt}) G \approx 40$ bars/km, implies that these values of σ_h would be capable of entrapping a dacitic melt column as thick as 1.7 km around the time of the porphyry copper mineralisation event, or a melt column ~ 3.8 km thick around the time of the high-sulphidation mineralisation event. We note that the large uncertainties in rheology of the lower-crustal rocks make these estimates very rough, but they serve to illustrate the feasibility of entrapping buoyant magmas in the lower crust in regimes of strong horizontal compressive stress. Magmas entrapped by the stress regime can resume ascent when either i). they evolve to greater compositional buoyancy by continued magmatic differentiation, or ii). far-field tectonic stress relaxes. The latter cause may account for the commonly reported approximate synchronicity of mineralisation in several districts along a mineral belt.

Thermal Modelling of Magma Chamber Longevity

A long-lived calc-alkaline magma reservoir is postulated to have evolved in the lower crust below the Tampakan district, trapped by the ambient stress regime during the early Pliocene collision in Mindanao. A reservoir life-span of ~ 7 M.y. is indicated by prolonged magmatism in multiple over-printing volcanic cycles (see the Geochronology and Petrochemistry sections), and is implied by long-term ramping trends in incompatible and volatile components of the melt that are observed in successive magmatic cycles which erupted in the district. Thermal constraints are discussed below to show that magma can be stored in the lower crust over time frames of 3 to 10 million years, typical of the duration of arc orogenic events, thus allowing inheritance of volatiles through multiple cycles of chamber recharge and fractional crystallisation.

Petrological, temperature and pressure profiles of the lithosphere have been defined in several volcanically active regions, based on the study of xenolith suites, which allow the determination of geothermal gradients (Fig. 22). Regional geothermal gradients derived from studies of xenolith suites need to be interpreted carefully because, in some studies, unusually high geotherms have been attributed to local warming of the lower crust or upper mantle by the prior passage of melt. For reliable geotherm estimation using geobarometry and geothermometry, mafic and ultramafic xenoliths must have equilibrated along the geotherm prior to intrusion of the ascending host magma (Takahashi, 1980). Consequently the temperature in the lower crust is best constrained from geotherms that are calculated from xenolith suites which were entrained into the first eruptions of monogenetic volcanic fields. In these fields, the thermal structure of the upper mantle and lower crust has not been perturbed by prior magmatism. Geothermal gradients tend to be steeper in volcanic island arcs than in passive continental settings because the crust is thinner, and has been thermally heated by subduction-related magmatism. The temperature in the vicinity of the crust-mantle boundary in the Ichinome-gata, Chugoku, Jeju Island, Mercaderes, Camp Creek and Ventura regions (Fig. 22) are all between ~ 150 and $\sim 250^\circ\text{C}$ hotter than the solidus of differentiation products of mantle-derived arc-basaltic melt having a normal initial content of dissolved H_2O (≥ 0.8 wt. %). These data indicate that if a large, evolving, hydrous calc-alkaline magmatic reservoir is trapped in the lower crust or at the Mohorovicic discontinuity, the temperatures of the surrounding rocks are sufficiently high to allow the reservoir to exist for several million years, or indefinitely, if compression in the lower crust prevents ascent of the residual melt. Consequently magma that has ponded at the crust-mantle boundary or at some other horizon of rheological contrast in the lower crust can undergo long-term evolution through multiple fractionation and replenishment cycles over the duration of a typical compressional deformation event and/or orogeny in the overlying crust (3 to 10 M.y.). Upper crustal sub-volcanic chambers have life-spans that are typically less than the 400 K.y., and which match the

lifespan of convergent margin stratovolcanoes that they build. Cooling of these shallow-level chambers is facilitated by the cooler country rocks in the upper crust and by convective groundwater systems. In contrast, the hot thermal regime surrounding lower-crustal magma reservoirs facilitates extremely slow cooling over several million years, and in some thermal regimes guarantees their indefinite longevity during periods of compression in the overlying crust.

Using the finite-element software program KWare HEAT Version 4.03.0131* (<http://www.ees1.lanl.gov/Wohletz/Heat.htm>; Wohletz and Heiken, 1992), and a range of appropriate geothermal gradients and thermal conductivities of country rocks, and varied thicknesses of horizontal sheet-like magma chambers, Rohrlach (2002) conducted single-stage cooling models and showed that deep-seated magma chambers emplaced into the lower crust could retain magma above the wet solidus on time-scales of 0.4 to over 8 M.y. for chamber thicknesses of 1 to 4 km and emplacement depths of 18 to 30 km.

In arc segments that are under tectonic compression, magmas are trapped in the lower crust by tectonic stress at depths where the normal, ambient thermal regime allows calc-alkaline magma reservoirs to reside at temperatures higher than the wet solidus for several million years, and in some circumstances, indefinitely. Given such long lifespans, there is a very high likelihood that deep magma chambers would experience intermittent replenishment of mantle-derived magma, and partial mixing of evolved resident and primitive replenishing batches. The evolution of fractionally crystallising, intermittently replenished, intermittently tapped chambers entails cyclic ramp-up in the residual melt's concentrations of volatile and other incompatible components, as described previously.

Model and Metallogenic Implications

Prior to the late Miocene collision in the northern Sangihe arc, relatively primitive, clinopyroxene ± olivine-dominated, H₂O poor, basaltic andesites and basalts erupted along the Sangihe arc. Mantle-derived basaltic arc magmas

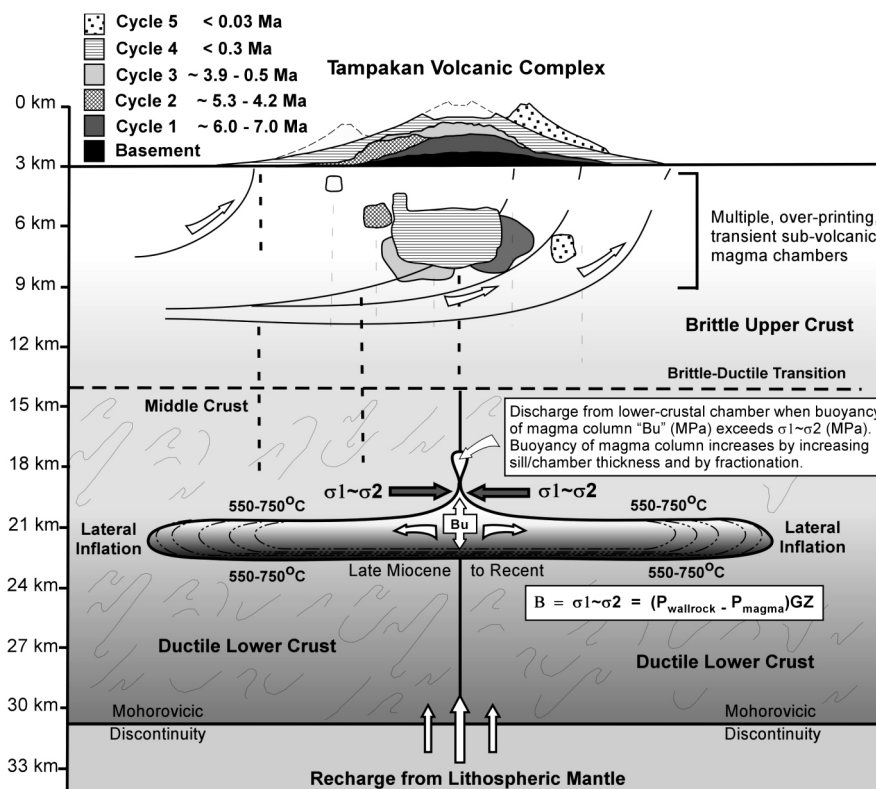


Figure 23: Dimensionally undistorted representation of the long-lived polygenetic Tampakan volcanic complex, with multiple short-lived (0.4 to 1.0 M.y.) upper-crustal magma chambers and volcanic cycles, each of which sequentially tapped a large and long-lived (7 M.y.), sill-like magma chamber near the Moho. During the late Miocene to Recent period of crustal compression, the deep melt reservoir experienced multiple cycles of replenishment and residual accumulation of volatiles and other incompatible components, and evolved by fractionation of ultramafic cumulates that were increasingly hornblende-dominated in later cycles. Tectonic compression entrapped the chamber at or near the Moho, although crustal shortening and magmatic underplating since the late Miocene have since lowered the Moho to present depths of 25 to 30 km. Magmas escaped periodically when the buoyancy of residual melt fractions overpowered the inhibiting stress, or when the horizontal stress relaxed intermittently. Water and chlorine concentrations were ramped by inheritance through successive million-year-scale recharge and differentiation cycles. Porphyry ore formed from water-rich melts that exsolved a magmatic-hydrothermal fluid phase *deep* in the upper crust, where chlorine was efficiently partitioned from the melt to a *high-density* fluid. High-sulphidation mineralisation formed from melts which had lower magmatic water contents and which therefore exsolved a magmatic-hydrothermal fluid at lower pressures where exsolution of two-phase 'dense' vapor + liquid favoured volatile transport of the high-sulphidation metal suite (Cu, Au, As, Te, V). Although the porphyry and high-sulphidation deposits formed from separate upper crustal hydrothermal systems at Tampakan, they are intimately related to the same long-lived lower crustal magmatic reservoir which was instrumental in imparting fertile characteristics to the magmatic system. Hydrothermal remobilisation of the older porphyry ore was probably important to generation of the giant accumulation of Cu in the high-sulphidation deposit.

had relatively unimpeded access to the upper crust. Crustal compression in the Tampakan district commenced in the Late Miocene (~6 Ma) and peaked in the middle Pliocene when subduction slowed and then stopped at the outward dipping northern Sangihe and Halmahera trenches, and convergence between the Philippine Sea and Eurasian Plates was partitioned into intraplate deformation and development of new Cotabato and Philippine Trench subduction thrusts. During early collision in the Tampakan district, ascending magmas that were derived from the wedge above the subsiding Molucca slab encountered increasing intensities of compressive stress within the crust. Magmas became entrapped at progressively deeper levels in the lower crust beneath the Tampakan district through the Pliocene and Pleistocene epochs. Pressure-depth estimates using Al-in-hornblende geobarometry record crystal fractionation to rhyolitic residual melt compositions at 5 to 6 kbars pressure and at mean depths of 20 ± 2.2 km depth within the lower crust of southeast Mindanao.

Detailed ^{238}U - ^{206}Pb , $^{40}\text{Ar}/^{39}\text{Ar}$, K/Ar and $^{87}\text{Sr}/^{86}\text{Sr}$ geochronological studies reveal that the Tampakan district contains a series of overlapping stratovolcanic centres that developed from the Late Miocene (at the onset of collision) to the present (during the waning stages of collision). Petrological and petrochemical trends reveal that magmatism in successive volcanomagmatic cycles became slightly more siliceous and much more hydrous over a time frame of 6 to 7 M.y. Hornblende and biotite become modally more important over time and appear at more mafic stages of the crystallisation sequence in successive magmatic cycles. U/Ti ratios in detrital zircon grains from the district, and other petrochemical indicators, track the progress of magmatic differentiation and cooling of magmas during the ~6-M.y. collision event, and provide a high-resolution record of magma chamber replenishment and crystallisation cycles in the long-lived magmatic series. The cyclic ramp-up of those element ratios coincides with a 7 M.y.-long "sawtooth" cyclic ramp-up in concentrations of volatiles and incompatible trace-elements relative to whole-rock SiO_2 in erupted andesites and dacites. Dissolved water contents climbed from 4.1 wt. % to 8.2 wt. % as SiO_2 in erupted magmas evolved from 57 to 67 wt. %. The deep magmatic reservoir was periodically tapped to form transient sub-volcanic chambers and four overprinting stratovolcanoes (Fig. 23).

In addition to the Tampakan district, some notable examples of long-lived and fertile centres include the Potrerillos district (Cobre, Norte and El Hueso deposits; Marsh *et al.*, 1997) and the Nevados de Payachata region (Choquelimpie high-sulphidation deposit; Wörner *et al.*, 1988). Within deeply exhumed districts, magmatic intrusive complexes also record a similar spatial focus of long-lived magmatism (e.g., the Fortuna and El Abra complexes associated with the Chuquicamata and El Abra porphyry copper deposits (Ballard, 2001).

Modelling of crustal stress in the southeast Mindanao collision zone reveals that entrapment of magmas by compressive stress within the crust is easily achieved at typical strain rates of collisional orogens, and is consistent

with the development of volcanic gaps in several other arc segments now undergoing collision with oceanic plateaux or other subduction-resistant features. Numerical thermal modelling of the syn-collisional Tampakan magmatic system, supported by compilation of arc-geotherm data from P-T studies of crust- and mantle-derived xenolith suites elsewhere, reveals that the longevity of a 1 to 4 km thick and 15 to 30 km wide, pancake-shaped, conductively cooling sill in the lower-crust is several million years. This chamber longevity allows its repeated replenishment from the mantle and can sustain multiple upper-crustal volcanic cycles.

During and following porphyry Cu-Au mineralisation, thrust faulting occurred within the Tampakan district, and was widespread in southeastern Mindanao. The Cycle 3 volcanic centre and its contained porphyry Cu deposit were uplifted by a district-scale ramp anticline that developed on a collision-stage thrust fault. The Cycle 3 stratovolcano underwent rapid, and perhaps catastrophic (?) denudation between 4.25 and 3.93 Ma, when two to three kilometres of overburden were removed, unroofing the Tampakan porphyry system and exposing lithostatically-pressured porphyry-stage veins at the palaeosurface.

The Tampakan high-sulphidation epithermal mineralisation formed between 3.39 and 3.20 Ma, during the latter part of Cycle 4a stratocone construction, at a palaeodepth of ~2 km (Rohrlach, 2002). Parental melts to high-sulphidation ore were less siliceous and had lower water contents than those that formed the preceding porphyry Cu mineralisation, allowing intrusion of high-sulphidation-stage melts to shallow crustal levels where more sulphur- and arsenic- and gold-rich fluids exsolved as a *vapor-dominated* two-phase fluid that may be typical of this deposit style (Hedenquist *et al.*, 1998).

Copper-ore-forming arc magmas of Phanerozoic age worldwide have a distinctive, shared set of lithophile trace-element characteristics that are well accounted for by general aspects of the genetic model above that we have described for the Tampakan ore-forming igneous suite - viz., magmatic differentiation of ordinary mantle-derived basaltic magmas mainly at relatively high pressure in long-lived magma chambers that undergo intermittent replenishment, tapping, and mixing during continuous fractional crystallisation. This process leads eventually to n^{th} -cycle residual melts having unusually high contents of dissolved H_2O (and probably of Cl and SO_3 and other relatively incompatible chemical components), relative to normal contents of major-oxide components that are buffered by the crystallising assemblage of common rock-forming minerals. The build-up of dissolved H_2O causes hornblende to advance in the mineral saturation sequence of successive cyclic units. Hornblende is a relatively strong sink for Y and heavier REEs (especially from Tb to Tm), leaving residual melts depleted in those components. High pressure (~5 to 10 kbar) increases the thermal stability (saturation temperature) of hornblende and markedly retards plagioclase in the saturation sequence of major minerals, for any given composition of the starting melt (e.g., Ulmer, 1988). A high content of dissolved H_2O further

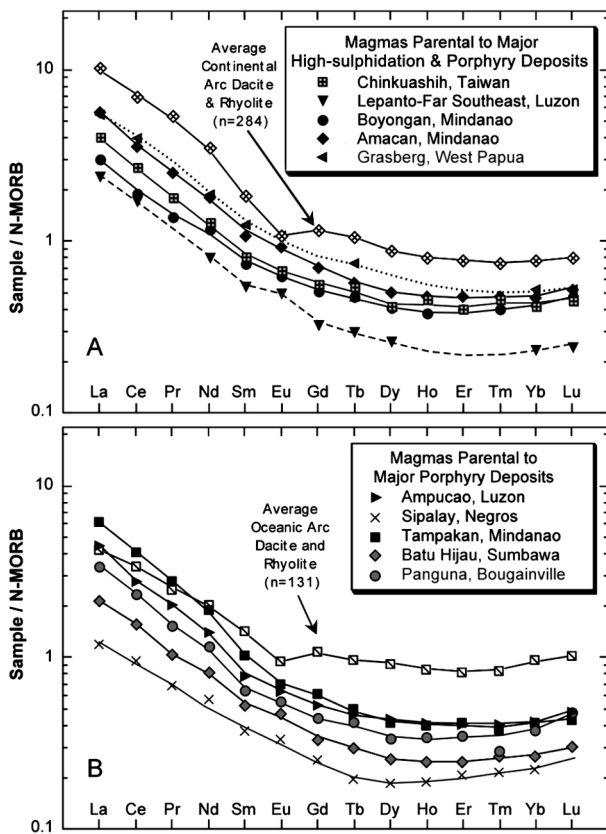


Figure 24: Abundances of REE in fresh or least-altered whole-rock samples of Pliocene and Pleistocene ore-forming porphyritic intrusives in compressive segments of the eastern Sunda and western Pacific arcs are compared with REE abundances in ordinary arc dacites and rhyolites from relatively non-compressive segments of 11 active epi-continental arcs (Andean Southern Volcanic Zone, northern Central America, Trans Mexico, Cascade, Alaska Peninsula, Kamchatka, North Honshu, Southwest Honshu, Ryukyu, western Sunda, New Guinea Highlands) and 12 intra-oceanic arcs (Aleutian, Kurile, Mariana, Izu-Bonin, North Luzon, Sangihe, Halmahera, Banda, Bismarck, Solomon, New Hebrides, Tonga). REE abundances in samples are ratioed to abundances of those elements in average Normal Mid-Ocean-Ridge Basalts (N-MORB; values of Sun and McDonough, 1989). The average felsic arc magmas in mostly unmineralised arc segments have a conspicuous negative Eu anomaly due to prior fractionation of a large proportion of intermediate-composition plagioclase (labradorite and andesine, mainly). The barren felsic suites, especially in oceanic arcs, also have a relatively flat pattern of middle to heavy REE's (Gd to Lu), due to fractionation of a large proportion of augite and little or no hornblende. In contrast, the Cu-ore-productive felsic arc magmas are more depleted in REEs of the Gd to Lu interval, and generally have a minimum at around Ho or Er, a shape caused by protracted fractionation of a large proportion of cumulus hornblende from exceptionally hydrous magmas. Data compiled by R.R. Loucks from >200 literature sources.

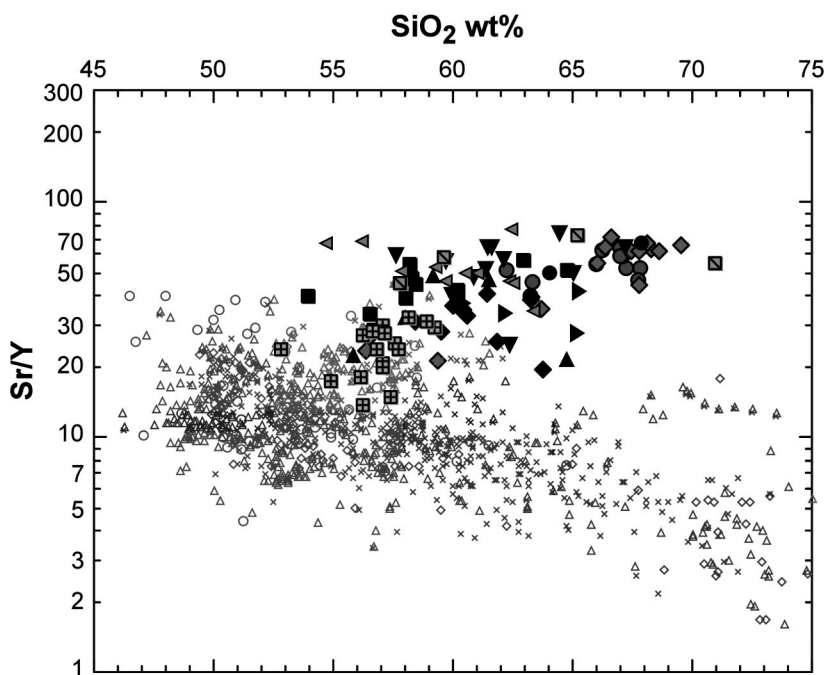


Figure 25: Rock suites temporally and spatially associated with major magmatic-hydrothermal Cu-Au deposits of Pliocene and Pleistocene age in Taiwan, Philippines, Sumbawa, New Guinea, and the Solomon Islands (black and grey solid symbols) are plotted for comparison with barren arc segments (smaller grey open symbols) in the northwest Pacific (Kurile, North Honshu, Ryukyu, and Izu-Bonin arcs) that contain no known significant Cu or Au deposits in the time and space range of the suites plotted. Unaltered or least-altered (to weak propylitic) samples of ore-related igneous suites are from the same volcanic-intrusive centre as hosts the deposit, and all are < 1 M.y. older than the mineralisation age at each locality, as determined from radiometric dates and structural relations to ore. All these deposits formed in regimes of strong horizontal compressive stress, so parental basaltic magmas were trapped at depth and are poorly represented in the eruptive and epizental intrusive igneous suites penecontemporaneous with mineralisation. Basalts erupted in these regions before and after the metallogenic epoch plot in the Sr/Y range 7 to 30 typical of tholeiitic to calc-alkalic arc basalts. Data compiled by R.R. Loucks from >100 literature sources.

Ore-Forming Igneous Suites in Western Pacific Arcs:

- Chinkuashih, Northern Taiwan
- ▼ Lepanto / Far Southeast, NW Luzon
- ▲ Black Mountain/Thanksgiving, NW Luzon
- ▶ Ampucao Au(-Cu) Porphyry, NW Luzon
- ◆ Santo Tomas II, NW Luzon
- Boyongan, East Mindanao
- Tampak, Central Mindanao
- ◆ Batu Hijau, Sumbawa, Indonesia
- ▲ Grasberg, West Papua, Indonesia
- Ok Tedi, Papua New Guinea
- Panguna, Bougainville, Solomon Arc

Unmineralised Reference Suites:

- Kurile Arc 43.8-50.9° N, <6 M.y.
- × N. Honshu Arc 35° -41° N, >138° E, <6 M.y. Old
- ◇ Central Ryukyu Arc 25-31° N, <5 M.y. Old
- ▲ Izu-Bonin Arc 27.1-34.9° N, <5 M.y. Old

delays the onset of feldspar saturation, and diminishes the modal proportion of plagioclase in hornblende-bearing assemblages (because hornblende consumes plagioclase-forming chemical components of the melt) and makes the crystallising plagioclase poorer in Na, Eu and Sr at any specified ratio of Na/(Na+Ca) in the melt (Panjasawatwong *et al.*, 1995; Blundy and Wood, 1991), so Cu-ore-forming magmas avoid plagioclase-induced depletion of Sr and Eu and hence lack a conspicuous negative Eu anomaly in their normalised REE patterns. Relatively sensitive discriminants of copper-fertile arc magmas may be formulated by ratioing relatively enriched elements to relatively depleted elements, such as the ratios Eu/Er or Sr/Y.

Fig. 24 illustrates the degree to which copper-ore-forming batches of subduction-generated calc-alkalic magma differ in REE abundances from ordinary metallogenically infertile calc-alkalic arc magmas of similar major-element chemical composition. Lang and Tittley, (1998) showed very similar REE distinctions between copper-ore-productive and

unproductive granitoid porphyry intrusives in Arizona. The plotted samples from ore-productive intrusives (from drill core beneath mineralised depths, or from satellite dykes emanating from the mineralised intrusive, or late syn-mineral intrusives in a composite complex, etc.) retain most plagioclase and hornblende in a petrographically fresh condition; advanced propylitic, sericitic and potassic alteration are associated with loss of most uni- and di-valent elements and cannot be used reliably. Spoon-shaped profiles of REE abundances, without significant Eu depletion, are distinctive of arc magmas that are chemically specialised for copper metallogeny. In a global survey (not shown), there is no significant chemical difference between magmas that produce major porphyry Cu(\pm Au) ore deposits and magmas that produce major high-sulphidation vein- and manto-type Cu-Au deposits.

In Fig. 25, the Sr/Y ratio in mafic-to-felsic differentiation series in arc segments that contain no known significant magmatic-hydrothermal Cu mineralisation is compared

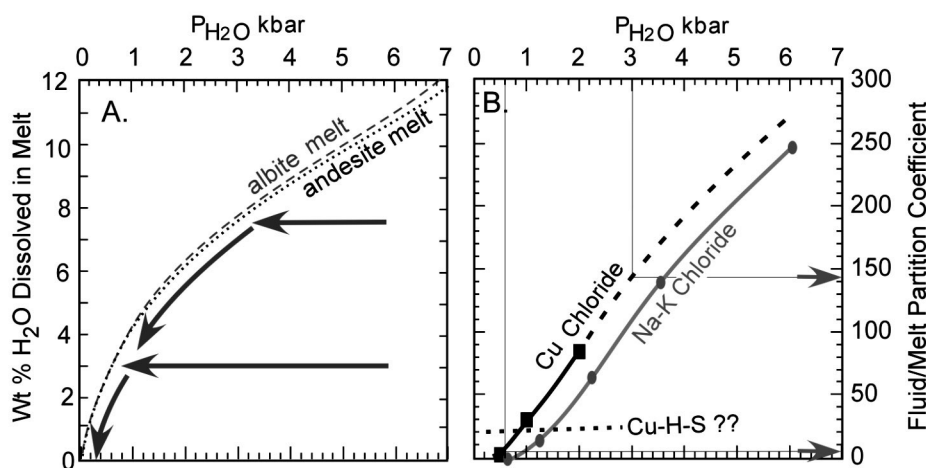


Figure 26: A. Dotted and dashed curves show the solubility of H₂O in silicate melts of andesitic and "alkali rhyolitic" (albite) composition as a function of confining pressure (Burnham, 1979b). If a water-undersaturated andesitic melt containing 3 wt % dissolved H₂O (typical of augite andesites) departed a lower-crustal magma chamber at 6 kbar (~22 km depth), its trajectory on this plot (lower horizontal arrow) would intercept the water saturation curve at ~0.6 kbar, and during further ascent of the melt+fluid mixture, the melt's content of dissolved H₂O would decrease along a trajectory like the arrow in the lower left. One- or two-phase aqueous fluid exsolved at $P \leq 0.6$ kb is entirely or almost entirely a low-density gas that is a poor solvent of dissolved solids. Alternatively, if a water-undersaturated andesitic melt containing 7.5 wt % dissolved H₂O departed a lower-crustal magma chamber at 6 kbar (cf. Tampakan pressures and dissolved H₂O contents in Table 1), its ascent trajectory (upper horizontal arrow) would intercept the water saturation curve at ~3 kbar or ~11 km depth, and during continued ascent the melt's content of dissolved H₂O would decline along the saturation curve as indicated by sloping arrows. Aqueous fluid exsolved at 3 kbar is a single-phase supercritical fluid of liquid-like density that is an effective solvent of dissolved solids.

B. The partition coefficient of alkali chloride between aqueous fluid and haplogranitic melt varies sensitively with P_{H_2O} or partial molar density of H₂O in the aqueous fluid, according to experiments at 810°C and 0.6 to 6.0 kbar by Shinohara *et al.*, (1989).

In these experiments, the melt contains ~700 to 2000 ppm Cl, in the typical range of felsic arc magmas (Wallace, 2005). Also plotted are values of fluid/haplogranitic melt partition coefficients of Cu¹⁺ as chloride complexes in the fluid (Williams *et al.*, 1995, mean of 2 relatively low-Cl experiments at 0.5 kbar and 850°C, having ~3500 ppm Cl in the melt and in the fluid; and mean of 6 relatively low-Cl experiments at 1 kbar and 800°C averaging ~1300 ppm Cl in the melt and ~14,500 ppm Cl in the fluid; and 1 experiment by Keppler and Wyllie, 1991, at 2 kbar and 750°C, having ~49 000 ppm Cl in the fluid and ~1000 ppm Cl in the melt, which is their only experiment that closely approximates Cl contents typical of natural felsic melts). The selected Cu partitioning experiments are all those having melt Cl contents like typical pre-eruptive arc dacites and rhyolites, as indicated by fluid salinities reported by Williams *et al* and by Keppler and Wyllie, in combination with the

$D_{Cl}^{fluid/melt}$ values of Shinohara *et al.*, (1989) at the relevant pressures. The experiments on Cu partitioning only span a P_{H_2O} range of 0.5 to 2 kbar, so we have estimated the values at higher pressure by extrapolation parallel to the well-constrained curve for alkali chlorides, inasmuch as aqueous CuCl^o has the same molecular structure as aqueous NaCl^o and KCl^o, and Cu is not expected to undergo significant configurational changes in these sulphur-free haplogranitic melts in the 2 to 6 kbar interval. Heinrich *et al.*, (1999) have reported analyses of natural fluid inclusions in sub-volcanic magmatic-hydrothermal systems which show that Cu, Au, and As are concentrated in fluid inclusions that trapped a low-salinity vapour phase, whereas inclusions that trapped a coexisting high-salinity brine have low contents of Cu, Au and As. They infer that Cu, Au, and As were probably partitioned from melt into vapour as metal-hydrosulphide (not chloride) complexes. Equilibrium values of $D_{Cu}^{fluid/melt}$ as Cu hydrosulphide complexes have not been experimentally determined, but the hypothetical dashed line labelled "Cu-H-S???" considers the possibility that CuCl exsolved at higher pressure may undergo a change of speciation to volatile Cu-H₂S complexes in sulphur-rich low-density aqueous fluids at magmatic temperatures and low pressures.

with the Sr/Y ratio in volcanic and hypabyssal intrusive rocks spatially and temporally associable with major Cu(±Au) ore deposits of porphyry and high-sulphidation types. Chinkuashih, Grasberg and Ok Tedi overlie Palaeozoic to Precambrian continental basement; other deposits are on Mesozoic-Cenozoic arc basement. The Kurile and Izu Bonin arcs are built upon oceanic lithosphere, whereas the Ryukyu and North Honshu arcs overlie mature continental basement of Palaeozoic or greater age. The age of the subducting oceanic lithosphere under some ore deposits is Mesozoic (Chinkuashih, Tampakan, Batu Hijau, Panguna) and Paleogene under the remainder of deposits, making partial melting of the subducting eclogitic slabs an implausible explanation for the high Sr/Y values of the ore-forming igneous suites (Peacock *et al.*, 1994). Compressive-stress entrapment of mantle-derived basaltic magmas in intermittently replenished, continuously crystallising uppermost-mantle or lower-crustal magma chambers can account for a differentiation trend from predominantly ordinary parental arc basaltic melts toward residual felsic melt fractions having high Sr/Y, as described in the Petrochemistry section above.

The reason that lithophile-trace-element indicators of unusually high hydration state of the melt are also indicators of exceptional copper metallogenic fertility seems to be that exceptionally hydrous melts are likely to begin exsolving a hydrothermal fluid at unusually great depth during their ascent from circum-Moho magma chambers. The higher the pressure at which the fluid exsolves, the denser it tends to be, and the more effective as a solvent of dissolved solids, so the more efficient it is in extracting relatively non-volatile copper chloride and other salts and silica from the parental melt. Fig. 26A illustrates the degree to which the pressure (depth) of onset of fluid saturation is sensitive to the dissolved H₂O content of the ascending, decompressing melt. Fluid that exsolves at shallow subvolcanic depths at which porphyry ore deposits form, is chiefly or entirely a low-density gas (with or without a very subordinate mass of conjugate hypersaline brine), whereas aqueous fluid that exsolves from the melt at mid-crustal pressures ≥ 3 kbar is a single-phase supercritical fluid of liquid-like density (Sourirajan and Kennedy, 1962). Figure 26B presents experimental evidence that the partition coefficient of NaCl and KCl from granitoid melt into exsolving fluid increases very sensitively with increasing density (pressure) of the exsolving fluid. In these 810°C experiments by Shinohara *et al.*, (1989), the granitoid melts have Cl contents in the range 700 to 2000 ppm that are typical of felsic arc magmas (Wallace, 2005). Experimental measurements of the partition coefficient of CuCl between granitoid melt and hydrothermal fluid at 800 to 850°C, selected on the basis of having Cl contents in the fluid and melt in same natural range as the experiments by Shinohara *et al.*, (1989) show a sensitivity of $D_{\text{CuCl}}^{\text{fluid/melt}}$ to fluid pressure and bulk fluid density that parallels the trend of $D_{\text{(Na,K)Cl}}^{\text{fluid/melt}}$ in the 0.5 to 2 kbar range of the available Cu data. On that basis, we have extrapolated the CuCl trend to higher pressures, parallel to the alkali chloride trend.

A very hydrous silicate melt containing 7.5 wt % dissolved H₂O (left panel) that began to exsolve a saline (~1.5 to 3.0 molal Cl) hydrothermal fluid at 3.0 kbar would initially have $D_{\text{Cu}}^{\text{fluid/melt}} \approx 140$, whereas the ascending melt having only 3 wt. % H₂O that began to exsolve low-salinity (~0.02 to 0.06 molal Cl) H₂O gas at 0.6 kbar would initially have only a $D_{\text{Cu}}^{\text{fluid/melt}} \approx 4$, as indicated by the arrow pointers in the right panel. If the Cu-rich, dense fluid that exsolves from a H₂O-rich melt at high pressure segregates buoyantly to the top of an ascending intrusion, the fluid can avoid having to give back its high Cu content to the melt as the ascending magma decompresses and $D_{\text{Cu}}^{\text{fluid/melt}}$ decreases to low values, and thereby preserve that fluid's advantage as an ore-forming fluid at subvolcanic depths. By the time the magma has ascended by dyke propagation to shallow subvolcanic depths, the accumulated fluid at the top of the intrusion would be a composite of fractions that exsolved earlier at higher pressure and fractions that exsolved later at lower pressure. Later fractions of lower-density fluid exsolving at lower pressure are increasingly efficient at extracting gaseous components (HCl, SO₂, H₂S etc.) from the silicate melt (enhancing the fluid's capacity to make high-sulphidation-type mineralisation), but they are much poorer at extracting relatively non-volatile components (chloride salts, silica, etc.) from the melt. Heinrich *et al.*, (1999) have presented empirical evidence that fluid inclusion populations which trapped conjugate magmatic aqueous gas and hypersaline brine have marked enrichments of Cu (as well as Au and As) in the low-density gas phase, relative to the brine. They suggest that partitioning of Cu into the gas phase as sulphide complexes is likely. Such low-pressure re-speciation of Cu from chloride complexes to sulphide complexes as the bulk fluid evolves in density and sulphur content need not affect our interpretations that porphyry- and many coeval high-sulphidation-type Cu deposits developed from unusually H₂O-rich magmas that must have begun to exsolve dense ore-forming fluid at mid-crustal depths.

Based on our case study of the Tampakan deposit and the chemistry of barren and fertile arc rocks globally, we conclude that the characteristic occurrence of major porphyry copper(-gold-molybdenum) and high-sulphidation gold-copper(-silver) deposits in focussed metallogenic districts and epochs framed by barren arc magmatism is governed and ultimately modulated by the transient stress state in the arc lithosphere, which in turn is mediated by changes in global geodynamics and arrival of buoyant, subduction-resistant features in the subducting plate.

References

- Anderson, D.J., Lindsley, D.H., and Davidson, P.M., 1993 - QUILF: A PASCAL program to assess equilibria among Fe-Mg-Mn-Ti oxides, pyroxenes, olivine, and quartz, *Computers and Geosciences* v. 19, pp. 1333-1350.
- Anderson, J.L. and Smith, D.R., 1995 - The effects of temperature and f_{O_2} on the Al-in-hornblende

- barometer, *American Mineralogist* v. 80, pp. 549-559.
- Aoki, K.-I., Yoshida, T. and Zhe, J.Y., 1989 - Petrology and geochemistry of Pleistocene dacitic and rhyolitic pyroclastic flows from southern part of northeast Honshu Japan, *Journal of Mineralogy, Petrology and Economic Geology*, v. 84, pp. 1-14.
- Arribas, A. Jr, Hedenquist, J.W., Itaya, T., Okada, T., Concepción, R.A. and Garcia, J.S. Jr., 1995 - Contemporaneous formation of adjacent porphyry and epithermal Cu-Au deposits over 300 ka in northern Luzon, Philippines, *Geology*, v. 23, pp. 337-340.
- Aurelio, M.A., Barrier, E., Rangin, C. and Muller, C., 1991 - The Philippine Fault in the late Cenozoic tectonic evolution of the Bondoc-Masbate-N.Leyte area, central Philippines, *Journal of Southeast Asian Earth Sciences* v. 6 (3/4), pp. 221-238.
- Baker, D.R. and Egglar, D.H., 1983 - Fractionation paths of Atka (Aleutians) high-alumina basalts: constraints from phase relations, *Volcanology and Geothermal Research* v. 18, pp. 387-404.
- Baker, L. and Rutherford M.J., 1992 - Anhydrite breakdown as a possible source of excess sulfur in the 1991 Mount Pinatubo eruption, *EOS, Transactions AGU* v. 73, p625.
- Baker, L. and Rutherford M.J., 1996 - Crystallisation of anhydrite-bearing magmas, *Transactions of the Royal Society of Edinburgh, Earth Sciences* v. 87, pp. 33-41.
- Ballard, J., 2001 - A comparative study between the geochemistry of ore-bearing and barren calc-alkaline intrusions, *Unpublished PhD thesis, Australian National University, Canberra*.
- Barrier, E., Huchon, P. and Aurelio, M.A., 1991 - Philippine Fault: a key for Philippine kinematics, *Geology*, v. 19, pp. 32-35.
- Beattie, P., 1994 - Systematics and energetics of trace-element partitioning between olivine and silicate melts: implications for the nature of mineral/melt partitioning, *Chemical Geology*, v. 117, pp. 57-71.
- Bindeman, I.N., Davis, A.M. and Drake, M.J., 1998 - Ion microprobe study of plagioclase-basalt partition experiments at natural concentration levels of trace elements, *Geochimica et Cosmochimica Acta* v. 62, pp. 1175-1193.
- Blatter, D.L. and Carmichael, I.S.E., 1998 - Plagioclase-free andesites from Zitácuaro (Michoacán), Mexico: petrology and experimental constraints, *Contributions to Mineralogy and Petrology*, v. 132, pp. 121-138.
- Blundy, J. and Wood, B.J., 1991 - Crystal-chemical controls on the partitioning of Sr and Ba between plagioclase feldspar, silicate melts, and hydrothermal solutions, *Geochimica et Cosmochimica Acta*, v. 55, pp. 193-209.
- Burnham, C.W., 1979a - The importance of volatile constituents; in Yoder, H.S. Jr. (Ed.), *The Evolution of the Igneous Rocks: Fiftieth Anniversary Perspectives*, Princeton University Press, Princeton, N.J., pp. 439-482.
- Burnham, C.W. 1979b - Magmas and hydrothermal fluids; in Barnes, H.L. (Ed.), *Geochemistry of Hydrothermal Ore Deposits*, New York, John Wiley and Sons, pp. 71-136.
- Burnham, C.W. and Ohmoto, H., 1980 - Late-stage processes of felsic magmatism, *Mining Geology Special Issue*, v. 8, pp. 1-11.
- Cardwell, R.K., Isacks, B.L. and Karig, D.E., 1980 - The spatial distribution of earthquakes, focal mechanism solutions and subducted lithosphere in the Philippine and northeastern Indonesian islands; in Hayes, D.E., (Ed.), *The Tectonic and Geologic Evolution of Southeast Asian Seas and Islands*, American Geophysical Union Monograph v. 23, pp. 1-35.
- Carroll, M.R. and Rutherford, M.J., 1988. Sulfur speciation in hydrous experimental glasses of varying oxidation state: results from measured wavelength shifts of sulfur X-rays, *American Mineralogist*, v. 73, pp. 845-849.
- Castillo, P.R., Janney, P.E. and Solidum, R.U., 1999 - Petrology and geochemistry of Camiguin Island, southern Philippines: insights to the source of adakites and other lavas in a complex arc setting, *Contributions to Mineralogy and Petrology*, v. 134, pp. 33-51.
- Cathles, L.M., Erendi, A.H.J. and Barrie, T., 1997 - How long can a hydrothermal system be sustained by a single intrusive event, *Economic Geology*, v. 92, pp. 766-771.
- Choi, S.H., Jwa, Y.-J. and Lee, H.Y., 2001 - Geothermal gradient of the upper mantle beneath Jeju Island, Korea: evidence from mantle xenoliths, *The Island Arc*, v. 10, pp. 175-193.
- Conceição, R.V., Mallmann, G., Koester, E., Schilling, M., Bertotto, G.W. and Rodriguez-Vargas, A., 2005 - Andean subduction-related mantle xenoliths: isotopic evidence of Sr-Nd decoupling during metasomatism, *Lithos* v. 82, pp. 273-287.
- Corpuz, E.S.G., 1992 - Petrology and geochemistry of the Central Mindanao arc, southern Philippines, *PhD Thesis, University of Canterbury, New Zealand*.
- Defant, M.J. and Drummond, M.S., 1990 - Derivation of some modern arc magmas by melting of young subducted lithosphere. *Nature*, v. 347, pp. 662-665.
- Domingo, E.G., Sevillo, D.J., Ferrer, N., Apostol, A., Aurelio, M., Quebral, R., Pubellier, M., Almeda, R., Ferrer, H., Cadawan, B., Comsti, E., Pena, R., Baluda, R., Yumul, G., Villamor, R., Rillon, E., Umbal, J., Diegor, W., Evangelista, D. and Pascual, M., 1995 - Guidebook for field trips GEOSEA '95 eighth regional conference on geology, minerals and energy resources of Southeast Asia, 19-23 February 1995, Philippines, pp. 61-72.
- Drake, M.J. and Weill, D.F., 1975 - The partition of Sr, Ba, Ca, Y, Eu^{2+} , Eu^{3+} and other REE between plagioclase feldspar and magmatic silicate liquid, *Geochimica et Cosmochimica Acta* 39, 689-712.

- Dunn, T. and Sen, C., 1994 - Mineral/matrix partition coefficients for orthopyroxene, plagioclase, and olivine in basaltic to andesitic systems: a combined analytical and experimental study, *Geochimica et Cosmochimica Acta*, v. 58, 717-733.
- Elburg, M.A. and Foden, J.D., 1998 - Temporal changes in arc magma geochemistry, northern Sulawesi, Indonesia, *Earth and Planetary Science Letters*, v. 163, pp. 381-398.
- Esperanca, S. and Holloway, J.R., 1984 - Lower crustal nodules from the Camp Creek Latite, Carefree, Arizona; in Kornprobst, J., (Ed.), *Kimberlites II: The mantle and crust-mantle relationships. Proceedings of the Third International Kimberlite Conference- Volume 2*, Elsevier, 1984.
- Esperanca, S., Carlson, R.W. and Shirey, S.B., 1988 - Lower crustal evolution under central Arizona: Sr, Nd and Pb isotopic and geochemical evidence from the mafic xenoliths of Camp Creek, *Earth and Planetary Science Letters*, v. 90, pp. 26-40.
- Ewart, A., 1982 - The mineralogy and petrology of Tertiary-Recent orogenic volcanic rocks: with special reference to the andesitic-basaltic compositional range; in Andesites: orogenic andesites and related rocks, Thorpe, R.S., (Ed.), Chichester: Wiley, pp. 26-87.
- Ewart, A. and Griffin, W.L., 1994 - Application of proton-microprobe data to trace-element partitioning in volcanic rocks, *Chemical Geology*, v. 117, pp. 251-284.
- Fujinawa, A., 1992 - Distinctive REE patterns for tholeiitic and calc-alkaline magma series co-occurring at Adatara volcano, northeast Japan, *Geochemical Journal*, v. 26, pp. 395-409.
- Hack, P.J., Nielsen, R.L. and Johnston, A.D., 1994 - Experimentally determined rare-earth element and Y partitioning behavior between clinopyroxene and basaltic liquids at pressures up to 20 kbar, *Chemical Geology*, v. 117, pp. 89-105.
- Hall, R., 1996 - Reconstructing Cenozoic SE Asia; in Hall, R. and Blundell, D., (Eds.), *Tectonic Evolution of Southeast Asia*, *Geological Society, Special Publication No. 106*, pp. 153-184.
- Hall, R., 2002 - Cenozoic geological and plate tectonic evolution of SE Asia and the SW Pacific: computer-based reconstructions, model and animations, *Journal of Asian Earth Sciences*, v. 20, pp. 353-431.
- Hamilton, W., 1979 - Tectonics of the Indonesian region, *US Geological Survey Professional Paper 1078*.
- Hart, S.R. and Dunn, T., 1993 - Experimental cpx/melt partitioning of 24 trace elements, *Contributions to Mineralogical Petrology*, v. 113, pp. 1-8.
- Hatherton, T. and Dickinson, W.R., 1969 - The relationship between andesitic volcanism and seismicity in Indonesia, the Lesser Antilles, and other island arcs, *Journal of Geophysical Research*, v. 74 (22), pp. 5301-5310.
- Hedenquist, J.W., Arribas, A. Jr. and Reynolds, T.J., 1998 - Evolution of an intrusion-centred hydrothermal system: Far Southeast-Lepanto porphyry and epithermal Cu-Au deposits, Philippines, *Economic Geology*, v. 93, pp. 373-404.
- Heinrich, C.A., Günther, D., Audétat, A., Ulrich, T. and Frischknecht, R., 1999 - Metal fractionation between magmatic brine and vapor, determined by microanalysis of fluid inclusions, *Geology*, v. 27, pp. 755-758.
- Hodell, D.A., Mead, G.A. and Mueller, P.A., 1990 - Variation in the strontium isotopic composition of seawater (8 Ma to present): implications for chemical weathering rates and dissolved fluxes to the oceans, *Chemical Geology*, v. 80, pp. 291-307.
- Holland, T. and Blundy, J., 1994 - Non-ideal interactions in calcic amphiboles and their bearing on amphibole-plagioclase thermometry, *Contributions to Mineralogy and Petrology*, v. 116, pp. 433-447.
- Housh, T.B. and Luhr, J.F., 1991 - Plagioclase-melt equilibria in hydrous systems, *American Mineralogist*, v. 76, pp. 477-492.
- Ikeda, Y., 1991 - Geochemistry and magmatic evolution of Pliocene-early Pleistocene pyroclastic flow deposits in central Hokkaido, Japan, *Journal of the Geological Society of Japan*, v. 97 (8), pp. 645-666.
- Imai, A., Listanco, E.L. and Fujii, T., 1993 - Petrologic and sulfur isotopic significance of highly oxidised and sulfur-rich magma of Mt Pinatubo, Philippines, *Geology*, v. 21, pp. 699-702.
- Jenner, G.A., Foley, S.F., Jackson, S.E., Green, T.H., Fryer, B.J. and Longerich, H.P., 1994 - Determination of partition coefficients for trace elements in high pressure-temperature experimental run products by laser ablation microprobe-inductively coupled plasma-mass spectrometry (LAM-ICP-MS), *Geochimica et Cosmochimica Acta*, v. 58, pp. 5099-5103.
- Kay, S.M. and Kay, R.W., 1985 - Role of crystal cumulates and the oceanic crust in the formation of the lower crust of the Aleutian arc, *Geology*, v. 13, pp. 461-464.
- Kennedy, A.K., Lofgren, G.E. and Wasserburg, G.J., 1993 - An experimental study of trace element partitioning between olivine, orthopyroxene and melt in chondrules: equilibrium values and kinetic effects, *Earth and Planetary Science Letters*, v. 115, pp. 177-195.
- Keppler, H. and Wyllie, P.J., 1991 - Partitioning of Cu, Sn, Mo, W, U, and Th between melt and aqueous fluid in the systems haplogranite-H₂O-HCl and haplogranite-H₂O-HF, *Contributions to Mineralogy and Petrology*, v. 109, pp. 139-150.
- Kimura, J.-I., Tanji, T., Yoshida, T. and Iizumi, S., 2001 - Geology and geochemistry of lavas at Nekoma volcano: implications for origin of Quaternary low-K andesite in the north-eastern Honshu arc, Japan, *The Island Arc*, v. 10, pp. 116-134.
- Kobayashi, K. and Nakamura, E., 2001 - Geochemical evolution of Akagi Volcano, NE Japan: implications for interaction between island-arc magma and lower crust, and generation of

- isotopically various magmas, *Journal of Petrology*, v. 42 (12), pp. 2303-2331.
- Kress, V.C. and Carmichael, I.S.E., 1991 - The compressibility of silicate liquids containing Fe₂O₃ and the effect of composition, temperature and oxygen fugacity and pressure on their redox states, *Contributions to Mineralogy and Petrology*, v. 108, pp. 82-92.
- Kushiro, I., 1987 - A petrological model of the mantle wedge and lower crust in the Japanese island arcs; in Mysen, B.O., (Ed.), *Magmatic processes: Physicochemical principles*, *The Geochemical Society*, Special Publication No. 1. *Lancaster Press Inc.* 1987.
- Lallemant, S.E., Popoff, M., Cadet, J.P., Bader, A.G., Pubellier, M., Rangin, C. and Deffontaines, B., 1998 - Genetic relations between the central and southern Philippine Trench and the Sangihe Trench, *Journal of Geophysical Research*, v. 103 (B1), pp. 933-950.
- Lang, J.R. and Titley, S.R., 1998 - Isotopic and geochemical characteristics of Laramide magmatic systems in Arizona and implications for the genesis of porphyry copper deposits, *Economic Geology*, v. 93, pp. 138-170.
- Lange R.L. and Carmichael I.S.E., 1990 - Thermodynamic properties of silicate liquids with emphasis on density, thermal expansion and compressibility; in Nicholls, J. and Russell, J.K., (Eds.), *Modern Methods of Igneous Petrology: understanding Magmatic Processes*. *Mineralogical Society of America, Bookcrafters Inc.*, Michigan.
- Larsen, L.M., 1979 - Distribution of REE and other trace elements between phenocrysts and peralkaline undersaturated magmas, exemplified by rocks from the Gardar igneous province, south Greenland, *Lithos*, v. 12, pp. 303-315.
- Luhr, J.F. and Aranda-Gómez, J.J., 1997 - Mexican peridotite xenoliths and tectonic terranes: correlations among vent location, texture, temperature, pressure, and oxygen fugacity, *Journal of Petrology*, v. 38, pp. 1075-1112.
- Marsh, T.M., Einaudi, M.T. and McWilliams, M., 1997 - ⁴⁰Ar/³⁹Ar geochronology of Cu-Au and Au-Ag mineralisation in the Potrerillos district, Chile, *Economic Geology*, v. 92, pp. 784-806.
- Middleton, C., Buenavista, A., Rohrlach, B., Gonzalez, J., Subang, L. and Moreno, G., 2004 - A geological review of the Tampakan copper-gold deposit, southern Mindanao, Philippines; in *Hi Tech and World Competitive Mineral Success Stories Around the Pacific Rim*, Proc. Pacrim 2004 Conference, Adelaide, 19-22 September, 2004, *AusIMM, Melbourne*, pp 273-187.
- Miyajima, H., 1990 - Petrology of Higashi-Izu monogenetic volcano group, implication of xenocrysts, time and spatial variation of ejecta, *Journal of Mineralogy, Petrology and Economic Geology*, v. 85, pp. 315-336.
- Moore, G. and Carmichael, I.S.E., 1998 - The hydrous phase equilibria (to 3 kbar) of an andesite and basaltic andesite from western Mexico: constraints on water content and conditions of phenocryst growth, *Contributions to Mineralogy and Petrology*, v. 130, pp. 304-319.
- Moore, G., Vennemann, T. and Carmichael, I.S.E., 1998 - An empirical model for the solubility of H₂O in magmas to 3 kilobars, *American Mineralogist*, v. 83, pp. 365-42.
- Morrice, M.G., Jezek, P.A., Gill, J.B., Whitford, D.J. and Monoarfa, M., 1983 - An introduction to the Sangihe Arc: volcanism accompanying arc-arc collision in the Molucca Sea, Indonesia, *Journal of Volcanology and Geothermal Research*, v. 19, pp. 135-165.
- Moyle, A.J., Doyle, B.J., Hoogvliet, H. and Ware, A.R., 1990 - Ladolam gold deposit, Lihir island; in Hughes, E., (Ed.), *Geology of the Mineral Deposits of Australia and Papua New Guinea*, *AusIMM, Melbourne*, pp. 1793-1805.
- Nicholls, I.A. and Harris, K.L., 1980 - Experimental rare-earth-element partition coefficients for garnet, clinopyroxene and amphibole coexisting with andesitic and basaltic liquids, *Geochimica et Cosmochimica Acta*, v. 44, pp. 287-308.
- Nagasawa, H. and Schnetzler, C.C., 1971 - Partitioning of rare earth, alkali and alkaline earth elements between phenocrysts and acidic igneous magma, *Geochimica et Cosmochimica Acta*, v. 42, pp. 1253-1263.
- Nielsen, R.L., Gallahan, W.E. and Newberger, F., 1992 - Experimentally determined mineral-melt partition coefficients for Sc, Y and REE for olivine, orthopyroxene, pigeonite, magnetite and ilmenite, *Contributions to Mineralogical Petrology*, v. 110, pp. 488-499.
- Ochs, A. and Lange, R.A., 1999 - The density of hydrous magmatic liquids, *Science*, v. 283, pp. 1314-1317.
- Ozawa, A., Tagami, T., Listanco, E.L., Arpa, C.B. and Sudo, M., 2004 - Initiation and propagation of subduction along the Philippine Trench: evidence from the temporal and spatial distribution of volcanoes, *Journal of Asian Earth Sciences*, v. 23, pp. 105-111.
- Panjasawatwong, Y., Danyushevsky, L.V., Crawford, A.J. and Harris, K.L., 1995 - An experimental study of the effects of melt composition on plagioclase-melt equilibria at 5 and 10 kbar: implications for the origin of magmatic high-An plagioclase, *Contributions to Mineralogy and Petrology*, v. 118, pp. 420-432.
- Peacock, S.M., 1990a - Numerical simulation of metamorphic pressure-temperature-time paths and fluid production in subducting slabs, *Tectonics*, v. 9 (5), pp. 1197-1211.
- Peacock, S.M., 1990b - Fluid processes in subduction zones, *Science*, v. 248, pp. 329-337.
- Peacock, S.M., Rushmer, T. and Thompson, A.B., 1994 - Partial melting of subducting oceanic crust, *Earth and Planetary Science Letters*, v. 121, pp. 277-244.
- Peng, G., Luhr, J.F. and McGee, J.J., 1997 - Factors

- controlling sulfur concentrations in volcanic apatite, *American Mineralogist*, v. 82, pp. 1210-1224.
- Polvé, M., Maury, R.C., Bellon, H., Rangin, C., Priadi, B., Yuwono, S., Joron, J.L. and Soeria-Atmajda, R., 1997 - Space- and time- controlled magmatic evolution of Sulawesi (Indonesia): constraints on the Cenozoic geodynamic history of the Sundaland active margin, *Tectonophysics*, v. 272, pp. 69-92.
- Poulson, S.R. and Ohmoto, H., 1990 - An evaluation of the solubility of sulfide sulfur in silicate melts from experimental data and natural samples, *Chemical Geology*, v. 85, pp. 57-75.
- Prouteau, G., Maury, R.C., Sajona, F.G., Cotton, J. and Joron, J-L., 2000 - Behaviour of Nb, Ta and other HFSE in adakites and related lavas from the Philippines, *Island Arc*, v. 9, pp. 487-498.
- Pubellier, M., Quebral, R., Rangin, C., Deffontaines, B., Muller, C., Butterlin, J. and Manzano, J. 1991. The Mindanao collision zone, a soft collision event within a continuous strike-slip setting; *Journal of Southeast Asian Earth Sciences*, v. 6, pp. 239-248.
- Pubellier, M., Quebral, R., Deffontaines, R. and Rangin, C., 1993 - Neotectonic map of Mindanao island, Philippines, *Explanatory Note*.
- Pubellier, M., Gaelle Bader, A., Rangin, C., Deffontaines, B. and Quebral, R., 1999 - Upper plate deformation induced by subduction of a volcanic arc: the Snellius Plateau (Molucca Sea, Indonesia and Mindanao, Philippines), *Tectonophysics*, v. 304, pp. 345-368.
- Quebral, R.D., Pubellier, M. and Rangin, C., 1996 - The onset of movement on the Philippine Fault in Eastern Mindanao: A transition from a collision to a strike-slip environment, *Tectonics*, v. 15(4), pp. 713-726.
- Rangin, C., 1991 - The Philippine Mobile Belt: A complex plate boundary, *Journal of Southeast Asian Earth Sciences*, v. 6 (3/4), pp. 209-220.
- Rodriguez-Vargas, A., Koester, E., Mallmann, G., Conceição, R.V., Kawashita, K. and Weber, M.B.I., 2005 - Mantle diversity beneath the Colombian Andes, Northern Volcanic Zone: constraints from Sr and Nd isotopes, *Lithos* v. 82, pp. 471-484.
- Rohrlach, B., Madera, A. and Watt, R., 1999 - Geology, alteration and mineralisation of the Tampakan copper deposit, in Proc. Pacrim 99, Conference, Bali, Indonesia, *AusIMM, Melbourne* pp 517-525
- Rohrlach, B.D. and Loucks, R.R., 2000a - An extended calibration range for the magnetite-ilmenite Fe-Ti-exchange geothermometer and oxygen barometer, 2000 Annual Report, Research School of Earth Sciences, *Australian National University*, Canberra, ACT.
- Rohrlach, B.D. and Loucks, R.R., 2000b - Refinement of a silicate melt "geohygrometer" based on the depression of feldspar crystallisation temperature by water dissolved in the silicate melt, 2000 Annual Report, Research School of Earth Sciences, *Australian National University*, Canberra, ACT.
- Rohrlach, B.D., 2002 - Tectonic evolution, petrochemistry, geochronology and palaeohydrology of the Tampakan porphyry and high sulphidation epithermal Cu-Au deposit Mindanao, Philippines, *Unpublished PhD thesis, Australian National University*, Canberra, Australia, November 2002.
- Rohrlach, B.D., Loucks, R.R. and Palin, J.M., 2003 - Isochoric ascent of lithostatically-pressured, dense magmatic vapor during gold-enargite ore formation, *13th V.M. Goldschmidt Conference 2003: Frontiers in Geochemistry, 7-12th September 2003, Kurashiki, Japan*. Abstracts Volume.
- Ruxton, B.P. and McDougall, I., 1967 - Denudation rates in northeast Papua from potassium-argon dating of lavas, *American Journal of Science*, v. 265, pp. 545-561.
- Rye, R. O., Bethke, P. M. and Wasserman, M. D., 1992 - The stable isotope geochemistry of acid sulphate alteration, *Economic Geology*, v. 87, pp. 225-262.
- Sajona, F.G., 1994 - Petrographic and geochemical analyses of four igneous rock samples of the Western Mining Corporation from the northwestern flanks of Mt Matutum, Mindanao, Philippines, *Unpublished Report to WMC*, Makati, Metro-Manila.
- Sajona, F.G., Bellon, H., Maury, R.C., Pubellier, M., Cotton, J. and Rangin, C., 1994 - Magmatic response to abrupt changes in geodynamic settings: Pliocene-Quaternary calc-alkaline and Nb-enriched lavas from Mindanao (Philippines), *Tectonophysics*, v. 237 (1-2), pp. 47-72.
- Sajona, F.G., Bellon, H., Maury, R.C., Pubellier, M., Quebral, R.D., Cotton, J., Bayon, F.E., Pagado, E. and Pamatians, P., 1997 - Tertiary and Quaternary magmatism in Mindanao and Leyte (Philippines): geochronology, geochemistry and tectonic setting, *Journal of Asian Earth Sciences*, v. 15, pp. 121-153.
- Sajona, F.G., Maury, R.C., Pubellier, M., Leterrier, J., Bellon, H. and Cotton, J., 2000 - Magmatic source enrichment by slab-derived melts in a young post-collision setting, central Mindanao (Philippines), *Lithos*, v. 54 (3/4), pp. 173-206.
- Sakuyama, M. and Nesbitt, R.W., 1986 - Geochemistry of the Quaternary volcanic rocks of the northwest Japan arc, *Journal of Volcanology and Geothermal Research*, v. 29, pp. 413-450.
- Scaillet, B. and Evans, B.W., 1999 - The 15 June 1991 eruption of Mount Pinatubo. I. phase equilibria and pre-eruption P-T-fO₂-fH₂O conditions of the dacite magma, *Journal of Petrology*, v. 40 (3), pp. 381-411.
- Seno, T. and Kurita, K., 1978 - Focal mechanisms and tectonics in the Taiwan-Philippine region; in Uyeda, S., Murphy, R.W. and Kobayashi, K., (Eds.), *Geodynamics of the Western Pacific*, Proceedings of the International Conference on Geodynamics of the Western Pacific-Indonesian

- Region, March 1978, Tokyo. Supplementary Issue of *Journal of Physics of the Earth*. Tokyo.
- Shinohara, H., Iiyama, J.T. and Matsuo, S., 1989 - Partition of chlorine compounds between silicate melt and hydrothermal solutions: I. Partition of NaCl-KCl, *Geochimica et Cosmochimica Acta*, v. 53, pp. 2617-2630.
- Shuto, K. and Yashima, R., 1990 - Lateral variation of major and trace elements in the Pliocene volcanic rocks of the Northeast Japan arc, *Journal of Mineralogy, Petrology and Economic Geology*, v. 85, pp. 364-389.
- Silver, E.A. and Moore, J.C., 1978 - The Molucca Sea collision zone, Indonesia, *Journal of Geophysical Research*, v. 83 (B4), pp. 1681-1691.
- Sisson, T.W., 1994 - Hornblende-melt trace-element partitioning measured by ion microprobe, *Chemical Geology*, v. 117, pp. 331-344.
- Sourirajan, S. and Kennedy, G.C., 1962 - The system H₂O-NaCl at elevated temperatures and pressures, *American Journal of Science*, v. 260, pp. 115-141.
- Stern, C.R., Huang, W-L. and Wyllie, P.J., 1975 - Basalt-andesite-rhyolite-H₂O: Crystallization intervals with excess H₂O and H₂O-undersaturated liquidus surfaces to 35 kilobars, with implications for magma genesis, *Earth and Planetary Science Letters*, v. 28, pp. 189-196.
- Streck, M.J. and Dilles, J.H., 1998 - Sulfur evolution of oxidised arc magmas as recorded in apatite from a porphyry copper batholith, *Geology*, v. 26, pp. 523-526.
- Subang, L.L., Buenavista, A.G., Gonzales, J.M., Moreno, G.P., Baratang, V.T.B. Jr., Sebua, M.C. and Santos, N.A., 2004 - Geology and Mineralisation of the Porphyry-High-Sulphidation Epithermal Cu-Au Deposit at Tampakan, Southern Mindanao, Philippines, *Geological Society of the Philippines GeoCon 2004 Modern Technology and Advancement in Geosciences, Dec 8-10, Sulo Hotel, Quezon City, Philippines*, 72p.
- Sun, S.-S. and McDonough, W.F., 1989 - Chemical and isotopic systematics of oceanic basalts: implications for mantle composition and processes, in Saunders, A.D. and Norry, M.J., eds., *Magmatism in the Ocean Basins*, *Geological Society of London, Special Publication* 42, pp. 313-345.
- Suzuki, Y., 2000 - Petrogenesis of felsic magma in the Higashi-Izu monogenetic volcano group, *Bulletin of the Volcanological Society of Japan*, v. 45, pp. 149-17.
- Takahashi, E., 1980 - Thermal history of lherzolite xenoliths-1. Petrology of lherzolite xenoliths from the Ichinomegata crater, Oga Peninsula, Northeast Japan, *Geochimica et Cosmochimica Acta*, v. 44, pp. 1643-1658.
- Talbot, C.J., 1999 - Can field data constrain rock viscosities?, *Journal of Structural Geology*, v. 21, pp. 949-957.
- Tamura, S.-I. and Shuto, K., 1989 - Lateral variation of major and trace elements in the late Miocene volcanic rocks from central part of northeast Japan, *Journal of Mineralogy, Petrology and Economic Geology*, v. 84, pp. 444-459.
- Tamura, Y., 1994 - Genesis of island arc magmas by mantle-derived bimodal magmatism: evidence from the Shirahama group, Japan, *Journal of Petrology*, v. 35, pp. 619-645.
- Tatsumi, Y., Murasaki, M., Arsadi, E. M. and Nohda, S., 1991 - Geochemistry of Quaternary lavas from NE Sulawesi: transfer of subduction components into the mantle wedge, *Contributions to Mineralogy and Petrology*, v. 107, pp. 137-149.
- Titley, S.R. and Beane, R.E., 1981 - Porphyry copper deposits - Part I. Geologic settings, petrology and tectogenesis, *Economic Geology - 75th Anniversary Volume*, pp. 216-269.
- Togashi, S., Tanaka, T., Yoshida, T., Ishikawa, K., Fujimaki, H. and Kurasawa, H., 1992 - Trace elements and Nd-Sr isotopes of island arc tholeiites from frontal arc of northeast Japan, *Geochemical Journal*, v. 26, pp. 261-277.
- Ujike, O. and Stix, J., 2000 - Geochemistry and origins of Ueno and On-take basaltic to andesitic rocks (<3 Ma) produced by distinct contributions of subduction components, central Japan, *Journal of Volcanology and Geothermal Research*, v. 95, pp. 49-64.
- Ulmer, P., 1988 - High-pressure phase equilibria of a calc-alkaline micro-basalt: implications for the genesis of calc-alkaline magmas, *Carnegie Institution of Washington Geophysical Laboratory Annual Report 1987-1988*, pp. 28-35.
- Umino, S. and Yoshizawa, E., 1996 - Petrology of ultramafic xenoliths from Kishyuku Lava, Fukuejima, Southwest Japan, *Contributions to Mineralogy and Petrology*, v. 124, pp. 154-166.
- Wallace, P.J., 2005 - Volatiles in subduction zone magmas: concentrations and fluxes based on melt inclusion and volcanic gas data, *Journal of Volcanology and Geothermal Research*, v. 140, pp. 217-240.
- Weber, W.B.I., Tarne, J., Kempton, P.D. and Kent, R.W., 2002 - Crustal make-up of the northern Andes: evidence based on deep crustal xenolith suites, Mercaderes, SW Colombia, *Tectonophysics*, v. 345, pp. 49-82.
- Williams, T.J., Candela, P.A. and Piccoli, P.M., 1995 - The partitioning of copper between silicate melts and two-phase aqueous fluids: an experimental investigation at 1 kbar, 800°C and 0.5 kbar, 850°C, *Contributions to Mineralogy and Petrology*, v. 121, pp. 388-399.
- Wörner, G., Harmon, R.S., Davidson, J., Moorbath, S., Turner, D.L., McMillan, N., Nye, C., Lopez-Escobar, L. and Moreno, H. 1988 - The Nevados de Payachata volcanic region (18°S/69°W, N.Chile) I. Geological, geochemical, and isotopic observations, *Bulletin of Volcanology*, v. 50, pp. 287-303.
- Wohletz, K. and Heiken, G., 1992 - Volcanology and geothermal energy, *University of California Press*, Berkeley and Los Angeles, California. 432 p.

